2020

Application of heat pumps and thermal storage systems for improved control and performance of microgrids

Ali Baniasadi
Edith Cowan University

Edith Cowan University

Copyright Warning

Application of Heat Pumps and Thermal Storage Systems for Improved Control and Performance of Microgrids

This thesis is submitted for the degree of

Doctor of Philosophy

Ali Baniasadi

School of Engineering

Edith Cowan University

2020

USE OF THESIS

The Use of Thesis statement is not included in this version of the thesis.

Abstract

The high penetration of renewable energy sources (RES), in particular, the rooftop photovoltaic (PV) systems in power systems, causes rapid ramps in power generation to supply load during peak-load periods. Residential and commercial buildings have considerable potential for providing load flexibility by exploiting energy-efficient devices like ground source heat pump (GSHP). The proper integration of PV systems with the GSHP could reduce power demand from demand-side. This research provides a practical attempt to integrate PV systems and GSHPs effectively into buildings and the grid. The multi-directional approach in this work requires an optimal control strategy to reduce energy cost and provide an opportunity for power trade-off or feed-in in the electricity market. In this study, some optimal control models are developed to overcome both the operational and technical constraints of demand-side management (DSM) and for optimum integration of RES.

This research focuses on the development of an optimal real-time thermal energy management system for smart homes to respond to DR for peak-load shifting. The intention is to manage the operation of a GSHP to produce the desired amount of thermal energy by controlling the volume and temperature of the stored water in the thermal energy storage (TES) while optimising the operation of the heat distributors to control indoor temperature.

This thesis proposes a new framework for optimal sizing design and real-time operation of energy storage systems in a residential building equipped with a PV system, heat pump (HP), and thermal and electrical energy storage systems. The results of this research demonstrate to rooftop PV system owners that investment in combined TSS and battery can be more profitable as this system can minimise life cycle costs.

This thesis also presents an analysis of the potential impact of residential HP systems into reserve capacity market. This research presents a business aggregate model for controlling residential HPs (RHPs) of a group of houses that energy aggregators can utilise to earn capacity credits. A control strategy is proposed based on a dynamic aggregate RHPs coupled with TES model and predicting trading intervals capacity requirements through forecasting demand and non-scheduled generation. RHPs coupled with TES

are optimised to provide DSM reserve capacity. A rebound effect reduction method is proposed that reduces the peak rebound RHPs power.

Declaration

I, Ali Baniasadi, hereby declare that this thesis does not, to the best of my belief and knowledge:

- Incorporate without acknowledgement any material previously submitted for a degree or diploma in any institution of higher education;
- Contain any material published previously or written by another person except where due reference is made in the text; or contain any defamatory material.

Signed: Ali Baniasa 

Dated: 31.01.2020

I would like to dedicate this thesis to my inspirational wife.

Acknowledgements

It is a genuine pleasure to express my deep sense of thanks and gratitude to my supervisors, faculty, friends, and family. I would like to gratefully acknowledge my principal supervisor, Professor Daryoush Habibi, for his valuable guidance and continuous support during my research. I would also like to express my sincere gratitude to Dr Mohammad Masoum and Dr Waleed Al-Saedi for their generous support with various sources of information and critical reviews throughout this research work. Furthermore, I would like to thank Dr Octavian Bass and my fellow Smart Energy group members for all their kind advice, assistance, guidance and generous personal support.

I would like to express my profound gratitude to my beloved wife for her understanding, timely patience and encouragement. This journey would never be possible without her endless love and unconditional support. I am sincerely grateful to my parents and other family members for their invaluable cooperation, encouragement, and blessings, even from afar. Finally, I would also like to thank my friends for their unconditional support throughout this research journey.

List of Publications Arising From This Thesis

1. **A. Baniasadi**, D. Habibi, O. Bass and M. A. S. Masoum, "Optimal Real-Time Residential Thermal Energy Management for Peak-Load Shifting With Experimental Verification," in IEEE Transactions on Smart Grid, vol. 10, no. 5, pp. 5587-5599, Sept. 2019. doi: 10.1109/TSG.2018.2887232

2. **A. Baniasadi**, D. Habibi, W. Al-Saedi, M. A. S. Masoum, C. K. Das, and N. Mousavi, "Optimal Sizing Design and Operation of Electrical and Thermal Energy Storage Systems in Smart Buildings," Journal of Energy Storage, 2020 Apr 1;28:101186. doi.org/10.1016/j.est.2019.101186

3. **A. Baniasadi**, D. Habibi, W. Al-Saedi and M. A. S. Masoum, "A Cost-effective Thermal and Electrical Energy Storage Management Strategy for Smart Buildings," 2019 IEEE PES Innovative Smart Grid Technologies Europe (ISGT-Europe), Bucharest, Romania, 2019, pp. 1-5. doi: 10.1109/ISGTEurope.2019.8905537

4. **A. Baniasadi**, D. Habibi, W. Al-Saedi, and M. A. S. Masoum, "PV Self-Consumption Enhancement with Optimal Residential Thermal Energy Management," 2019 9th International Conference on Power and Energy Systems (ICPES), Perth, Australia

5. **A. Baniasadi**, D. Habibi, W. Al-Saedi, M. A. S. Masoum, and N. Mousavi, "Potential Integration of Residential Heat Pump Systems into Reserve Capacity Market," [redacted] (Under Review).

Contents

List of Figures

List of Tables

Glossary

AC	Air conditioner.
AEMO	Australian energy market operator.
ANN	Artificial neural network.
BSS	Battery storage system.
BTM	Building thermal mass.
DDRC	Dynamic demand response controller.
DLC	Direct load control.
DR	Demand response.
DRP	Demand response program.
DSM	Demand side management.
DTS	Dynamic temperature set-point.
FCU	Fan coil unit.
GSHP	Ground source heat pump.
HP	Heat pump.
HVAC	Heating, ventilating, and air conditioning.
IRCR	Individual reserve capacity requirement.
LCC	Life cycle cost.
MPC	Model predictive control.
NSG	Non-schedule generation.
OBTS	Optimal BSS and TSS sizing.
PSO	Particle swarm optimisation.
RC	Reserve capacity.
RCM	Reserve capacity mechanism.
RER	Rebound effect reduction.
RES	Renewable energy resources.
RHP	Residential heat pump.
RTB	Real-time temperature boundary.
RTP	Real-time pricing.
SBEMS	Smart building energy management system.
SOC	Battery state of charge.
SWIS	South West interconnected system.
TCL	Thermostatically controlled load.
TEMS	Thermal energy management system.
TES	Thermal energy storage.
TOU	Time-of-use.
TSS	Thermal storage system.
WEM	Wholesale electricity market.
WST	Water storage tank.
β	Impact coefficient of DTS.
$\dot{m}_{af}$	Mass air flow rate through the FCU (m^3/s).
$\dot{m}_{ex}$	Mass water flow rate through the boreholes (l/min).
$\dot{m}_f$	Mass water flow rate through the FCU (l/min).
$\dot{m}_{GHP}$	Mass water flow rate of GSHP (l/min).
$\dot{m}_{HP}$	Mass water flow rate of HP (L/min).
$\dot{m}_r$	Mass water flow rate through fan coil (L/min).
$\dot{m}_{td}$	Mass water flow rate through the building (l/min).
λ	Solar radiation absorption factor.
$\mathcal{Z}$	Electricity price ($Cent/kWh$).
ψ	Binary decision variable.
ρ	Density of the water (kg/m^3).
$\underline{T}_{in}, \overline{T}_{in}$	Lower and upper boundaries of indoor temperature set-point ($^\circ C$).
$\underline{T}_{sp}, \overline{T}_{sp}$	Lower and upper boundaries of indoor temperature set-point ($^\circ C$).
C_g	Cost of electricity purchased from grid (\$).

C_l	Thermal capacity of the thermal mass ($J/^\circ C$).
c_p	Specific heat capacity of water ($J/(g.^\circ C)$).
c_{ap}	Specific heat capacity of air ($J/(g.^\circ C)$).
C_{batt}	Capacity of BSS (kWh).
C_{BSS}	Capital, replacement, and maintenance costs of BSS (\$).
C_{HP}	Cost of HP power consumption (\$).
C_{in}	Thermal capacity of the building ($J/^\circ C$).
C_{TSS}	Capital and maintenance costs of TSS (\$).
D	Diameter of the WST (m).
h_c	Stored chilled water height (m).
I_s	Solar radiation (W/m^2).
I_g	Internal heat gain (W).
I_g	Internal heat gain (kW).
m_c	Volume of stored chilled water (l).
m_t	Volume of stored water (l).
m_w	Volume of the warm water in the TES (l).
$m_{TSS,0}$	Initial chilled/hot water volume stored in TSS (L).
m_{TSS}	TSS stored chilled/hot water volume (L).
$NRTP$	Normalised real-time electricity price ($Cent/kWh$).
P_{ch}	Battery charging power (kW).
P_{dch}	Battery discharging power (kW).
P_f	Power consumption of fan (W).
P_g	Power purchased from grid (kW).
P_{hl}	Internal heat loads (W).
P_{hl}	Power usage of base load (kW).
P_{HP}	Power consumption of HP (kW).
P_{PV}	PV output Power (kW).
R_{in}	Thermal resistance between building and ambient ($^\circ C/W$).
R_{io}	Thermal resistance between building and thermal mass ($^\circ C/W$).
S_r	Solar radiation (W/m^2).
SOC_0	Initial SOC of BSS (%).
SOC_{TES}	TES State of charge (%).
T_c	Stored chilled water temperature ($^\circ C$).
T_d	Dynamic indoor temperature set-point ($^\circ C$).
T_l	Building's lumped thermal mass temperature (°C).
T_l	Building's lumped thermal mass temperature ($^\circ C$).
T_o	Ambient temperature ($^\circ C$).
T_w	Top layer temperature of TES ($^\circ C$).
T_{af}	Supply FCU air temperature ($^\circ C$).
$T_{b,in}$	Water temperature to the boreholes ($^\circ C$).
$T_{b,out}$	Water temperature from the boreholes ($^\circ C$).
T_{fr}	Outlet water temperature of FCU ($^\circ C$).
T_f	Inlet water temperature of FCU ($^\circ C$).
T_{GHP}	Output water temperature of the GSHP ($^\circ C$).
T_{HP}	Output water temperature of the HP ($^\circ C$).
T_{in}	Indoor temperature ($^\circ C$).
T_{return}	Temperature of return water from building (°C).
T_{TSS}	Chilled/hot water temperature stored in TSS (°C).
W_{GHP}	Power consumption of GSHP compressor (W).
Q_c	Stored cooling energy in WST (W).
Q_{ex}	Heat transfer rate of boreholes (W).

Q_{f_1}	Heat transfer rate of FCU from water (W).
Q_f	Heat transfer rate of FCU to air (W).
Q_{GHP}	Heat transfer rate of GSHP (W).
Q_{HP}	Thermal energy generated by HP (kW).
Q_{td}	Thermal energy demand (kW).
Q_{TSS}	Thermal energy stored in TSS (kW).

Chapter 1

Introduction and Topical Overview

1.1 Background and Motivation

Environmental and economic considerations are the main motivations for moving energy generation from fossil fuels towards renewable energy sources. However, there are some issues to address for integrating new sources in deregulated power systems, such as flexible loads and demand side management [5]. Recent developments in the field of controllable devices such as heat pumps (HPs) and electricity market deregulation have led to a renewed interest in energy efficiency and demand response [6]. DR is a change in the power consumption patterns by energy consumers in response to price signals over time or to price incentives [7]. The main goal of DR is to integrate the required demand to the available energy resource without the need for new generation capacity [8]. Based on the definition of DR and its aim, HP can be actively managed to match the intermittent RES to the price of electricity efficiently.

There are two categories for DR programs as price-based (including time-of-use pricing, real-time pricing, critical peak pricing) and incentive-based [9]. In the midst of the pricing-based strategies, the RTP has considerable potential to address intermittent RE integration issues [10]. However, the response of customers to these strategies are highly

unpredictable, and will be largely dependent on customers' perception of their gains from these strategies. When they wish to benefit from participating in the price-based program, they can manipulate the operation of their appliances so that they turn on during off-peak periods [11]. Therefore, in order to hinder the adverse effect of this issue on the success of the strategy, an efficient control method is needed.

Some challenges are now being faced in the power systems because of widespread penetration of the intermittent RES. Electricity generation conventionally would follow the load. In a system with large RES penetration, a management system is required that can adjust the demand and/or the generation in response to the intermittency in energy generation from wind and PV sources [12]. On the other hand, DSM has the highest potential for changing the patterns of end-use energy consumption and reducing costs over time. This can be accomplished through load shifting, predictive control strategies, and flexible loads [13]. The best initiative to reduce the gap between supply and demand is an optimal integration of controllable devices with RES. This is the main motivating principle of this research in order to provide experimental solutions to achieve optimal control, DSM and optimal integration of RES with HPs.

Furthermore, due to the fact that the generation of RES is highly variable and distribution electricity networks face economic and technical challenges to keep power balance in real-time and scheduled-time operations. Addressing this challenge often needs application of additional demand-side flexibility in power systems mainly through ancillary service provision of electricity end-users. Ancillary services are described as services that are essential to support the management of power system security and reliability and transmission of electric power from seller to purchaser in acceptable quality [14]. There are two groups for this service; 1) first group contains scheduling, system control and dispatch, and reactive supply and voltage control, 2) second group includes regulation and frequency response, energy imbalance, and reserve power. The need for more flexibility in power systems has resulted in the application of DR programs to distributed energy storage systems. The residential buildings have been stated as a possible resource for demand-side flexibility. TES inherent in building structural materials can be accessible through HVAC, including GSHPs which are coupled to electricity grids. Thereby, the

ancillary service provision of the residential buildings may have significant potential to improve power grid stability.

There are some significant issues that should be considered to design an effective energy management model to to optimally integrate RES with HP. These issues are power demand prediction, forecast weather condition, and control and state variables. According to high consumption of energy in space heating/cooling and hot water in buildings, GSHP could highly decrease energy consumption on the demand-side by implementing an optimal control strategy. GSHP is a very high energy efficiency equipment that brings appropriate flexibility for grid, in particular when combined with TESs. Furthermore, GSHP is more efficient than air source heat pump which is used widely in buildings. The main reason of this excel is consequence of extracting heat from the ground which is an approximately constant temperature source, warmer than the air in cold seasons and cooler in hot seasons [15].

The integration of RES such as wind, PV, fuel cell, micro-hydro and storage batteries into buildings and small communities is encouraging for DSM. However, exploiting novel technologies in power systems requires intelligent load management to meet increasing demand and cost function. Subsequently, there is a vital need to develop an optimal control strategy and integrate RES to realise net-zero energy buildings, cost-effective billing and positive-energy buildings [16, 17]. The high level control strategy such as MPC can effectively manage multi-variable dynamic constrained systems and optimisation issue that minimises the cost function [3]. However, far too little attention has been paid to integrate RES into GSHP. Therefore, lack of a proper optimal strategy to optimum integration of RES and GSHP is the main motivation of this research.

More specifically, the main challenges of the proposed research can be stated as:

- Real-time scheduling for demand-side that needs accurate prediction (like prices, weather condition and RES generation) and forecasting error reduction.
- The deployment of an appropriate modelling technique will be needed for achieving optimum RES integration with GSHP coupled with thermal storage tanks, which will benefit customers economically.

- HPs should be controlled optimally on the distribution network to save energy and increase the reserve power while maintaining system stability, control and flexibility.

1.2 Aims

The main question that this research will address is how heat pumps can be managed with optimal control strategies in buildings and in distribution grids. Thus, the following aims are considered:

1. Design, analyse and implement an optimal strategy to shift peak-load. in buildings, by controlling the power consumption of GSHP
2. Optimal operation of electrical and thermal energy storage systems in smart buildings according to the availability of RES generation.
3. Optimal sizing of electrical and thermal energy storage systems in smart buildings.
4. Predict the flexibility of HP pool in the distribution network to enhance reserve capacity.

1.3 Thesis Contributions

The contributions of this thesis are about managing heat pumps by proposing optimal control strategies in building and in distribution grid. The main contributions of this thesis are as follows:

- This research develops an optimal real-time thermal energy management system (TEMS) for smart buildings to respond to DRP by employing two thermal storage systems (WST and BTM) for peak-load shifting while enhancing the efficiency and maintaining the temperature within the thermal comfort zone. This research also proposes a real-time DTS approach based on real-time pricing tariffs is developed to enhance the efficiency of smart building by shifting up to 100% of HP loads from peak-price hours.

- This research presents a cost-effective approach to minimise the operation cost for smart homes as well as to increase the PV self-consumption. A model of an integrated home energy management system (IHEMS) consists of rooftop PV system and HP coupled with thermal energy storage system is proposed.
- This research presents a new optimal BSS and TSS sizing (OBTS) solution for thermal and electrical storage systems to minimise annual electricity costs of smart buildings with rooftop PVs while minimising life cycle cost. Optimal BSS and TSS charging and discharging are key elements of the proposed OBTS that is considered in the optimal sizing. These elements have not been largely considered together by other literature studies for optimal TSS and BSS sizing. Moreover, cost comparison for different case studies is presented.
- This research develops a control scheme for real-time smart building energy management system (SBEMS) to increase PV self-consumption and reduce electricity costs. The real-time charging and discharging of BSS and TSS are achieved by using the proposed SBEMS based on RTP.
- This research presents a dynamic aggregate model of residential heat pumps coupled with thermal energy storage systems for providing demand side management reserve capacity.

1.4 Thesis Outline

This thesis is organised into nine chapters as follows:

- Chapter 1 introduces the research overview, including research significance and motivation, aims of the thesis, and contributions of the thesis in the relevant fields. This chapter also presents ideas on the research visions and expected outcomes in terms of operation and sizing of electrical and thermal energy storage using various approaches.
- Chapter 2 discusses the background and literature review of integrating HPs with RES systems in the power grid and their impacts. This chapter presents all relevant control strategies along with both their advantages and disadvantages. Research gaps are identified and the research questions are proposed.

- Chapter 3 focuses on a new building pre-cooling/preheating system using a real-time dynamic temperature set-points strategy. The implementation of a new comprehensive control strategy based on DTS supports the full advantage of BTM to make the system more flexible. The system includes a GSHP, a water storage tank and two fan coil units (FCUs). The WST is used to store chilled/hot water produced by the GSHP and deliver it when needed. The presence of the WST allows the GSHP to efficiently operate whenever the electrical energy prices are low. In this chapter, experimental verifications of the proposed TEMS to reduce power consumption of the GSHP and FCU with load shifting is presented.

- Chapter 4 presents an approach to resolve the issues associated with variations in rooftop PV power by minimising the peak demand of smart buildings. This is done by integrating a HP-PV system model that consists of a rooftop PV and a HP which is used as a controllable load. The implemented residential thermal energy management strategy consists of a model predictive control to minimise the operation cost of HP, and a real-time temperature boundary (RTB) strategy based on real-time pricing tariff. Furthermore the occupants' thermal comfort is also taken into account while shifting the HP electricity load.

- Chapter 5 demonstrates a cost-effective approach to minimise the operation cost for smart homes. A model of an integrated home energy management system is proposed in this chapter. This system encompasses a rooftop PV system, battery and HP coupling with a thermal storage tank as controllable load. Colonial competitive algorithm is employed to minimise the operation cost. The efficiencies of battery charging and discharging are considered as well as battery charging method. HP with TST is considered to shift its load towards the low electricity price periods or whenever PV production is available. Furthermore, the occupants' thermal comfort is also considered while shifting HP electricity load. The IHEMS model is implemented in Smart Energy Laboratory at Edith Cowan University to verify the simulation results.

- Chapter 6 provides an effective sizing strategies for HPs coupled with TSS to respond to DRP while minimising life cycle cost. The aims of this chapter are to find the optimal sizes of TSS and BSS based on TOU tariff to increase PV self-consumption. Then, after determining the optimal BSS and TSS sizes, developing

a smart management strategy to decrease the electricity cost of residential buildings. The well-known heuristic PSO approach is applied for optimal thermal and electrical storage component sizing. After determining optimal BSS and TSS sizes, MPC is applied for real-time optimal operation of smart buildings.

- Chapter 7 proposes a new business energy aggregate model to provide DSM reserve capacity. Artificial neural network is applied to forecast demand and wind and PV power generation. The model predicts trading intervals capacity requirements in each trading day. Then, the proposed control strategy minimises the RHPs power consumption to reduce IRCR. Energy aggregators can use i) the proposed RHPs coupled with TES aggregate model to provide DSM reserve capacity and consequently earn capacity credits, ii) the changing temperature set-point strategy to reduce IRCR. The proposed rebound effect reduction method is then implemented to reduce peak rebound effect.

- Chapter 8 summarises the concluding remarks of all chapters and provides suggestions for future research directions.

Chapter 2

Background and Literature Review

In this chapter, the literature on energy efficiency and DSM is reviewed. Renewable energy has an enormous impact on decreasing greenhouse gas emissions. Therefore, the Australian Government has established the Renewable Energy Target scheme to achieve the aim of increasing renewable energy [18]. The Large-scale Renewable Energy Target has been established to create a financial incentive for expanding renewable power stations such as wind and solar farms, and hydroelectric power stations. Meanwhile, the Small-scale Renewable Energy Scheme focuses on supply and demand side. The plan is to make up the partial amount of energy coming from Small-scale Renewable Energy Scheme. This scheme has been providing a financial incentive to install PV panels, wind turbines, hydro systems, solar water heaters, and heat pumps. Therefore, the major challenges would be optimal operational control and to manage energy feed-in in order to keep the system stable. Additionally, the mentioned schemes and initiatives are considered in the planning for integration of RES and flexible loads.

This chapter aims to provide a background on demand response programs and heat pump applications. The integration of heat pumps are categorised into the building level and the distribution network level. Related works for each HP application are reviewed to identify the research gaps. This chapter begins with Section 2.1 which includes an overview of microgrid and demand response programs. A discussion on HP technologies

and applications with related works are then presented in Section 2.2. In Section 2.3, the effect of thermal and electrical energy storage sizing in building level is investigated and related works are reviewed. Based on the findings of different HP applications in microgrid and identifying the existing gaps for improving the solutions, the author presents the relevant research questions for this thesis in Section 2.4.

2.1 Microgrid

Microgrid (MG) includes controllable loads, network control system, DERs, and storage devices and is designed to provide reliable and stable power for the local energy system in both connected-grid and islanded mode [19]. MG has various consumers such as residential buildings, commercial buildings and industrial loads that are supplied by local DER (PV panels, wind turbines and other generators) and energy storage system. In a microgrid, it is essential to maintain the power supply-demand balance for stability because the intermittent PVs and wind turbines are difficult to predict and their generation may fluctuate drastically based on the availability of the primary sources (e.g., solar and wind). Likewise, MG can provide better power balancing and enhance operational efficiency by controlling flexible loads like HPs and EVs [20]. This control usually comprises controller, communication system, energy management system, and demand-side management system [21].

Nanogrid (NG) is the analogous of a smart grid [22, 23] which can be connected with the rest of the grid or it can independently operate in islanded mode [22]. NG and MG are not necessarily mutually exclusive and the connection of multiple NG can form an MG. They both comprise of energy sources, not necessary but often, renewable energy storage systems and some sort of load [24]. However, there are some distinctions between NGs and MGs. They have different potential markets. A power structure of an NG can be obtained at a relatively low cost compared to MGs [23]. Moreover, NGs structure can be confined to a single home/small building , the technical objectives, hardware and software often vary from that of MGs [25, 26].

2.1.1 Energy management system

Energy management system is applied for data gathering, device control, and optimises the operation of an MG to accomplish certain operational objectives (e.g., minimise costs). It also operates power prediction from RESs, load forecasting and power planning [27]. Due to the importance of EMS in power systems, many EMS studies [27–33] have been investigated in the literature. Intermittency and variability of DER (e.g., PVs and wind turbines) and uncertainty in controllable loads complicate the MG management, which the EMS must be able to cope with. Moreover, since many devices managed by the EMS are located on the demand side, they require certain level of autonomy and local intelligence that the EMS must be able to provide.

Recently, EMS in microgrids is formulated as a real-time optimisation problem for day-ahead scheduling. Most of these studies forecast the power of the RES, the demand, and the market, which is practically difficult to achieve due to the intermittency and variability of RES, uncertainty in flexible loads, and the randomness in real-time pricing. Several models for MG optimisation have been proposed including heuristic methods such as bee colony algorithms, particle swarm optimisation and game theory [27, 30, 32]. Some approaches use stochastic programming to formulate EMS [33]. Monte Carlo simulations are also applied to generate some scenarios for EMS as a deterministic problem. Other studies [28, 29, 31] consider the energy management modeling and experimental implementation of optimal scheduling in a MG. They consider the load and the availability of power in short term and focus on how to efficiently solve the optimisation problem in real-time according to weather forecasts. Most of these studies implement MPC technique that has widely been identified as a control methodology for industrial and process applications. In this technique, constraints can be formulated which makes it highly popular for EMS.

2.1.2 Demand side management

Demand side management is a popular modification in terms of load management in order to develop better efficiency and operations in the electrical energy system [6]. The application of DSM methods has been applied to disturb the natural diversity of loads. DSM has been used to redistribute the load to reschedule operation or take advantage of

storage in the form of thermal, chemical or mechanical energy or intermediate products to continue operating during the interruptions [11]. DSM can be divided into following two groups: a) energy efficiency (EE), and b) demand response.

2.1.2.1 Energy efficiency

EE refers to methods and means for reducing the energy required in the provision of products or services, especially compared to conventional or standard approaches. There is an effective connection between EE and reducing energy demand which results in downsizing more expensive system components such as generation and storage. Also, EE helps to maintain reliability when encountering supply interruptions [34]. Often the reducing energy consumption being provided by heating, cooling. Efficient HP systems are an example of such an energy efficient technology: they require significantly less energy and maintain expected standards.

2.1.2.2 Demand response

Demand response is an adapted demand which comes either as a result of price responsiveness or to prevent any power system jeopardy [14]. DR offers the utility better utilisation of assets particularly transmission circuits which without DR, are loaded to capacity for a very short duration of the day, which is uneconomical considering the capital cost [35]. DR shows potential in its techno-economical solutions to make electricity demand more flexible which allows private customers to alter their demand profiles to fit the needs of the energy supply. In the DR programs, electric utilities provide some reward to their residential customers since they modify their energy consumption in specific time period. Furthermore, utilities provide a signal to their customers (electricity price) that are intended to steer the power consumption so as to get an aggregate demand that better matches the needs of the power generation. DR can be grouped into two categories, Price-based DR and Incentive-based DR [9].

Price-based DR Price-based DR points to customers intentionally managing energy consumption due to different prices [9]. Additionally, depending on the DR program, the price signal can be deterministic or stochastic. Price-based DR can be grouped further into a real-time DR program, critical peak pricing DR program, and TOU program. The most straightforward out of all of them is TOU, where customers are usually presented with two different price periods by utilities, specifically peak price and off peak price periods. However, even very good TOU tariffs would not obtain the majority of the efficiency benefit that would result in the use of actual real-time prices [36]. The objective is to shift the maximum amount of consumption from peak to off peak periods to achieve system efficiency, all the while giving customers financial benefits such as a reduced energy payment. Exploiting smart meter and advanced ICT infrastructure, bidirectional communication between customer and system operator is now achievable which allows customers to participate in the real time DR program. As the name suggests, the real time DR program includes power prices that reveal the actual situation of the electricity market and power system and are sent to the customer to respond. Electricity consumers are charged prices that typically rise and fall on an hourly basis and are broadcasted either day-ahead or hours ahead before the actual delivery time [37].

Incentive-based DR Incentive-based DR programs provide an opportunity for customers to gain financial rewards through changing (load increment/decrement) consumption profiles. The goal of these programs is to control the energy consumption profile at times of peak periods or critical events [9]. These programs can also be beneficial since the DR from the customer can be anticipated beforehand and thus give more flexibility to the operators in controlling the loads. However, customer preferences are violated in doing so and once in a while, even privacy is not taken into consideration. Key incentive-based DR programs include direct load control, emergency DR, interruptible rates, and demand bidding or buyback.

2.1.2.3 DSM for the residential buildings

For a long time, loads from large-scale industries have operated as reserves used for maintaining the power balance. However, the DSM is a natural opportunity in the

residential sector to increase power system operational efficiency by developing smart grid and effective ICT infrastructure [38]. Much research has focused on the potential and activation of domestic DR [17, 38, 39]. Domestic appliances can be sorted into critical appliances and flexible appliances. HPs, HVAC, electric water heater (EWH), and electric vehicles are some major flexible appliances whereas lighting and television are considered as critical appliances due to their operational characteristics. In terms of the DR program, the focus of this study will be on HP. The significant reason for choosing the HP for DR applications is because of their flexible energy consumption as well as the large influence they have on the domestic daily load profile. The goal of DR program is customer comfort which can be readily measured as compared to other appliances. The HP system is direct electric space heating/cooling (or simply HVAC) and HP integrated with thermal storage. These installations have great thermal storage capacities like the hot water tank, and so they enable the shifting of energy demand without changing the customer's comfort level.

2.2 Heat Pump

The residential sector amounts to 30-40% of total energy consumption in the world [8]. Hot water and space heating/cooling are responsible for the major amount of energy consumption in the building sector. On the other hand, a well-known equipment such as heat pump is mostly used for heating and cooling of residential buildings. HPs have an important impression on the future electric system for various reasons. First of all they are energy efficient in the production of thermal energy at domestic and commercial level. Next, they reduce the dependency on fossil fuels for individual heating demands. Heat pumps, with their thermal storage tanks, can store energy for a period of time and use the energy gradually, enabling them to operate flexibly.

HP units are largely used for keeping water and indoor temperatures at desirable level by take advantage of sources, like air, water, the ground and waste heat. Two heat exchangers, including an evaporator and another a condenser, a compressor, and an expansion device are the main components of a HP unit. The compressor pressurises the refrigerant vapour which leads to a higher temperature. The compressed refrigerant stream is condensed at high pressure which high temperature is achieved. The achieving

heat is delivered to the heat sink. Depending on the source and sink temperatures, additional energy is required for the compression process. A compressor that is driven by an electric motor is utilised for compression in residential applications [13].

There are several types of HP that are classified by heat sources like ambient air, water or ground. Air source heat pumps absorb the energy in the surrounding air and delivers it through out a building. The power consumption of this type of heat pump follows the inside temperature of the building where it is connected closely, since the delivering mechanism is through the air which has a low time constant, when compared to delivering the energy through a system of pipes in the floor. There is no means of storing energy for longer periods of time in such a system. A better approach with more flexibility is the air-water or ground-water type of heat pump system. The sink and source temperatures affect the unit efficiency as an increased temperature difference between sink and source results in a lower COP. Therefore, the COP changes throughout the year. The utilisation of the ground as a heat source for HP leads to the higher COP in comparison with air. Furthermore, air may cause frosting of the evaporator which additional energy is required for defrosting [13].

There is no dispute that the ground source heat pump has a better year-round efficiency than the air source heat pump. The ground stays warmer than the air in the winter season which means that the efficiency of the heat pump will be better. The ground source heat pump therefore has better characteristics in terms of flexible consumption in the winter time than the air-source heat pump [40]. However, the ground source heat pump system is more expensive to install than an air-source system due to digging labour costs.

Many developments in HP technology have been done recently [5, 13], which has resulted in enhancing COP. Several attempts have been made to improve the COP and energy efficiency by presenting different models [41, 42]. However, there are some challenges in system design and integration that should be revised.

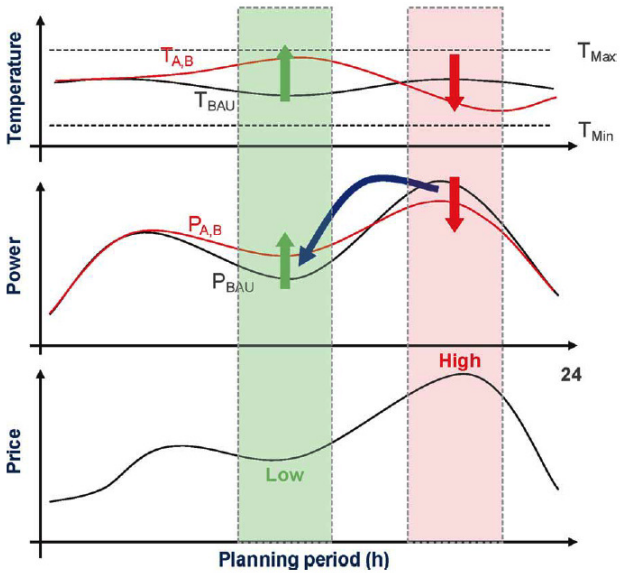

Figure 2.1: Heat pump shift load approach [35]

2.2.1 Building level integration

In residential buildings, the type of heat source and sink, heating distribution system, and thermal storage system determines the type of HP system. Frequently, water is utilised for radiator, floor heating system, and domestic hot water, whilst air is used in ventilation and heat recovery applications.

The importance of HP for DSM is because of the type of storage. Water tank, borehole thermal energy storage (BTES) and building thermal mass are thermal storages which contribute to DSM application [43]. In fact, thermal storage makes DSM possible by shifting thermal demand from high price to low price periods (Figure 2.1) [44].

Thermal storage is used as space heating/cooling and also for DHW. Reference [45] uses hot water tank and building materials for provision of flexible DR with consideration of thermal comfort. This shows the benefits of utilisation of these storage systems to reduce substantial cost through decreasing thermal discomfort for dwelling occupants.

There is a possibility of using a BTES when a GSHP integrates with solar collector as shown in [46]. It is important to note that the excess PV and wind electricity generation can convert to heat and store the heat seasonally in BTES.

Increasing the usage of RES, the reduction of cost and peak load shifting are the major objectives of wind and PV integration with HP at building level. These aims are achievable by exploiting HPs and make them respond to some signals like prices or current RES generation. The integration of PV with HP in buildings is mainly for increasing self-consumption. It is because of less attractive PV feed-in-tariffs and giving the incentives to promote self-consumption. As a result, the most economic option for PV generation is PV self-consumption where HPs can help to increase the self-consumption rate [47, 48].

2.2.1.1 Related research

Several types of distributed energy resources and controllable loads have been considered as demand response providers including plug-in electric vehicles [49, 50], various types of energy storage [51], residential electric water heaters [52], and domestic heat pumps [53]. Among domestic loads, electric devices such as heat pumps and heating, ventilating, and air conditioning systems have a significant potential to facilitate DRP [2, 38, 39, 54].

Changing temperature set-point based on real-time pricing tariffs is a potential solution for the utilisation of BTM, although considering the thermal comfort of occupants is an important constraint. The variable temperature set-point strategies presented in [2],[55] change the temperature set-point when the electricity price is higher than a threshold price which is determined based on consumers preferences. However, neither of these two strategies can considerably shift the HVAC loads. Furthermore, their simulations are not verified by experimental results. Braun [56] presented an overview of research related to the use of BTM for shifting and reducing peak cooling loads in commercial buildings based on TOU tariff. Henze et al. [57] concentrated on the usage of both BTM and TES by presenting an optimal control based on common TOU rate differentials. Kim [58] proposed a price-based DR strategy for an office building to co-optimise energy costs of HVAC units and thermal discomfort levels of occupants. In this context, day-ahead pre-cooling operation was scheduled in the early mornings to reduce peak load demand in peak-load hours based on TOU tariffs. However, real-time pre-cooling/pre-heating strategies are more effective than conventionally scheduled pre-cooling operations. In this study, the proposed DTS is designed to shift up to 100% of

HVAC loads from peak-load hours while taking advantage of a water storage tank. The temperature set-point is changed based on RTP and maximum price of electricity.

Heat pumps coupled with TES systems are mainly used to achieve efficient space heating and cooling, but in recent decades a more efficient technology, ground source heat pumps, has not only made the system more efficient, but has also been recognised as a promising technology for demand-side management [40, 59, 60]. Carvalho et al. [40] proposed a TOU strategy using a GSHP as a flexible load combined with the building thermal mass to reduce the operation costs on the customer side. The GSHP consumes electrical power in off-peak hours to pre-heat a service building. The building pre-heat method provides a 34% reduction in the electricity costs [40].

Additionally, it is more effective to develop a control strategy for heat pumps coupled with TES to respond to DRP. A building thermal energy management system based on DRP requires weather, occupancy disturbance, building thermal load, and energy price predictions to improve the building energy efficiency, load shifting and reduce total energy consumption. Among all proposed control methodologies for controlling indoor temperature, the model predictive control approach can effectively predict the future behaviour of the system to minimise energy consumption while considering thermal comfort [60–67]. Mantovani et al. [61] mostly concentrated on the thermal comfort level and energy efficiency optimisation in a commercial building using an MPC controller. However, the authors do not take advantage of pre-heating/pre-cooling for electricity cost reduction. The study by Yao et al. [63] proposed an innovative strategy to reduce peak power demand via predictive thermal energy management using an MPC-based controller. However, the authors considered a fixed temperature set-point and simulation results were not verified by experimental tests. A bi-level MPC optimisation framework for commercial buildings is proposed in [67] to integrate with a 33-node distribution grid by controlling the HVAC load to minimise building operation cost and maximise building allowable loads. However, this optimisation framework does not take advantage of a WST for peak-load shifting.

2.2.2 Distribution network level integration

Integration of HPs into a distribution grid will alter the way they are used at building level. New control strategies will be required for HP integration. However, this level of integration usually has issues with building. In grid integration, HPs provide ancillary services (AS) to the grid that can be categorised in three groups: a) voltage regulation, b) congestion management, and c) reserve power.

Voltage regulation: In LV grid, the most important problem is voltage violation. As a result, any distributed control for the LV distribution network should be a solution for this issue. To clarify this point, each consumer can adapt HP control for possible voltage regulation for their own point of connection. The references [68, 69] use DIgSILENT Power Factory to model HPs in the LV grid in order to calculate HP demand required and simulate the electric network to study the effect on local voltage. The results indicate that HPs can help coping with voltage violation.

Congestion management: Congestion may occur in transmission lines and transformers and lead to differences in the locational marginal pricing systems. Also, increasing the number of DERs and flexible loads which are integrated at the distribution level can possibly result in congestions [70, 71]. In [71], an incentive-based DR program for real-time congestion management is presented. This program is used to control the consumption of the flexible loads, i.e. the EV and the HP consumption, considering the imbalance issue and the costs of providing flexibility services.

Reserve power: In recent years, conventional fossil-fueled power plants are being replaced by decentralised RES. Subsequently, the main providers of reserve power are being changed from centralised conventional power plants to energy storage devices and flexible loads. It means that reserve power is needed even further to balance electricity generation and demand and to regulate frequency in the electric grid. HPs are currently an attractive initiative [38]. In 2016, Young-Jin Kim et al. demonstrated that a variable speed heat pump can be effectively utilised as distributed energy storage to lessen grid frequency deviation and required frequency regulation reserve capacity while ensuring

the thermal comfort of occupants [72]. Reference [38] demonstrates that the direct control approach can be exploited to provide reserve power and shows the success of this approach in a field test with 54 different heat pumps while the occupants did not experience any thermal discomfort.

2.2.3 Related works

Different methods have been implemented for integrating and controlling HPs in a smart grid. Individually, the control of HP is for supplying thermal energy to meet the thermal comfort of occupants. But this task will be extended when it integrates with RES at building level and in the distribution network and operates under time variable electricity prices. Most control approaches in this field try to achieve better results for minimising operation cost and increasing energy efficiency of the system besides optimal usage of maximum available renewable electricity generation.

The control of distributed flexible loads in distribution grids needs an aggregator to access flexibility from HPs by participating in the electricity market [38]. There are two different corresponding signals that can be described by direct load control and indirect load control. When the distributed controllable loads are directly controlled by broadcast links, it refers to direct control. When this control happens indirectly by a one-way signal that can be broadcast by a virtual power plant or an aggregator is called indirect control load [38].

Recent research focus on modern control methods that contributes to the development of predictive, adaptive and optimal control techniques. These modern techniques can achieve optimal results by handling constraints. For example, operating a HP is related to some sort of external signals so that HP should be scheduled accordingly. Hereupon, predictive methods such as MPC are the best initiatives to predict real-time signals like weather, prices, PV and wind generation and handle future disturbances like occupancy and constraints of the system [73]. Reference [61] develops an MPC technique for controlling indoor temperature in a shopping center. Several extensions based on economic optimisation and hybrid control considering external signals are investigated and include the variation of the supply water temperature, and minimising

the cost of operation based on RES tracking. However, electricity price and ambient temperature are not predicted by MPC.

Heat pumps are potential devices to provide flexibility to the power system beside supplying thermal energy to residential buildings. The need for flexibility in the power systems is becoming more and more important due to increased RES. To achieve more flexibility, optimal HP integration strategy is required to avoid wasting cost and instability in power systems. Hence, a comprehensive review is needed to achieve optimal integration.

References [74–76] developed an open-loop optimal control method for a grid-connected RES system at building level to supply the power of a heat pump water heater and other domestic loads based on TOU electricity tariff and energy cost minimisation. The case study is done for different configurations in a hotel. Reference [74] presents an optimal control strategy for a grid-connected PV system for a heat pump water heater that brings cost saving during load shifting and with consideration of TOU tariff. But this strategy is designed for a specific configuration which is not regular. To clarify this point, the battery is only charged by the grid in off-peak. Due to this, excess RE generation cannot be used for charging the battery. In [75] a diesel generator is added as a backup to the model in [74]. Although the optimal control strategy utilised the diesel generator in the peak TOU tariff to minimise energy cost, it results in increasing the initial investment cost and CO_2 emissions. Reference [76] proposed an optimal energy management strategy for wind-PV-fuel cell hybrid system in order to minimise energy cost and maximise fuel cell power output. The model indicated a daily optimal energy saving of 27.68% and a cost saving of 33.8%. These reductions in energy and cost are achieved by the optimal operation of the fuel cell as a backup and the required hot water temperature, taking into account the TOU tariff. However, this study did not consider the initial investment cost of electrolyzer and fuel cell that are still expensive and physical constraints for avoiding equipment degradation.

As shown above, studies [74–76] have only been carried out in a small number of areas. For example, indoor temperature and thermal comfort of occupants are not considered as a building thermal mass. These works developed an open-loop optimal control method to integrate heat pump water heater into RES hybrid systems. There

is a need to implement the application of close-loop techniques like MPC to reduce the uncertainties and future disturbances resulting from occupants, hot water demand, ambient temperature, solar radiation and wind velocity variations. Additionally, it is better to integrate more energy-efficient devices such as ground source heat pump into RES system in this case. These studies considered TOU tariff for DR. There is an enormous difference between even the best TOU design and RTP. It means that setting TOU rates in advance and fixing them over the hours results in missing the majority of the potential efficiency benefits of real-time energy pricing [36].

In [47], the authors have developed a rule-based strategy of energy flexibility in a house with PV for cost-optimal and PV self-consumption optimisation. The flexible sources in the system were a GSHP with an auxiliary electric resistance heater and TES, a battery and controllable appliances. A case study of a Finnish low-energy house was carried out to evaluate the impacts of the controls. As a result, electricity cost savings of 13–25%, along with 8–88% reduction in electricity exported to the grid while cost-optimal control were achieved. The HP coupled with TES and a battery were demonstrated more effective to provide flexibility than the controllable devices in the case study. However, this study did not consider the effect of forecast error by a special predictive technique like MPC which may provide a more flexible approach to system robustness. Moreover, more efficient demand management by adding other energy sources like solar and wind with a better control strategy could be fruitful to increase energy cost-savings.

A two-stage stochastic programming model was proposed and analysed in [45] to manage thermal energy storage in the form of hot water storage and building mass at residential level in order to reduce cost. Day-ahead DR optimisation was conducted considering the high degree of uncertainties, including ambient temperature, electricity and hot water consumption, occupant movement, and imbalance prices. The authors developed a new expected thermal discomfort for more efficient utilisation of flexibility and determination of consumption for lost comfort in DR contracts. The presented case study, of a portfolio of 50 residential flats with 5 aggregation cases (various combined heat and power and air source heat pumps) indicated a cost reduction while decreasing the expected thermal discomfort. Although this study illustrated a significant cost reduction by focusing on thermal energy storage and penalised thermal comfort, an optimal thermal management with RES integration was not developed.

2.3 Energy Storage System

The installed capacity of PVs has significantly increased in recent years. The PV system is one of the top-ranked renewable resources in many countries including USA, China, Japan, India, and Australia. In 2017, the global installed (on-grid and off-grid) PV capacity reached 98 GW which was nearly one-third of the total 402 GW load [77]. However, the renewable energy buyback rate is expected to significantly drop in the near future. This buyback price reduction is due to power system challenges, such as frequency regulation, reverse power and voltage imbalance issues which are caused by high PV penetration. A potential solution that may be beneficial for both end-users and utilities is to increase PV self-consumption. This can be efficiently achieved using energy storage systems and residential flexible loads such as heat pumps and electric vehicles [39, 78]. Energy storage systems are frequently being applied to minimise various issues of RES-penetrated power networks. A comprehensive review of various energy storage systems is presented in [51].

Accordingly, residential customers can reduce their electricity costs by capitalising their dispatched power. This can be done by i) optimising the capacities of renewable energy resources and energy storage systems, ii) utilising HPs and heating, ventilation, and air conditioning systems coupled with thermal energy storage systems and, iii) implementing demand response programs to spread the HP load throughout the day based on electricity price tariffs and the availability of RESs [79, 80]. In Australia, residential end-users have moved to install rooftop PV systems to reduce electricity bills. However, they still have to pay for electricity due to high electricity prices during peak-load hours when PV production is not sufficient. A practical solution is to implement demand response programs, flexible loads, and energy storage systems to take full advantage of PV power production.

Electrochemical storage systems (e.g., Lead-acid and Li-ion batteries) have limitations including short lifespan, limited number of cycles, and high initial cost that make them unaffordable for most applications [81]. Comparatively, thermal storage systems and pumped-hydro storage systems [82, 83] are eco-friendly options that can provide more sustainable solutions. More importantly, TSSs make HVAC systems flexible with suitable responses to time-varying electricity prices. Hence, a combination of TSSs and

electrical storage systems could provide a more economical and eco-friendly solution compared to utilisation of only electrical storage systems. Therefore, the motivation of this study is to provide a low-cost solution to end-users with a low environmental impact using TSSs and battery storage systems for energy management applications.

2.3.1 Related works

Many researchers have focused on finding optimal component sizes of RES and storage systems for smart buildings. Some papers have applied flat electricity tariffs or average load as input data to find optimal sizes of RESs and electrical energy storage [84, 85]. Most publications rely on simple charging algorithms [86, 87]. Recent research has considered optimal battery charging and discharging in their sizing strategies. However, the effect of flexible loads such as HPs and HVAC systems on RES and BSS sizes as well as PV self-consumption have not been investigated.

Thermal energy storage such as building thermal mass and thermal storage tanks are broadly identified as effective means of shifting loads from peak to off-peak hours in buildings [45, 56, 57, 88–92]. End-users can gain additional cost-saving advantages from TES by implementing DRP and spread the heat pump load throughout the day based on time-varying electricity prices during peak and off-peak hours [88]. Shah et al. [90] presented an optimal DR algorithm to reduce the electrical water heating costs based on time-of-use tariff by taking advantage of TES while considering hot water consumption for 24 hours. Good et al. [45] focused on a day-ahead optimisation to provide more flexibility for the power system by utilising TES of hot water and building thermal mass of 50 residential flats while determining the expected energy and discomfort costs.

In [93], a stochastic approach based on a Monte Carlo simulation (MCS) and particle swarm optimisation was proposed for sizing a smart household energy system, taking into account the demand uncertainty. A convex programming method for finding optimal size and control of energy in smart homes, with PV generation and battery storage has been introduced in [94]. This structure is employed for three different buildings in California and Texas. The optimal size and control are investigated over several time horizons, considering maximum power exportation to the grid, BSS cost, and load demand patterns. In [95], the authors used a mixed integer non-linear programming

method to perform optimal size and operation of the battery storage system for a smart home. In [96], mixed-integer linear programming (MILP) was implemented to find the optimal battery and PV sizes for a determined location considering both demand and time-of-use tariff. Another MILP was also applied to optimally schedule the PV-battery system, with the aim of reducing electricity bills. However, the effect of flexible loads such as HPs and HVAC systems on RES and BSS sizes were not considered in the aforementioned studies.

In [97], an MILP framework was applied to quantify the required battery capacity. However, the solution depends on different DR-based load patterns. The sizing and analysis of renewable energy and BSSs were introduced in [98]. A hybrid model was proposed using MILP to maximise the use of renewable energy and reduce load demand on the grid. Weather prediction was used to determine the optimal size of the wind turbine as well as the thermal load and PV profiles for a residential building. The aforementioned literature presents useful backgrounds; however, the effect of thermal energy storage sizing on battery size in smart buildings has not been considered in these publications.

The effects of different electricity pricing tariffs on PV and electrical energy storage systems are investigated in [99]. In their work, the profitability and sizing of a PV system with a battery are analysed from an economic perspective for residential buildings. However, the effect of DRPs is not considered in the sizing of components. The authors [100] have developed an MILP model for the optimal sizing and operation of HP based building energy systems. Their analysis demonstrated that the size of the HP is slightly affected by the scenario assumptions, while the optimal sizing of PV significantly depends on load profiles. However, the effect of flexible HP coupled with TSS on the dimension of BSS has not been considered. An MILP algorithm is introduced in [101]. This algorithm is presented to find the optimal size and operation of electric boiler and thermal storage in combination with a PV system. A considerable storage size was only obtained during the large fluctuation in electricity prices or by using the large PV size. The authors [102] investigate the parameters that affect the optimal size of BSS for grid-connected PV systems. The subject was to improve the self-consumption of PV systems by determining the battery size based on electricity tariffs, and battery performance and price. The battery size was largely affected by feed-in electricity price. Similarly, the

pricing structure is applied to find the optimal size of PV and BSS systems of a smart house in [103].

Boeckl et al., [104] have presented a technical consideration sizing method to design PV and battery systems for different households. This paper considers different household load profiles based on a behaviour model and life patterns of different end-users in a stochastic method. However, considering DR is crucial to design a PV battery system which has been ignored in aforementioned paper. Another work [105] presented an analytical strategy for sizing battery storage based on minimising energy cost for a battery storage owner. This paper developed a simple analytical method to size battery for peak-load shaving. However, DRPs are already practical by developing smart meters. Therefore, controlling HVAC systems as the devices that consume the most power in residential buildings is important to consider for designing a battery. The sizing of rooftop PV systems with HPs and BSS with the focus on changing economics and regulatory is evaluated in [106]. In [107], the authors presented an optimisation model to investigate the effect of HPs on the size of a PV system with BSS. The results showed that HPs as shiftable loads are required to avoid under-sizing of PV systems. However, the effect of HPs coupled with TSS on BSS size has been ignored. An interesting research on electrical and heating components sizing is presented in [108]. The authors have applied forecast-based operation approaches for PV-battery and power-to-heat systems to improve economics of the house. The results show reduction in levelised costs of electricity compared to a self-consumption maximising strategy. In [109], the authors have investigated the effects of thermal and electrical loads, TSS, EV, and power sharing among neighbours on PV system sizing for residential buildings. A genetic algorithm is adapted to optimise: i) the quantity of PV capacity installed on each facade of the building, and ii) the size of electric storage to increase PV self-consumption when the system is profitable. An optimisation design strategy is provided in [110] for implementing building-integrated PV with electricity storage in the early conceptual and preliminary design process of a building. The method optimises the size and positions of the PV panels and size of the BSS to enhance the net present value of the whole system during the project lifetime. However, the effects of load management and thermal storage have not been considered to attain high PV self-consumption rates. Furthermore, the impacts of HP load management on the capacity design of TSS and BSS are not included in the aforementioned studies.

2.4 Research Questions

On the basis of the findings and challenges as identified through the above literature survey, the present research is carried out by addressing following research questions (RQs):

- RQ1: How to introduce a framework for GSHP load management considering real-time electricity tariff and thermal comfort to increase energy efficiency and peak-load shifting? How this framework allows the occupants to select system operation to reduce the cost or achieve the best thermal preference? How the optimisation results can be validated through the experimental tests?
- RQ2: How to develop an optimisation approach for scheduling the operation of HP integrated with PV system to minimise the customer's energy expenses and increase PV self-consumption? How much PV self-consumption and electricity costs can be improved when a battery added to HP-PV system?
- RQ3: How to develop an optimal sizing design of battery and thermal energy storage to minimise annual electricity costs of smart buildings with rooftop PVs while minimising life cycle cost? How much economic benefits can be achieved through sizing of i) thermal energy storage, ii) battery, and iii) thermal energy storage and battery for rooftop PV owners? How to develop a real-time smart building energy management system based on real-time pricing tariff to reduce the operation costs?
- RQ4: How to present a business energy aggregate model for residential HPs to allow energy aggregators or retailers participate in reserve capacity market by providing demand side management reserve capacity? How to establish a dynamic aggregate model of residential heat pumps coupled with thermal energy storage systems and proposing an optimisation control strategy based on the RHPs aggregate model? How to reduce the rebound effect when changing the temperature set-point of RHPs?

Chapter 3

Optimal Real-Time Residential Thermal Energy Management for Peak-Load Shifting

This chapter addresses the research question RQ1 and proposes an optimal real-time thermal energy management system (TEMS) for smart homes to respond to DRP for peak-load shifting [1]. The proposed TEMS combines two model predictive controllers to manage two thermal energy storage systems, a water storage tank and the building thermal mass, to schedule residential heat pump loads to off-peak periods. The intention is to manage the operation of a ground source heat pump to produce the desired amount of thermal energy by controlling the volume and temperature of the stored water in the WST while optimising the operation of the heat distributors to control indoor temperature. The key contributions are the development of a new control strategy for GSHPs coupled with WST based on building identification to minimise total energy consumption and cost. This chapter also proposes a real-time indoor dynamic temperature set-point strategy based on real-time pricing tariffs for enhancing peak-load shifting of heat pump loads with an acceptable variation in thermal comfort. Simulation and

[1] The presented chapter has been published as: **A. Baniasadi**, D. Habibi, O. Bass and M. A. S. Masoum, "Optimal Real-Time Residential Thermal Energy Management for Peak-Load Shifting With Experimental Verification," in **IEEE Transactions on Smart Grid**, vol. 10, no. 5, pp. 5587-5599, Sept. 2019. doi: 10.1109/TSG.2018.2887232

experimental results demonstrate that the proposed TEMS has significant potential for real-time peak-load shifting.

3.1 Introduction

The growing penetration of renewable energy resources in power systems increases the risk of physical infrastructure damage to conventional generators. This infrastructure damage arises because the intermittent nature of RES causes rapid ramps in power generation to supply demand during peak-load hours. On the other hand, the growing demand for power in buildings, during peak-load hours in particular, boosts the need for load-shifting. Therefore, the need for flexibility is a crucial issue on the demand side. Flexible loads and decentralised energy storage can support RES to maintain the balance between demand and supply [39, 111, 112]. These elements also enable consumers to participate in demand response programs in residential and commercial buildings [54].

This chapter focuses on a new building pre-cooling/pre-heating system using a real-time dynamic temperature set-points strategy. The implementation of a new comprehensive control strategy based on DTS supports the full advantage of BTM to make the system more flexible. The system includes a GSHP, a water storage tank and two fan coil units. The WST is used to store chilled/hot water produced by the GSHP and deliver it when needed. The presence of the WST allows the GSHP to efficiently operate whenever the electrical energy prices are low.

The main contributions of this chapter are summarised as follows.

- An enhanced optimal real-time thermal energy management system for smart buildings is developed to respond to DRP by employing two thermal storage systems (WST and BTM) for peak-load shifting while improving the efficiency and keeping the temperature within a desirable thermal comfort zone.
- A real-time DTS strategy based on real-time pricing (RTP) tariffs is developed to improve the efficiency of smart building by shifting up to 100% of HVAC loads from peak-load hours. The proposed cost-aware DTS allows the occupants to select system operation to reduce the cost or achieve the best thermal preference.

- Experimental verification of the proposed TEMS is undertaken to reduce power consumption of the GSHP and FCU with load shifting. In particular, the TEMS responds more effectively to DRP compared with the controller presented in [2].

3.2 System Modelling and Identification

3.2.1 System description

Figure 3.1 shows the thermal energy system installed in the Smart Energy Laboratory (SELAB) at Edith Cowan University (ECU), Joondalup, Western Australia. It consists of a GSHP with an electrical ground circulation pump (Pump1), a WST, two electrical circulation pumps (Pump2 and Pump3), and FCUs. The schematic of this system is shown in Figure 3.2. The chilled/hot water is produced by the GSHP and stored in the WST. The water is distributed to the laboratory building via the FCUs and the heat exchanged water is then returned to the WST.

Figure 3.3 presents the two main control loops used to manage the building heating/cooling system. The proposed MPC of Section III is implemented by these two control loops. The FCU loop controls the fan speed to control building temperature while considering thermal comfort. The GSHP loop is responsible for controlling the temperature and the volume of stored water in the WST based on electricity tariffs. The GSHP loop helps to increase peak-load shifting while supplying enough chilled/hot water for the thermal load.

The thermal system is monitored by LabVIEW software. The controllers are implemented in the MATLAB environment. Data is transferred between MATLAB and LabVIEW over a TCP/IP connection in order to modify the set-points.

3.2.2 SELAB building thermal model

The SELAB building is modeled by the heat dynamic state-space model proposed in [64] and [113]:

$$\begin{bmatrix} \dot{T}_l \\ \dot{T}_{in} \end{bmatrix} = \begin{bmatrix} -\frac{1}{R_{in} \cdot C_l} & \frac{1}{R_{in} \cdot C_l} \\ \frac{1}{R_{in} \cdot C_{in}} & -(\frac{1}{R_{io} \cdot C_{in}} + \frac{1}{R_{il} \cdot C_{in}}) \end{bmatrix} \begin{bmatrix} T_l \\ T_{in} \end{bmatrix} + \begin{bmatrix} 0 \\ \frac{1}{C_{in}} \end{bmatrix} Q_f + \begin{bmatrix} 0 & 0 & 0 \\ \frac{1}{R_{io} \cdot C_{in}} & \frac{\lambda}{C_{in}} & \frac{1}{C_{in}} \end{bmatrix} \begin{bmatrix} T_o \\ S_r \\ I_g \end{bmatrix} \tag{3.1}$$

It is assumed that T_{af} is fixed and the thermal energy rate that is delivered to the SELAB by the FCU is given by $Q_f = \dot{m}_{af} c_{ap} (T_{af} - T_{in})$. Therefore, the discrete control input is denoted by $\mathbf{U} = \dot{m}_{af}$. If the state and disturbance vectors are denoted by $\mathbf{X} = [T_l \ T_{in}]^\intercal$ and $\mathbf{V} = [T_o \ S_r \ I_g]^\intercal$, then the discrete-time state space model can be represented by

$$\mathbf{X}(k+1) = A\mathbf{X}(k) + B\mathbf{U}(k) + D\mathbf{V}(k) \tag{3.2}$$

where the matrices A, B and D are defined as

$$A = \begin{bmatrix} A_{11} & A_{12} \\ A_{21} & A_{22} \end{bmatrix}, B = \begin{bmatrix} 0 & B_1 \end{bmatrix}^\intercal, D = \begin{bmatrix} 0 & 0 & 0 \\ D_1 & D_2 & D_3 \end{bmatrix} \tag{3.3}$$

These matrices are identified using a nonlinear regression algorithm [113] by measuring $T_{in}(k)$, $T_o(k)$, $S_r(k)$, $I_g(k)$, and $Q_f(k)$. According to the conservation of energy, the heat transfer in the FCU is defined as $Q_{f_1}(k) = \dot{m}_f c_p (T_f(k) - T_{fr}(k))$ which is equal to $Q_f(k)$. Therefore, by measuring $\dot{m}_f$, $T_f(k)$ and $T_{fr}(k)$, then $Q_f(k)$ can be calculated.

The SELAB building thermal model is identified and validated via two tests:

- Test I - The HVAC system is activated and the indoor temperature is measured. Figure 3.7 shows the $T_f(k)$ and $T_{fr}(k)$ measurements. Note that $\dot{m}_f$ is constant and equal to 10 l/min. Therefore, $Q_f(k)$ is calculated as an input for this test. In addition, Figure 3.5 presents the measurements of ambient temperature and solar irradiation as the data set for the identification of the thermal model of SELAB building. In this test, a low pass filter (LPF) is implemented to reduce the noise associated with the temperature sensor. Note the fine agreements of modelled and

Table 3.1: Parameters of identified SELAB building model.

$A_{11} = 0.9641$	$A_{12} = 0.0205$	$B_1 = 0.3966$	$D_1 = 5.212 \cdot 10^{-2}$
$A_{21} = 0.1362$	$A_{22} = 0.9028$	$D_2 = 2.656 \cdot 10^{-3}$	$D_3 = 4.474 \cdot 10^{-4}$

measured daily indoor temperatures shown in Figure 3.6. The root mean square error (RMSE) of the model is 0.284°C and the coefficient of variation of RMSE (CV(RMSE)) index is 2.52%. CV(RMSE) determines the accuracy of a model by considering offsetting measured and simulated data errors [114]. ASHRAE Guide 14 [114] considers a building model calibrated if the hourly CV(RMSE) values are under 30%. Table 6.3 presents the identified building model parameters based on Test I results.

- Test II - The HVAC system is off ($Q_f = 0$). Figure 3.8a shows the measured solar irradiation and ambient temperature for 7 days. The validation result is presented in Figure 3.8b. The RMSE of the model is 0.288°C and CV(RMSE) index is 3.57%.

3.2.3 Ground source heat pump model

GSHPs utilise the relatively constant ground temperature to warm the system's circulating liquid in winter, and cool it in summer for space heating and cooling, and domestic hot water applications [53]. The installed GSHP at the SELAB building manipulates three boreholes to exploit a higher quality source of heat as shown in Figures 3.1-3.2. Pump 1 circulates water through tubes in the boreholes. The GSHP is directly connected to the WST. The GSHP only operates in on and off modes.

The performance of the GSHP is heavily dependent on the temperature difference (ΔT) between the source side and the load side of the GSHP. ΔT is the difference between the temperature of the water returned (from the boreholes) $T_{b,out}$ (monitored by LabVIEW) and the GSHP output water temperature T_{GHP}. The heating/cooling capacity can then be obtained based on the flow rates and temperatures on the source side and the load side. Therefore, the coefficient of performance (COP) is expressed by [53]:

$$\text{COP} = \frac{Q_{GHP}}{W_{GHP}} \tag{3.4}$$

Figure 3.1: Thermal energy system installed in the Smart Energy Laboratory (SELAB) at Edith Cowan University (ECU), Western Australia.

An ideal borehole heat exchanger is considered and hence, Q_{GHP} is determined based on the compressor power consumption while utilising the heat taken (given) from (to) the ground (Q_{ex}). In this chapter, it is assumed that the GSHP operates in the cooling mode and hence, when the GSHP is running, it generates chilled water at a determined mass flow rate. Therefore, according to the conservation of energy for the cooling mode

$$|Q_{GHP}|+W_{GHP} = |Q_{ex}| \tag{3.5}$$

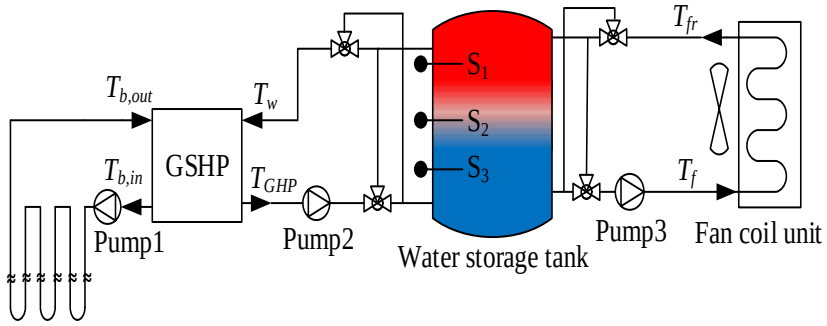

Figure 3.2: Schematic of the thermal energy system.

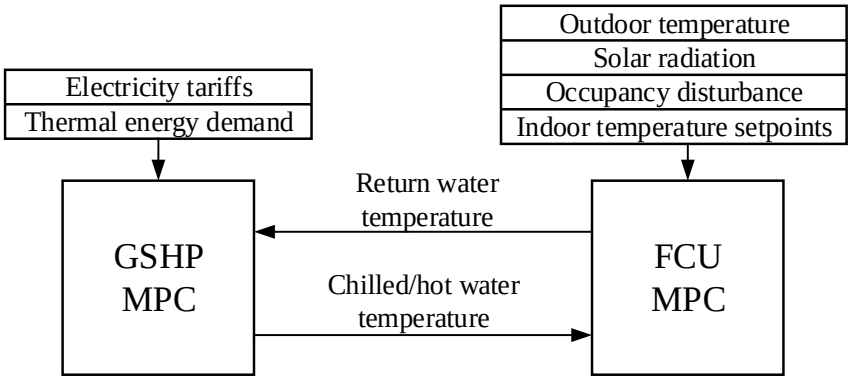

Figure 3.3: Control system.

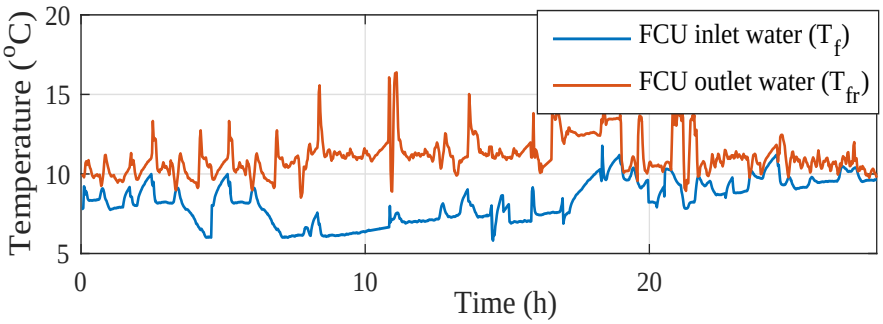

Figure 3.4: FCU inlet and outlet water temperature

$$Q_{ex} = \dot{m}_{ex} c_p (T_{b,out} - T_{b,in}) \tag{3.6}$$

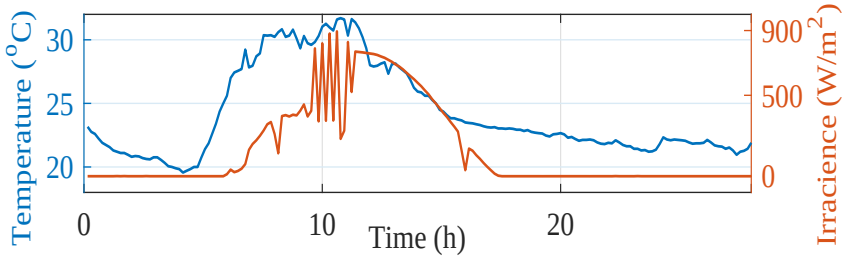

Figure 3.5: Ambient temperature and solar irradiation data set for Test I

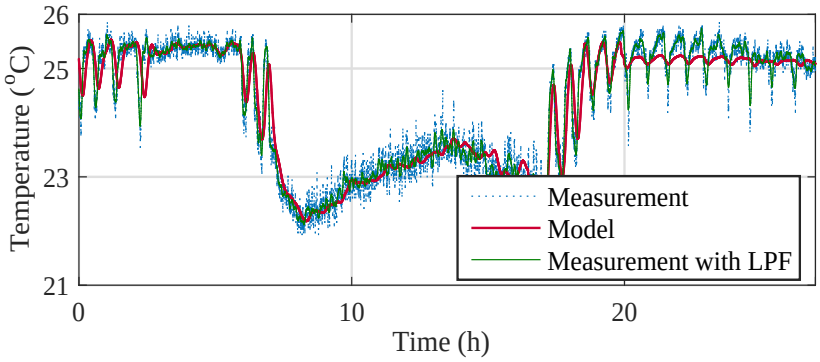

Figure 3.6: Indoor temperature

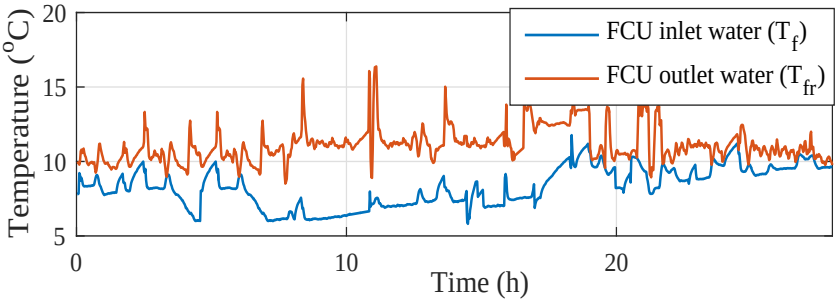

Figure 3.7: FCU inlet and outlet water temperature

3.2.4 Water storage tank model

The installed WST is modelled based on the stratified two-layer tank separated by a thermocline layer that is developed in [65, 115] and is validated with the collected data from SELAB. The WST is used for both heating and cooling modes. Nonetheless, the WST is modelled in cooling mode for making it easy to explain. Hence, in the following section, the attention is on the height and temperature of stored chilled water at the

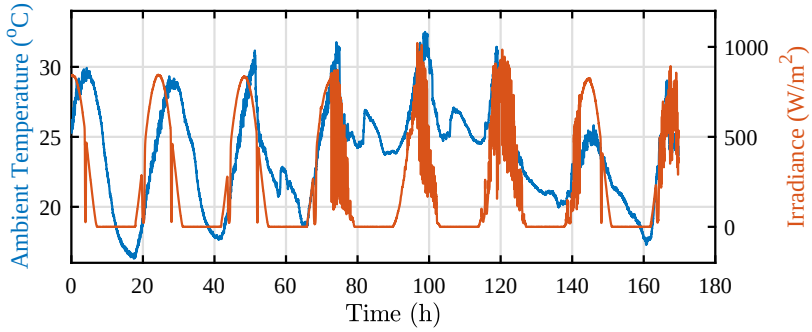

(a) Ambient temperature and solar irradiation data set for Test II

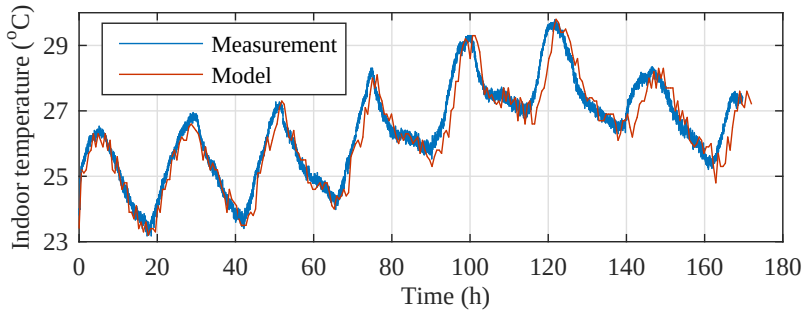

(b) Indoor temperature

Figure 3.8: Test II results- validation of SELAB building model.

bottom of the WST. In cooling mode, the circulation water map is: return water from FCU at the top at the temperature T_w and chilled water produced by GSHP at the bottom at the temperature T_c. As the WST is connected to the closed-loop system, the volume of stored water m_t is always constant and equal to the sum of the volume of return water m_w and chilled water m_c

$$m_t = m_c + m_w, \quad m_c = \rho\pi D^2 h_c/4 \tag{3.7}$$

where h_c is the height of the stored chilled water, D is the diameter of the WST and ρ is the density of the chilled water.

Note that the mass water flow rates for both sides of the thermal system (for the GSHP ($\dot{m}_{GHP}$) and for the FCU ($\dot{m}_f$)) are constant and $\dot{m}_{GHP} > \dot{m}_f$. Therefore, the chilled water is stored in the WST when the GSHP is on; otherwise, the WST discharges. The dynamics of the system can be described by the change in the volume (m_c) and

temperature of the chilled water layer (T_c) in the stratified WST. Therefore, the WST model based on the heat and mass flow balance concept is expressed by the following first order non-linear differential equation:

$$\frac{\mathrm{d}Q_c}{\mathrm{d}t}(m_c,T_c) = Q_c^{in} - Q_c^{out} = \dot{m}_{GHP} c_p T_{GHP} - \dot{m}_f c_p T_f \tag{3.8}$$

$$\frac{\mathrm{d}m_c}{\mathrm{d}t} = \dot{m}_{GHP} - \dot{m}_f \tag{3.9}$$

The WST is charged since the GSHP is operating. It is because of constant rates of mass water flow and $\dot{m}_{GHP} > \dot{m}_f$. In addition, the model is simplified by neglecting the losses to the surrounding environment, hence, it can be assumed $T_f = T_{GHP}$. Therefore, the heat flow Equation (3.8) can be rewritten as

$$\frac{\mathrm{d}Q_c}{\mathrm{d}t}(m_c,T_c) = \frac{\mathrm{d}m_c}{\mathrm{d}t} \cdot T_c + m_c \cdot \frac{\mathrm{d}T_c}{\mathrm{d}t} = (\dot{m}_{GHP} - \dot{m}_f) T_{GHP} \tag{3.10}$$

The derivative of temperature and the derivative of height of the bottom layer water at each time step can be expressed as

$$\frac{\mathrm{d}T_c}{\mathrm{d}t} = \frac{(\dot{m}_{GHP} - \dot{m}_f)(T_{GHP} - T_c)}{m_c} \tag{3.11}$$

$$\frac{\mathrm{d}h_c}{\mathrm{d}t} = \frac{4(\dot{m}_{GHP} - \dot{m}_f)}{\rho \pi D^2} \tag{3.12}$$

When the GSHP is off ($\dot{m}_{GHP} = 0$), the WST is discharged. Hence, the inlet water temperature of FCU is equal to the temperature at the bottom layer of the WST $T_f = T_c$.

3.2.5 Fan coil units model

The installed FCU at the SELAB building is modelled using the data-driven effectiveness ε-NTU method which is presented in [116] and is developed in [61]. In this method, the return air temperature from the heat exchanger (T_{af}) is ideally equal to the inlet water temperature of the heat exchanger (T_f). The equation of an ideal infinite-length FCU assuming $\dot{m}_f c_p > \dot{m}_{af} c_{ap}$ is:

$$Q_{f,ideal} = \dot{m}_{af} c_{ap} (T_f - T_{in}) \tag{3.13}$$

Therefore, the FCU can be practically modelled as follows:

$$Q_f = \varepsilon(\mathbb{C}, \text{NTU}) \cdot Q_{f,ideal} \tag{3.14}$$

$$\mathbb{C} = \frac{\dot{m}_f c_p}{\dot{m}_{af} c_{ap}}, \quad \text{NTU} = \frac{UA}{\dot{m}_{af} c_{ap}} \tag{3.15}$$

where UA and ε are heat transfer coefficient and effectiveness, respectively. UA is a function of air flow rate $\dot{m}_{af}$ and water flow rate $\dot{m}_f$. $\dot{m}_f$ is considered constant to avoid solving complex equations.

On the other hand, the FCU-MPC requires a steady-state fan model to obtain the fan power. A third-order polynomial regression equation can approximate the electric power of the fans. Since the electric power of the FCU is a function of the total supplied air mass flow rate, the fan power model can be given by

$$P_f = \alpha_3 \dot{m}_{af}^3 + \alpha_2 \dot{m}_{af}^2 + \alpha_1 \dot{m}_{af} + \alpha_0 \tag{3.16}$$

where α_0, α_1, α_2, α_3 are fan model parameters that are identified by measuring P_f while changing the fan speed. The parameters are given as follows: $\alpha_0 = 26.506$, $\alpha_1 = 244.757$, $\alpha_2 = -101.974$, and $\alpha_3 = 37.659$.

3.3 Formulation of Proposed TEMS Based on System Identification

The system model is used to formulate and implement the proposed TEMS that includes MPCs based on a new DTS strategy for FCU and GSHP coupled with WST. The flowchart of the proposed TEMS is shown in Figure 3.9.

3.3.1 Proposed dynamic temperature set-point based on RTP

Variable indoor temperature set-point T_d enables the DRP to effectively utilise the building pre-cooling/pre-heating. Since DTS will also affect the GSHP control, the optimal DTS should be determined prior to the GSHP control. To shift FCU load while maintaining indoor temperature within thermal comfort limits, an hourly model

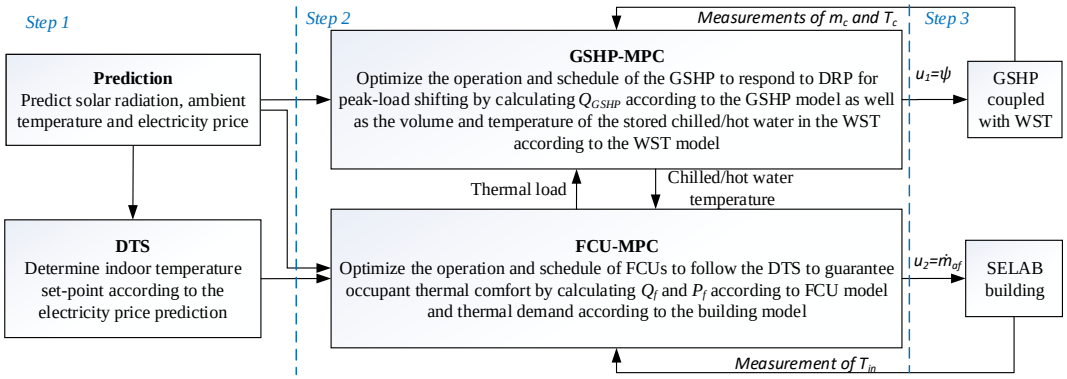

Figure 3.9: Flowchart diagram for the implementation of the proposed optimal real-time thermal energy management system for smart homes to respond to DRP for peak-load shifting.

is designed for both cooling and heating modes based on dynamic electricity pricing as follows:

$$\frac{T(i) - \underline{T}_{sp}}{\overline{T}_{sp} - \underline{T}_{sp}} = \frac{\mathcal{Z}(i) - \mathcal{Z}_{min}}{\mathcal{Z}_{max} - \mathcal{Z}_{min}} \tag{3.17}$$

$$\delta(i) = \beta\left(\frac{T(i) - T_{sp}}{T_{sp} - \underline{T}_{sp}}\right) \quad \forall i = 1, 2, \ldots, 24 \tag{3.18}$$

The indoor temperature is normalised based on RTP tariff and upper and lower boundaries of T_{sp} in Equation (3.17). The temperature difference from T_{sp} ($\delta(i)$) is determined in Equation (3.18) and β is an impact coefficient which changes the intensity of DTS. β is considered to reflect customer's preference in reducing the cost or choosing more desirable thermal comfort. The DTS responds to the price fluctuation and remains indoor temperature at the comfort zone at both cooling and heating modes.

T_d in the cooling mode is given by

$$T_d(i) = \begin{cases} T_{sp} - \delta_{max}, & \text{if } \delta(i) < 0.75\delta_{max} \\ & \quad \text{and } \delta(i+1) > 0.75\delta_{max} \\ T_{sp} + \delta(i), & \text{otherwise.} \end{cases} \tag{3.19}$$

T_d in the heating mode is given by

$$T_d(i) = \begin{cases} T_{sp} + \delta_{max}, & \text{if } \delta(i) < 0.75\delta_{max} \\ & \quad \text{and } \delta(i+1) > 0.75\delta_{max} \\ T_{sp} - \delta(i), & \text{otherwise.} \end{cases} \tag{3.20}$$

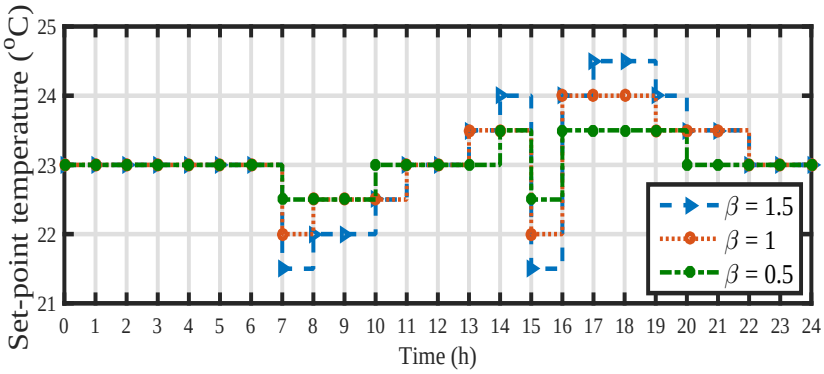

Figure 3.10: Temperature set-points for different β values in discrete step of 0.5 °C.

$$\underline{T}_{sp} \leq T_d \leq \overline{T}_{sp} \tag{3.21}$$

$$0 \leq \beta \leq T_{sp} - \underline{T}_{sp} \tag{3.22}$$

where δ_{max} corresponds to the condition $T_d = \overline{T}_{sp}$. $\delta > 0.75\delta_{max}$ indicates the peak-load hours based on RTP. β can be changed based on Equation (3.22). For example, lower β increases thermal comfort while higher β results in more energy saving. Figure 3.10 shows the indoor temperature set-points for 24 hours with discrete steps of 0.5 °C generated by the proposed DTS strategy based on the RTP tariff of Figure 3.11, for cooling mode. Note that, the DTSs are established between 7 am and 10 pm. Figure 3.10 shows that the proposed DTS pre-cools the building during low price periods (7 am-11 am) and before the peak price hours (3 pm-4 pm) (BTM charging mode) and DTS increases the temperature set-point during high price periods and peak-load hours (BTM discharging mode).

The impacts of various β will be examined on energy consumption and peak-load shifting by establishing a lower indoor temperature set-point during low-price tariff periods. During higher price periods, the building pre-cooling can supply space cooling and the FCU will be off. As a result, the GSHP will be off and the GSHP and FCU loads will be shifted by taking advantage of the building pre-cooling without violating the thermal comfort limits.

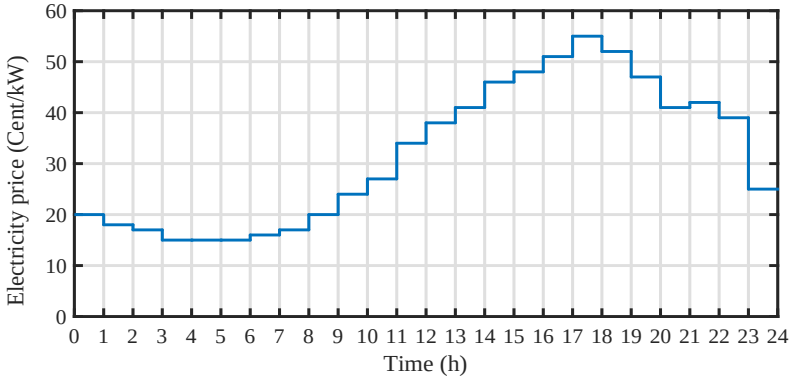

Figure 3.11: Hourly electricity price profile from AEMO [1].

3.4 Objective function

Two optimal controllers are required to find the optimal thermal energy system operation. One optimal control is to switch the GSHP on/off based on DRP to minimize the GSHP power consumption while producing sufficient chilled water. Another optimal control is applied to control the fan speed to minimise electrical and thermal energy consumption while keeping the indoor temperature within a desirable comfort range. The objective function of GSHP optimisation is to minimise electricity costs of GSHP subject to WST constraints. In this study, the objective function of GSHP optimization can be expressed as follows:

$$\min \quad \sum_{i} C_d \tag{3.23}$$

subject to

$$T_c^{min} \leq T_c \leq T_c^{max} \tag{3.24}$$

$$m_c^{min} \leq m_c \leq m_c^{max} \tag{3.25}$$

where C_d is the electricity cost. The volume and temperature of stored chilled water are limited based on the water capacity of WST and the requested temperature range by FCU, respectively. The objective function of FCU optimisation is to optimise the operation of FCU to minimise electrical energy consumption and minimise the deviation of indoor temperature from temperature set-points subject to indoor temperature

constraints. The objective function is:

$$\min \quad \sum_i P_f + \sum_i T_{in} - T_d \tag{3.26}$$

subject to

$$T_{in}^{min} \leq T_{in} \leq T_{in}^{max}, \tag{3.27}$$

$$\underline{T}_{sp} \leq T_d \leq \overline{T}_{sp} \tag{3.28}$$

3.5 MPC scheme with proposed DTS

The MPC uses the system model to predict the future evolution of the plant to generate the control action on receding control strategy [65, 66]. Two MPC controllers are established in this chapter.

GSHP-MPC The goal of this controller is to switch the GSHP on/off in order to shift GSHP power consumption based on DRP while producing sufficient chilled water. For this purpose, a cost function is designed for the MPC of GSHP based on RTP tariffs. The objective function of the GSHP-MPC is a trade-off between minimising the total electricity cost and producing enough chilled water subject to dynamic constraints:

$$\min_{u_{1k}} \quad \sum_{j=k}^{k+N-1} (\mathcal{Z}(j|k)(\psi(j|k)) \tag{3.29}$$

subject to

$$x_1(j+1|k) = f_1(x_1(j|k), u_1(j|k), d_1(j|k)), \quad \forall j = k, k+1, \ldots, k+N-1 \tag{3.30}$$

$$y_1(j|k) = g_1(x_1(j|k), u_1(j|k), d_1(j|k)), \quad \forall j = k, k+1, \ldots, k+N \tag{3.31}$$

where N is the prediction horizon, k is an arbitrary starting point in the vector. $\mathcal{Z}$ is the electricity tariff at time step j, ψ is the binary decision variable $u_1 = \{\psi\}$ while state

variable is $x_1 = \{m_c, T_c\}$ and disturbance is $d_1 = \{\dot{m}_f\}$. ψ is defined by

$$\psi(j) = \begin{cases} 1, & \text{if the GSHP is on} \\ 0, & \text{otherwise.} \end{cases} \tag{3.32}$$

The GSHP dynamic Equations (3.4)-(3.6) and the WST dynamic Equations (3.7)-(3.11) are the main dynamics of the GSHP system while Equation (3.30) relates to the WST dynamic and Equation (3.31) includes the GSHP dynamic.

FCU-MPC The objective of this controller is to control the fan speed to minimise electrical and thermal energy consumption while keeping the indoor temperature within a desirable comfort range. The objective function of FCU-MPC is a trade-off between minimising total energy consumption and minimising the deviation of indoor temperature from the temperature set-point subject to dynamic constraints:

$$\min_{u_{2,k}} \quad \sum_{j=k}^{k+N-1} (P_f(j|k)) + \sum_{j=k}^{k+N-1} (T_{in}(j|k) - T_d(j|k)) \tag{3.33}$$

subject to

$$x_2(j+1|k) = f_2(x_2(j|k), u_2(j|k), d_2(j|k)), \quad \forall j = k, k+1, \ldots, k+N-1 \tag{3.34}$$

$$y_2(j|k) = g_2(x_2(j|k), u_2(j|k), d_2(j|k)), \quad \forall j = k, k+1, \ldots, k+N \tag{3.35}$$

where decision variable $u_2 = \{\dot{m}_{af}\}$, state variable $x_2 = \{T_{in}\}$, and disturbances $d_2 = \{T_o, S_r, P_{hl}\}$. The building dynamic Equations (3.1)-(3.3) and the FCU dynamic Equations (3.13)-(3.16) are the main dynamics of the FCU-MPC while Equation (3.34) corresponds to the building dynamic and Equation (3.35) relates to the FCU dynamic.

3.6 Simulation and Experimental Setup

3.6.1 Simulation setup

The model-based optimisation problem is solved over a finite horizon. The non-linear equations and the non-convex terms due to bilinear system dynamics as well as the binary

and integer decision variables result in the formation of a non-convex mixed-integer non-linear programming (MINLP) problem. The non-convex MINLP is transformed into a linear model to obtain the global optimal solutions. The non-linear equations are approximated by linearising system dynamics at the operating points using piecewise linear equations, which result in a mixed-linear programming problem. In this chapter, the SCIP solver is implemented to solve the MILP MPC problem. The horizon prediction is $N = 24$ hours and the control sampling time is 10 minutes. The control horizon is equal to the prediction horizon. The control horizon decreases as the time step k increases. The purpose of reducing the control horizon toward the end of the day is the reduction of the computational time and complexity. Each day at the first time step ($k = 1$), the MPC utilises the present m_c, T_c and T_{in} values; as well as the predicted ambient temperature, solar irradiation and the electricity price. The current values are used for feedback by resetting the MPC state. Note that the MPC has previously captured all the values of the previous day's variables related to the building and WST models as the initial values. Therefore, the MPC obtains the optimal combination of control variables' set points corresponding to the lowest energy consumption while maintaining indoor temperature in thermal comfort zones along the time-varying control horizon. All simulations are performed using MATLAB and run on an Intel Core i5-3470M CPU at 3.20 GHz computer with an 8 GB RAM. The amount of time needed to compute the optimal solutions was between 3.5 seconds and 54 seconds. The computational time decreases when the control horizon reduces as the day progresses.

3.6.2 Experimental Setup

Simulations and experimental verifications are performed for the thermal energy system installed at the SELAB (Figures 3.1-3.2). The system consists of a water to water GSHP (7.1 kW of cooling capacity and 10.3 kW of heating capacity) with 3×65 m vertical boreholes, a 1000 liter stainless steel WST (insulated with 100 mm of insulation layer), circulation pumps and FCUs.

A control scheme is designed and modelled for the SELAB thermal energy system that will shift GSHP load based on DRP and minimise the electrical and thermal energy consumptions without violating any zone temperature limits. In order to demonstrate

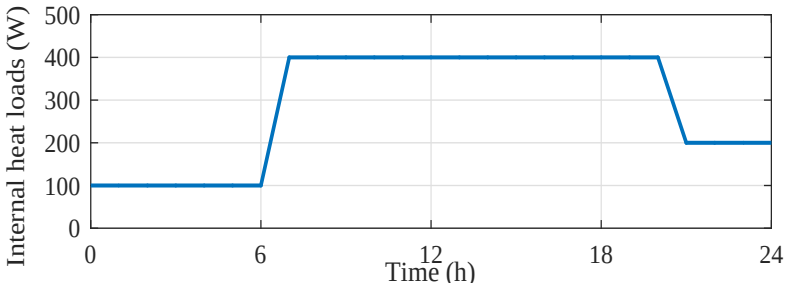

Figure 3.12: The internal heat loads for SELAB associated with 4 occupants.

Table 3.2: Variables and operating constraints used for the simulations and experimental verifications.

Variables	T_{in}	$[\underline{T}_{sp}, \overline{T}_{sp}]$	$\dot{m}_{GHP}$	$\dot{m}_f$	m_c	T_c
Unit	°C	°C	l/min	l/min	m^3	°C
Constraints	[21, 25]	[21.5, 24.5]	30	10	[0.1, 1]	[5, 8]

the model and the proposed controller, the RTP profile is considered which is based on the wholesale electricity price from the Australian energy market operator (AEMO) website [1]. The hourly RTP for a typical day in January 2018 is shown in Figure 3.11. Tests are also run considering an internal heat load profile for the SELAB building. Figure 3.12 shows the internal heat loads associated with 4 occupants.

The experiments at SELAB are performed with the operating constraints of Table 3.2. The WST is set to $m_c = 0.1$ m^3 at $T_c = 7\,^\circ$C in the first time step. The volume of stored chilled water is calculated by measuring the difference between the inlet and outlet water flow rates of the WST. The temperature of the stored chilled water is measured using temperature sensors S_1, S_2, and S_3 installed in the WST. The indoor temperature set-point is considered $T_{sp} = 23\,^\circ$C.

The temperature set-points determined by the proposed DTS strategy (equation 3.19) based on given lower and upper temperature bounds 21.5 °C and 24.5 °C, respectively (Table 3.2, column 3).

3.7 Simulation and Experimental Verification

This section presents and compares detailed simulation and experimental results for the SELAB thermal energy system (Figures 3.1-3.2). Four cases are considered

and tested including the conventional thermostatic control (Case I), MPC with fixed electricity pricing (Case II), MPC with dynamic demand response controller (DDRC) of Ref. [2] (Case III), and the proposed MPC with DTS based on RTP tariffs (Case IV). Experimental results of Cases II-IV validate the simulation results. The weather data are collected by the weather station at SELAB. These tests are conducted under the same conditions on days with similar ambient temperature and solar radiation profiles. The simulation results of Cases I-IV and the measurements are used to investigate the performance, capabilities and advantages of the proposed MPC.

3.7.1 Case I: Base case with conventional thermostatic control

Figure 3.13 shows the results for thermostatic control (own device control). It is a hysteresis controller that switches the FCU off when the indoor temperature is lower than 22.5 °C and activates it when the indoor temperature reaches 23.5 °C. This is the conventional thermal energy system used in most buildings. In this figure, the top plot shows the on/off signal for the GSHP, the middle plot is the corresponding daily indoor temperature control, and the bottom plot is the air flow rate required to keep the room temperature at the desired set-point of 23 °C.

3.7.2 Case II: MPC with fixed electricity pricing

Figure 3.14 shows the results for indoor temperature control with MPC under fixed electricity price. The first and second plots (from the top) show the GSHP on/off signal to control the WST temperature and the stored chilled water volume. The next plot shows the controlled indoor temperature within the thermal comfort zone of 21 °C and 25 °C. The last plot depicts the manipulated air flow to the building so that the FCU system can maintain the indoor temperature in the thermal comfort zone. Note that the designed controllers for this case study are able to operate the WST more efficiently. In particular, the MPC controller provides over 8.2% reduction in power consumption compared with the thermostatic controller of Case I. In addition, this test shows over 11.46% reduction in thermal discomfort.

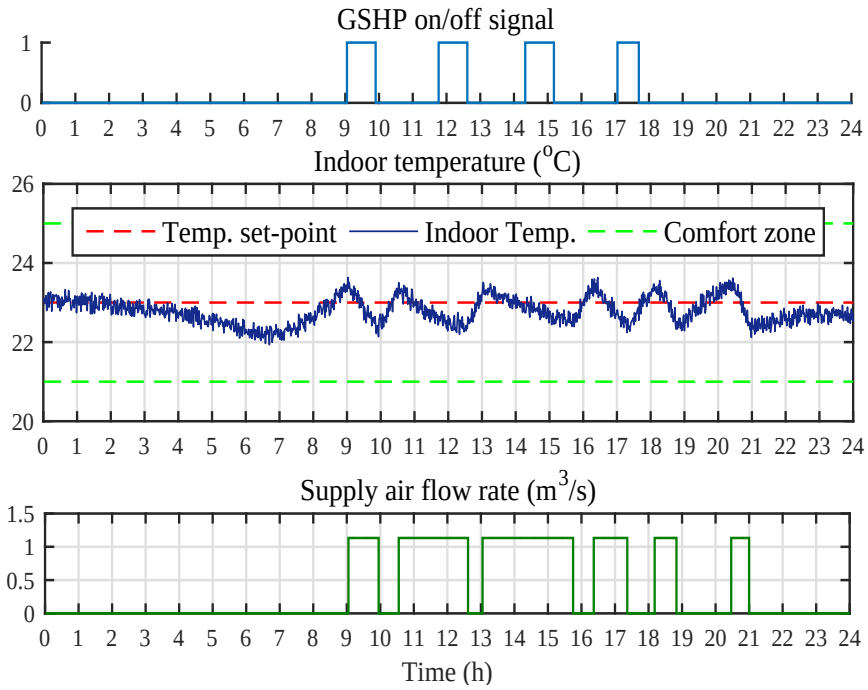

Figure 3.13: Case I (Base Case with Thermostatic Control)- Performances of the GSHP and the FCU.

3.7.3 Case III: MPC with the DDRC

Peak-load shifting is analysed based on the proposed MPC strategy of Reference. [2] (that uses a dynamic demand response controller). The DDRC strategy changes the temperature set-point when the electricity price is higher than the threshold price. Otherwise, the temperature set-point is maintained at its initial value that was set by the customer. Additionally, the threshold price is determined by customer's preference. The results are presented in Figure 3.15. The first and second plots show the performance of GSHP-MPC. Note that the GSHP load is shifted based on RTP and the WST is filled with chilled water at the low-price tariff. The third and fourth plots demonstrate FCU-MPC performance. In this case, the DDRC of Reference [2] resulted in a 27.36% improvement in peak-load shifting in Case I, and a 10.26% improvement in Case II.

3.7.4 Case IV: Proposed MPC with DTS based on RTP tariffs

The aim of this experiment is to analyse the MPC controllers with DTS. In this test, the proposed DTS is applied for $\beta = 1$ to pre-cool the building before the peak-load

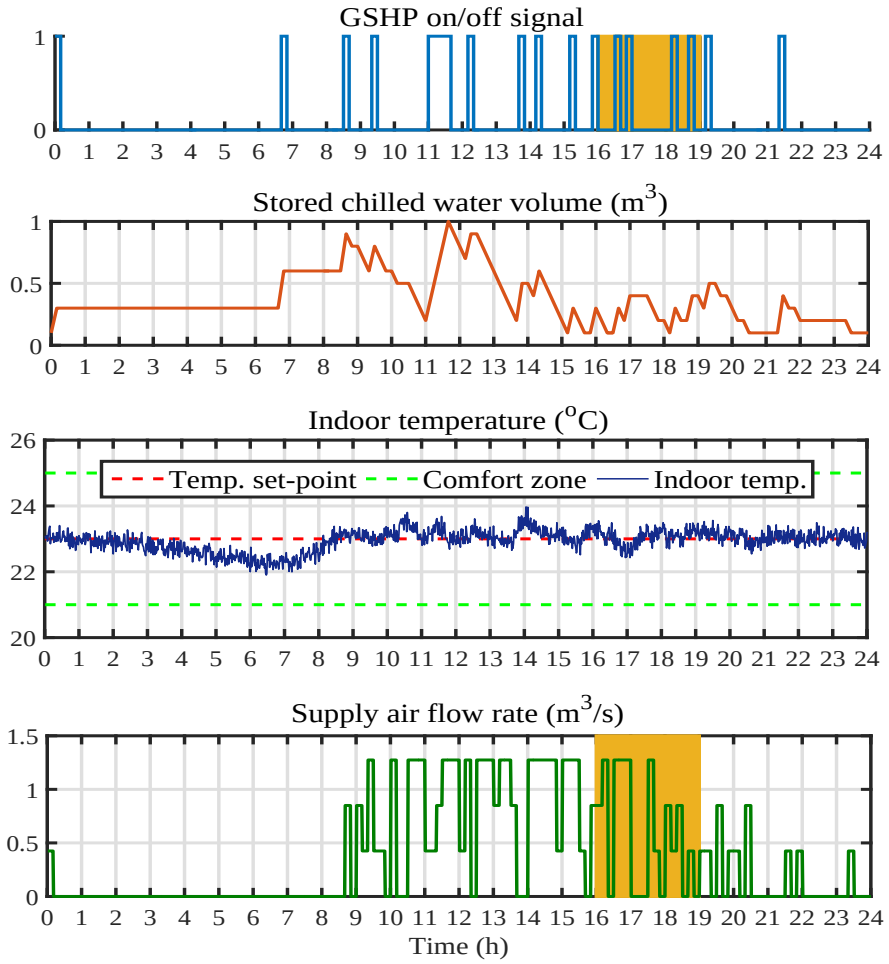

Figure 3.14: Case II (MPC with Fixed Electricity Pricing)- Operation of GSHP coupled with WST and FCU.

hours to reduce energy costs and shift the GSHP and FCU loads. The set-point can be changed between 22°C and 24°C for $\beta = 1$. Figure 3.16 shows the MPC results with $\beta = 1$. The proposed MPC strategy for $\beta = 1$ reduces the total power consumption to 7.18 kWh. In this case, the electricity consumption by the GSHP and FCU is reduced by 13.3%. In addition, this strategy is an effective way to shift the HVAC load from a high electricity price period while the indoor temperature is perfectly controlled. Results show reductions of 85% and 79% in peak-hours power consumption in compared to Cases I and III, respectively.

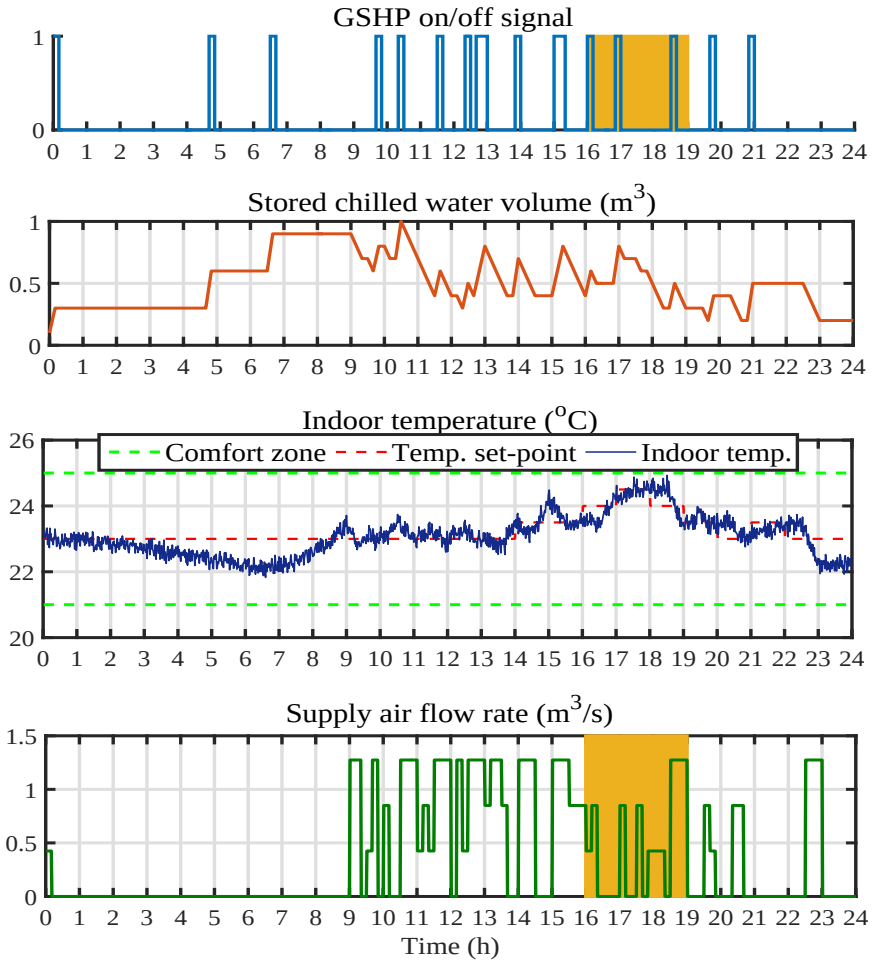

Figure 3.15: Case III (DDRC Strategy of Reference [2])- Operation of GSHP coupled with WST and FCU.

3.7.5 Experimental Verification of Cases II-IV

To verify the precision and performance of the proposed MPC with DTS, it is applied and implemented on the thermal energy system at the SELAB (Figures 3.1-3.2 and Section IV). Figures 3.17-3.19 demonstrate the experimental measurements that confirm the simulation results of Cases II-IV. In Figures 3.17-3.18, according to the first plot, the chilled water is supplied by GSHP whenever Pump1 is on. The water flow rate is 30 l/min and the temperature of the supply chilled water is between 5 and 8 °C. The second plot shows the return water temperature from the FCU. As a result of having desirable chilled water for the FCU, the return water temperature is in the range of

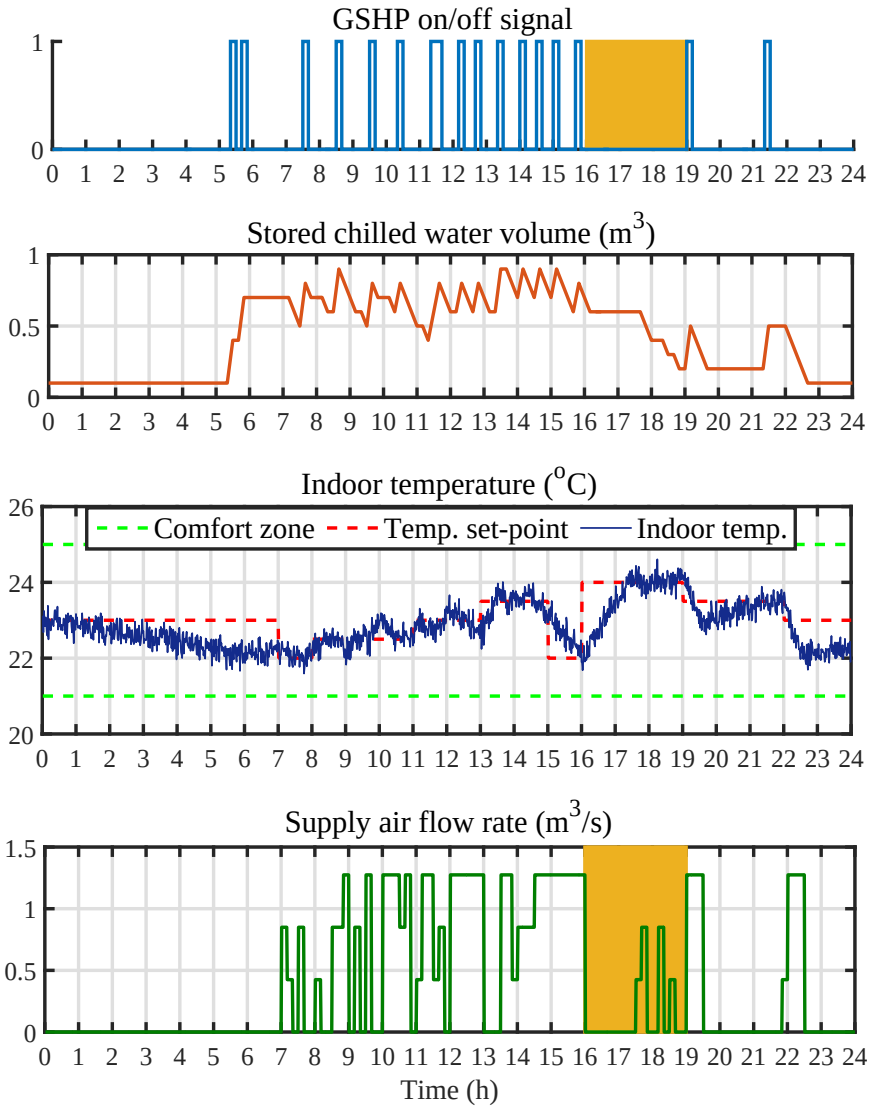

Figure 3.16: Case IV (Proposed MPC with DTS Strategy ($\beta = 1$) and RTP Tariffs)- Operation of GSHP coupled with WST and FCU.

8-13 °C. The total power consumption of the HVAC system is shown in the last plot of Figures 3.17-3.18.

Figure 3.19 confirms that the GSHP supplies chilled water to the WST (first plot) and the WST stores enough chilled water to supply the FCU (second plot) at the requested temperature range of 5-8 °C. After circulating chilled water through FCU, the returned water from FCU is in the expected range of 8-13 °C that is shown in the third plot.

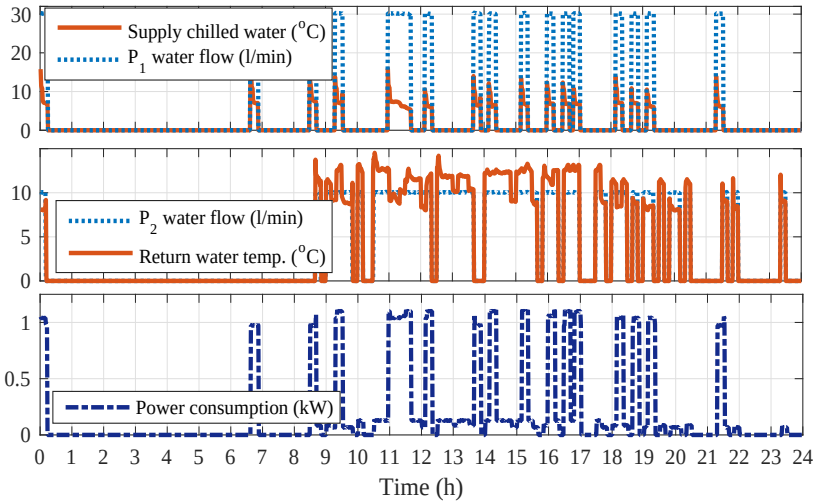

Figure 3.17: Experimental verification of Case II- Measured waveforms for operation of GSHP coupled with WST and FCU.

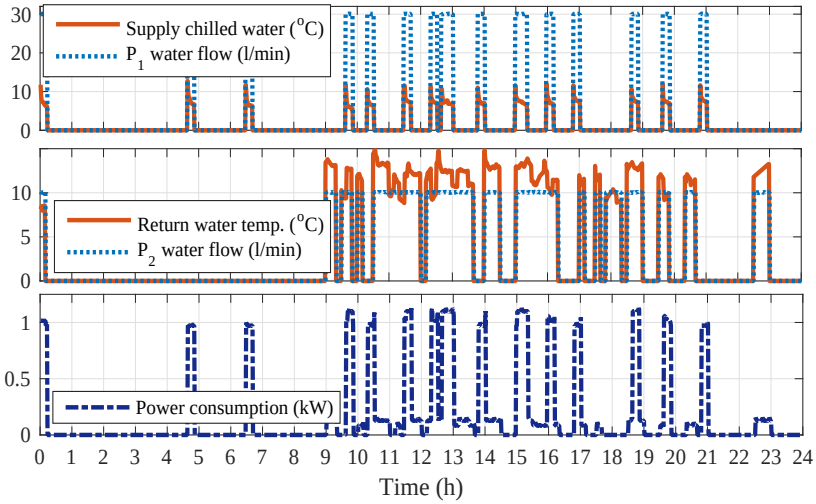

Figure 3.18: Experimental verification of Case III- Measured waveforms for operation of GSHP coupled with WST and FCU.

The last plot of Figure 3.19 shows the total power consumption of the HVAC system. The energy consumptions of GSHP and FCU during peak-load hours (16:00-19:00) are zero and 0.264 kWh, respectively. The difference between the power consumption of the experimental result and the simulation result is because the ground circulation pump is run about 75 seconds earlier than GSHP.

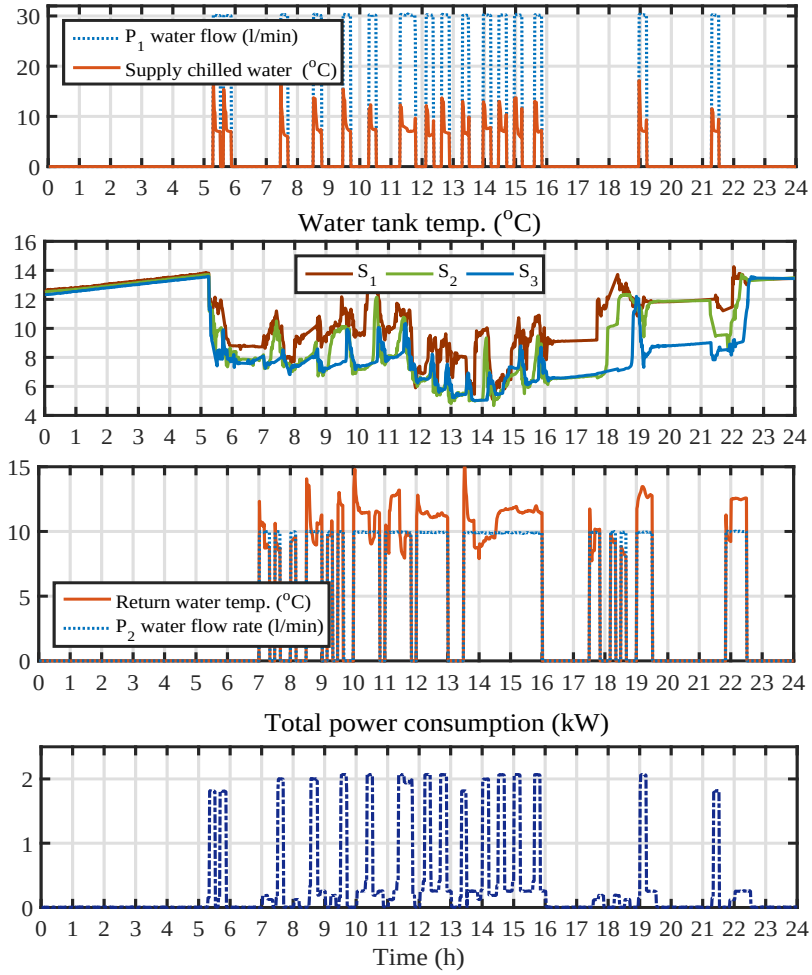

Figure 3.19: Experimental verification of Case IV- Measured waveforms for operation of GSHP coupled with WST and FCU.

3.8 Sensitivity Analysis and Discussions

Simulation and field measurement results including total energy consumption, cost saving, peak-load shifting, and indoor temperature deviation are summarised and compared in Table 3.3. It is of significant note that the proposed controller takes effective advantage of WST coupled with GSHP in terms of reducing the overall energy cost and shifting energy consumption from peak-load hours. The proposed TEMS with MPC controllers based on DTS (Case IV) enables the demand-side to efficiently respond to the DRP while allowing the end-user to take advantage of RTP. Detailed sensitivity analyses are also performed to illustrate the impacts of β on power consumption, peak-load

Table 3.3: Comparison of results for Cases I-IV (Figs. 3.13-3.19) with the percentage of improvement.

Cases	Total power consumption		Electrical energy cost		Power consumption in peak hours		Accumulated temp. deviation		Results
	kWh	%*	$	%*	kWh	%*	°C	%*	
Case I (Base case)	8.268	-	3.314	-	1.742	-	11.65	-	Fig. 3.13
Case II (Fixed electricity price)	7.614	7.91	2.902	12.43	1.41	19.05	5.26	54.84	Figs. 3.14,3.17
Case III (DDRC of Ref.[2])	7.227	12.59	2.729	17.65	1.265	27.36	11.45	1.71	Figs. 3.15,3.18
Case IV (Proposed MPC with DTS and RTP tariffs)	7.181	13.33	2.475	25.31	0.258	85.15	11.42	1.97	Figs. 3.16,3.20
Experimental verification of Case IV	7.213	-	-	-	0.264	-	11.83	-	Fig. 3.19

* Percentage of improvement with respect to Case I.

shifting, and indoor temperature. Table 3.4 and Figure 3.20 demonstrate the sensitivity of the proposed MPC to the intensity of DTS by changing the value of β from 0 to 1.5. Figure 3.20a shows changes of power consumption of GSHP and FCU for different β values. Interestingly, by increasing β, the power consumption will be reduced during peak-hours (4-7 pm) and the cost will be consequently decreased. However, the variation of indoor temperature will be increased but still within the comfort zone as shown in Figure 3.20b. Based on the detailed simulations, field measurements, and sensitivity analysis of Figures 3.13-3.20 and Tables 3.3-3.4, it can be observed that

- The proposed TEMS reduces the total energy cost by 25.31% as compared to 12.43% and 17.65% for Cases II and III, respectively (Table 3.3, column 5).
- The proposed TEMS has effectively shifted 85.15% of HVAC load from the peak-load hours as compared to only 19.05% and 27.36% for Cases II and III, respectively (Table 3.3, column 7).
- Increasing β will significantly shift HVAC loads from peak-load hours. For example, the peak-load shifting can be increased to over 88.23% with $\beta = 1.5$ (Figure 3.20a, Table 3.4).
- Increasing β will also reduce the total power consumption and cost by 20.16% and 30.74%, respectively (Figure 3.20a, Table 3.4, column 5).
- Decreasing β will decrease the deviation of indoor temperature from the set-point temperature. For example, with $\beta = 0$ (when the discomfort level is a concern of consumers) the energy consumption and cost increase during peak hours while the indoor temperature slightly varies around the designated temperature set-point (Figure 3.20b and Table 3.4, column 2). Note that for this scenario, the proposed TEMS will offer 47.46% improvement in temperature deviation compared to Case I (Table 3.4, column 2).

3.9 Conclusions

This chapter has advocated for the implementation of optimal real-time thermal energy management strategies for smart buildings with GSHP, WST and FCUs. This

Table 3.4: Sensitivity of proposed MPC to the intensity of DTS. Note that β values of 0, 1 and 1.5 correspond to best thermal comfort, best trade-off and low cost, respectively.

	$\beta = 0$	$\beta = 0.5$	$\beta = 1$	$\beta = 1.5$
Power consumption (kWh)	7.637	7.26	7.18	6.601
Electrical energy cost ($)	2.948	2.664	2.51	2.295
Power consumption in peak hours (kWh)	0.929	0.61	0.253	0.205
Accumulated temp. deviation (°C)	6.12	8.42	11.42	15.78

decreases the total power consumption of the GSHP and FCUs by shifting their loads based on DRP while providing adequate thermal comfort levels. This is done by combining two online closed-loop MPCs to manage two thermal energy storage systems, a water storage tank (WST) and the building thermal mass. The main advantages and contributions of the proposed MPC with DTS based on RTP tariffs compared to the existing technologies based on thermostatic control and the MPC with DDRC of Ref. [2] are:

- The proposed MPC with DTS can significantly reduce the total energy cost and overall cost by shifting up to 100% of HVAC (GSHP and FCUs) loads based on DRP depending on weather conditions while maintaining the indoor temperature within a desirable comfort range.
- The proposed MPC with DTS allows the end-user to take more advantage of RTP by increasing the DTS intensity coefficient. Large values of β will significantly shift HVAC loads from high price periods and consequently reduce the cost while the indoor temperature is still within the thermal comfort zone.

Furthermore, the proposed TEMS and simulation results are verified by experimental tests.

HVAC systems in residential buildings will be further studied in the coming chapters as a possible solution to improve the interaction of microgrid with the smart grid. This will be done by optimal sizing of electrical and thermal energy storage systems, and smart scheduling of heat pumps operation.

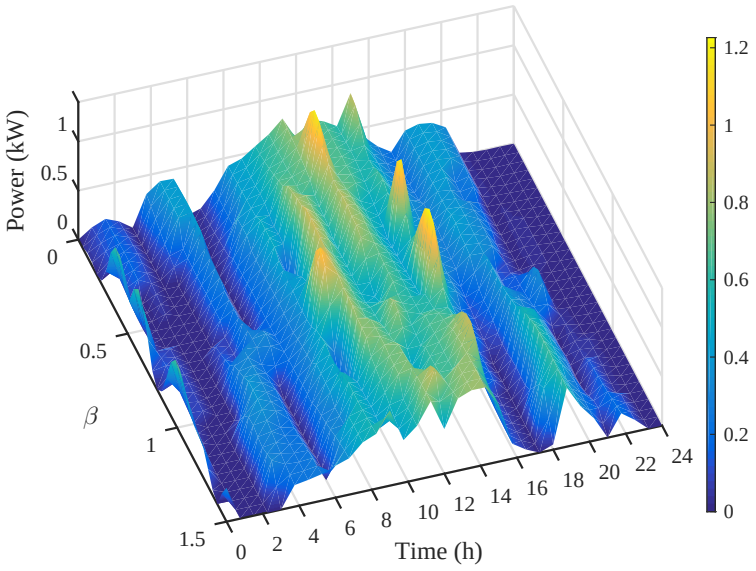

(a) Power consumption

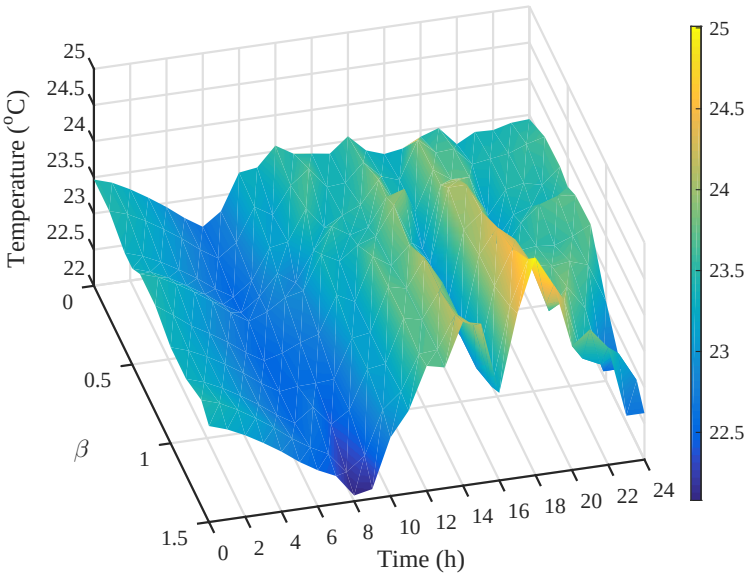

(b) Indoor temperature

Figure 3.20: Simulation results of sensitivity of DTS

The first research question (RQ1) has been completely addressed in this chapter. In this study, a GSHP is evaluated as a responsive load in a building. An optimal real-

time thermal energy management is proposed and applied in HVAC system to minimise total energy consumption while reducing the indoor deviation from the temperature set-points. The proposed DTS enables the DRP to effectively take advantage of building thermal energy mass. The DTS strategy also allows occupants to choose options for electricity cost reduction or the best thermal comfort by setting β.

Chapter 4

PV Self-Consumption Enhancement with Optimal Residential Thermal Energy Management

In smart residential buildings, variations in rooftop PV power causes a mismatch between generation and load demand. This chapter deals with shifting heat pumps loads to either lower electricity price period or whenever PV generation is available[1]. The proposed strategy is used for managing heat pump operation based on real-time pricing tariff to minimise the operation cost of a smart building, by controlling the room temperature. A real-time temperature boundaries is employed to increase the PV self-consumption. Simulation results demonstrate the cost benefits and effectiveness of the proposed thermal energy management strategy.

4.1 Introduction

In power system, the massive deployment of rooftop PV systems in the residential networks and commercial buildings has led to the rapid growth of PV power penetration.

[1]The presented chapter has been published as: **A. Baniasadi**, D. Habibi, W. Al-Saedi, and M. A. S. Masoum, "PV Self-Consumption Enhancement with Optimal Residential Thermal Energy Management," 2019 9th International Conference on Power and Energy Systems (ICPES), Perth, Australia

The integration of PV generation can offer environmental and economic benefits, in addition to introduce significant challenges for grid operations. On the other hand, buildings can consume about 40% of the total generated electricity [117]. HVAC system is one of the major energy consumers in residential buildings. HVAC systems can largely increase the demand in peak-load periods [118]. Therefore, thermal energy management in residential buildings can be utilised to increase the use of PV generation and thus decrease the peak demand, by exporting PV generation to the utility. HVAC systems also have a substantial potential to facilitate demand response program. Therefore, an optimal energy management strategy is largely required to enhance the utilisation of PVs. This strategy can be used for heat pumps as the heating/cooling suppliers to meet the space heating/cooling requirements.

Many researchers have presented various strategies to minimise the peak demand for residential buildings with the integrations of rooftop PVs. Ref. [74] focused on HP water heaters to reduce energy cost based on TOU tariff, by presenting an optimal scheduling model. Ref. [119] presented an optimal model to minimise energy and water consumption. The authors controlled an HP water heater and an instant heater which are integrated with a wind turbine, PV system, and diesel generator. However, space heating/cooling was not considered in both papers. In [90], an optimal DR methodology presented to decrease the electrical water heating costs based on TOU tariff. The authors considered the advantage of thermal energy storage by assuming the hot water consumption for one day. Reference [45] developed a day-ahead optimisation of TES based on DR. The aim was to utilise TES for hot water and thermal mass of 50 residential buildings, by considering the expected energy and discomfort costs. A scheduling approach for an energy system with a battery was proposed in [120]. This approach is employed to control the demand response for HVAC systems. The authors in [121] introduced a cost-optimal schedule method. A Mixed Integer Linear Programming optimisation technique is used for the better utilisation of solar energy in buildings. The demand caused by heating and partial thermal storage was investigated in [122]. An optimal thermal storage energy was determined by predicting the heat demand of the building.

To take advantage of the pre-cooling and pre-heating energies, a potential approach is applied to adopt temperature set-point based on real-time pricing tariffs. In [2] and

[55], authors proposed two variable temperature set-point strategies for changing the set-point temperature, when the electricity price is higher than a threshold price which is determined based on consumers preferences. However, neither of these two strategies can considerably shift the HVAC loads. A price based DR strategy for an office building to optimise energy costs of HVAC units and thermal discomfort levels of occupants is proposed in [58]. The TOU tariffs are used to generate day-ahead pre-cooling schedules for early morning hours to reduce the peak load demand. However, the real-time pre-cooling/pre-heating strategies are proven to be more effective than the conventionally scheduled pre-cooling operations. Therefore, in this study, the proposed RTB is designed to shift up to 100% of HVAC loads from peak-load hours while taking advantage of a TES. It is more effective to develop a control strategy for heat pumps coupled with TES to respond to DRP.

Among all proposed control methodologies for controlling indoor temperature, the model predictive control approach can effectively predict the future behaviour of the system to minimise energy consumption while considering thermal comfort [55, 61, 64, 65]. In [55], authors proposed a practical cost and energy efficient MPC method for HVAC load under real-time day-ahead electricity pricing tariff. A state-space model was developed to model the impact of inputs (outside temperature, HVAC operation, etc.) on the output (inside building temperature) at each control interval. Based on RTP tariff, around 8% reduction in overall energy consumption and 13% cost savings are achieved by this MPC controller. An MPC controller to optimise the thermal comfort level and energy efficiency in a commercial building is applied in [61]. However, the authors do not take advantage of pre-heating/pre-cooling for electricity cost reduction and PV self-consumption promotion.

Many researchers have investigated different approaches to promote PV self-consumption in residential buildings. Ref. [123] considered the cost optimal mix of the various complementary technologies such as batteries, electric vehicles, HPs and thermal energy storage to reduce the exporting PV power into the grid. In [124], a rule-based algorithm is employed to decrease energy exchanges with the aims of maximising PV self-consumption and considering both building and domestic hot water heating. The work in [125] considered an MPC multi-objective optimising energy management concept for a hybrid energy storage system. The model consists of PV system, battery, and combined heat

pump/heat storage device. The aim was to minimise the operation costs and increasing the PV self-consumption while ensuring user thermal comfort. However, the authors did not consider the variable temperature set-points based on RTP to increase PV self-consumption.

This chapter presents an approach to resolve the issues associated with variations in rooftop PV power, by minimising the peak demand of smart buildings. The aim is achieved by integrating the operation of HP-PV system which consists of rooftop PV and HP system. The latter is used as a controllable load. The implemented residential thermal energy management strategy consists of a model predictive control to minimise the operation cost of HP, and a real-time temperature boundary (RTB) strategy based on real-time pricing tariff. Furthermore, the occupants' thermal comfort is taken, into account while shifting the HP electricity load. The main contributions can be described as follows:

- A real-time heat pump control strategy is developed to increase the PV self-consumption and minimise the electricity bill.
- Real-time temperature boundaries is proposed to shift the load based on real-time pricing tariff.

4.2 System Model

4.2.1 Modelling of building thermal load

For a constructed building with given materials, design and equipment, the most important parameters that can impact the cooling/heating load are the ambient temperature, humidity, and solar radiation. Therefore, these parameters are considered as the input parameters of the building cooling/heating load prediction model. The impacts of delay of air temperature and solar radiation intensity's on the dynamic cooling/heating load are also considered in this chapter. The recorded values are used as input parameters to the model.

4.2.2 Modelling of thermal energy storage (TES)

In this chapter, TES model is adapted for heating and cooling modes which is based on a stratified two-layer tank separated by thermocline layer. TES is used in the cooling mode to simplify the description of the model. This is achieved by placing the return water from the radiator at temperature (T_w), at the top of TES, while the chilled water produced by the HP at temperature T_{HP} are directed to the bottom of TES. The volume of the stored water (m) in TES is always constant and equal to the sum of the volumes of return water (m_w) and chilled water (m_c) which is $m = m_w + m_c$. Therefore, the SOC of TES model based on the heat and mass flow balance can be described as follows:

$$SOC_i^{TES} = SOC_{i-1}^{TES} + \sum_i \frac{\dot{m}_{HP} - \dot{m}_r}{m} \times 100 \tag{4.1}$$

where $\dot{m}_r$ is the mass water flow rate through the radiator, and $\dot{m}_{HP}$ is the mass water flow rate of HP. The cooling energy stored in the TES can be calculated as follows:

$$Q_{TES} = m_c c_p (T_w - T_{HP}) \tag{4.2}$$

4.2.3 PV model

The PV power generation is calculated based on ambient temperature (T_o) and the solar irradiation data (I_s) [126, 127].

$$P_{PV} = I_s A_{PV} N_{PV} \eta_{PV} (1 - 0.005(T_o - 25)) \tag{4.3}$$

where A_{PV} is the area of PV module and N_{PV} is the number of PV module. η_{PV} is the efficiency of PV system, which is dependent on T_o and I_s.

4.3 Problem Formulation

4.3.1 Real-time temperature boundary (RTB) based on RTP

Real-time indoor temperature boundary $\chi(t)$ enables the DR to efficiently take advantage of the building pre-cooling and pre-heating. Most of the heat distributors such

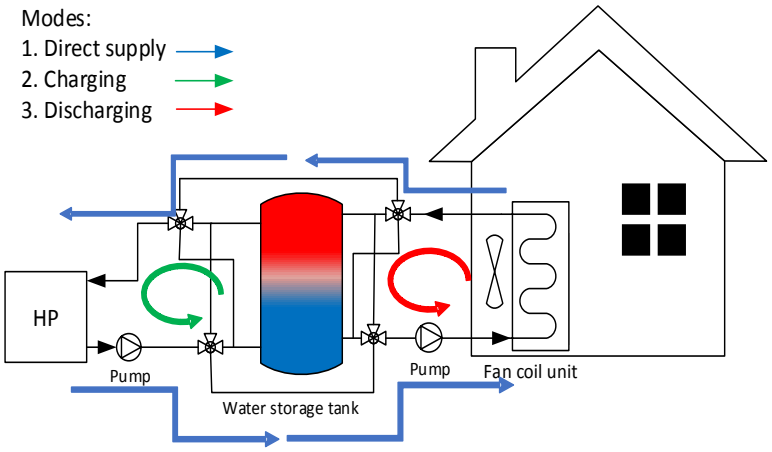

Figure 4.1: Residential air-conditioning system with and without a storage tank.

as radiators and fan coil units can regulate the room temperature by thermostats [128]. The on/off state of a relay can be determined by the hysteresis control rule as follow [128]:

$$\chi(t+1) = \begin{cases} 0 & \text{if } T_{in}(t) \leq \underline{T}_{in} + \mathcal{U} \\ 1 & \text{if } T_{in}(t) \geq \overline{T}_{in} + \mathcal{U} \\ \chi(t) & \text{otherwise,} \end{cases} \tag{4.4}$$

where the continuous state (T_{in}) is the building temperature and the discrete state (χ) is the state of the relay, which switches the heat distributor on or off according to the hysteresis control rule. The set-point offset ($\mathcal{U}$) is a control signal which is determined by the proposed RTB strategy based on DR signal as follows:

$$\mathcal{U} = \begin{cases} -1.5 & \text{if } P_{PV} \geq 0 \\ 0 & \text{if } NRTP(t) \leq 0.5 \\ (NRTP - 0.5) \times 2\ \mathcal{U}_{max} & \text{otherwise,} \end{cases} \tag{4.5}$$

where $\mathcal{U}_{max}$ represents the maximum set-point offset which can be determined by customers or based on thermal comfort zone. $NRTP$ represents the normalised real-time price.

4.4 Objective Function

The objective here is to switch the HP on/off in order to shift HP power consumption based on DRP while producing sufficient chilled/hot water. For this purpose, the cost function is designed for the MPC of HP based on RTP tariffs and the availability of PV power. The stored chilled/hot water in TES should be produced and consumed on the same day to prevent the thermal losses. In this chapter, the objective function can be expressed as follows:

$$\min \quad \sum_{i} C_{el} \tag{4.6}$$

subject to

$$T_{HP}^{min} \leq T_{HP} \leq T_{HP}^{max} \tag{4.7}$$

$$SOC_{TES}^{min} \leq SOC_{TES} \leq SOC_{TES}^{max}, \tag{4.8}$$

where C_{el} is the electricity cost. The temperature of chilled/hot water are restricted into the indoor temperature range which is determined by Section 4.3.1. The SOC of TES is limited to the capacity of storage tank.

4.5 Model predictive control-based for HP

MPC is adopted to use the system model to predict the future evolution of the plant, thus generate the control action on receding control strategy [65, 66]. Therefore, MPC is implemented to predict a thermal demand based on weather condition and building thermal model. The objective function is formulated for the trade-off between minimising the total electricity cost and producing enough chilled/hot water as subject to dynamic constraints which are given by:

$$\min_{u_k} \quad \sum_{j=k}^{k+N-1} (NRTP(j|k)(HP(j|k)) \tag{4.9}$$

where N is the prediction horizon, $NRTP$ is the normalised electricity tariff at time step j, HP is the binary decision variable $u = \{HP\}$ while state variable is $x =$

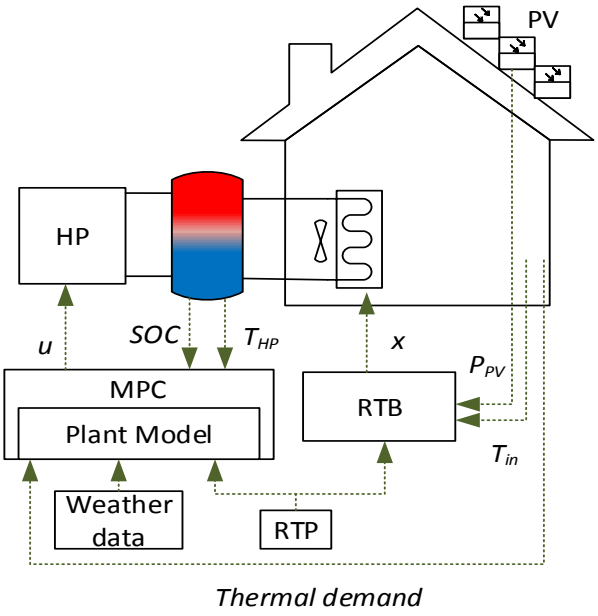

Figure 4.2: Schematic control structure of the HP-PV MPC.

$\{SOC_{TES}, T_{HP}\}$, and d is disturbance. Thus, HP is defined by

$$HP(j) = \begin{cases} 1, & \text{if the AC is on} \\ 0, & \text{otherwise.} \end{cases} \tag{4.10}$$

The overall schematic of the control structure of HP-PV MPC is shown in detail in Figure 4.2. The plant model is described in detail in Section 4.2. The horizon prediction is $N = 24$ hours, and the control sampling time is set to 5 minutes. Figure 4.3 shows the proposed HP-PV MPC structure.

4.6 Simulation Results

In this chapter, the thermal system consists of 1000 litre storage tank, and water source HP with 7.1 kW cooling capacity (1.92 kW power consumption) and 10.3 kW heating capacity. The electrical system encompasses of 18 series mono-crystalline PV modules each with rating 285 W, which produce 5.1 kWp.

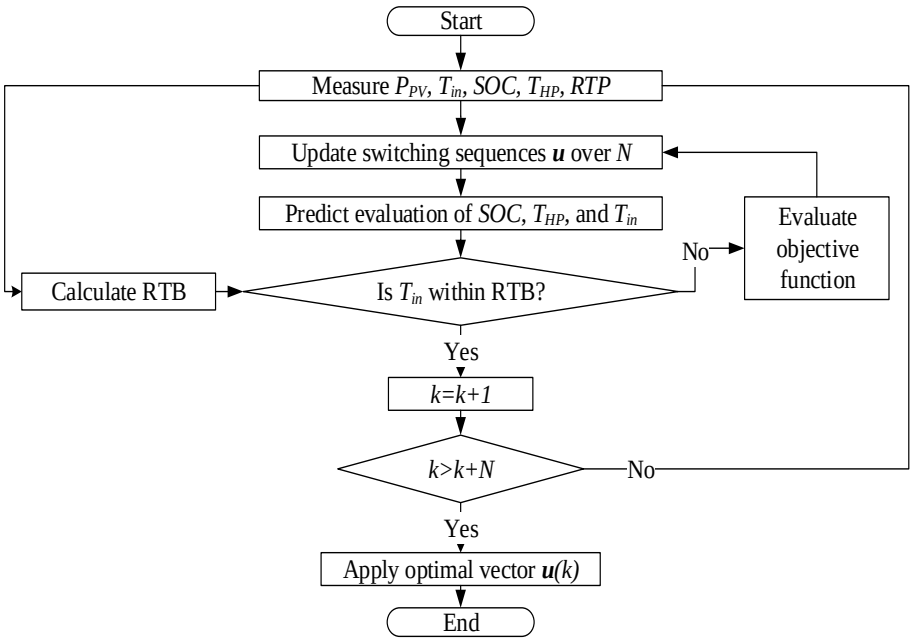

Figure 4.3: Flowchart of proposed HP-PV MPC.

In this section, the system operation is demonstrated in detail for two typical days in summer and winter. Figure 4.1 shows the water source HP system for a residential building. This system can directly supply the thermal demand, while the load can be also supplied by the thermal storage tank. The thermal demand is calculated based on weather condition and thermal building model [79]. The proposed strategy changes the RTB based on the forecasted PV generation and RTP to minimise the price by shifting the AC load. Figure 4.4 shows the wholesale electricity market in Western Australia [1] and solar irradiation for a typical day in summer. Figure 4.5 depicts the AC operation without the water storage tank. The AC load is shifted by RTB strategy. MPC is also implemented to operate HP online based on RTP to control the state of charge of the storage tank. This section shows the system operation for a typical day in summer and winter. The simulations are carried out for the following three scenarios.

4.6.1 Residential air-conditioning system without storage tank

Typical air-conditioning system operates based on thermostat control. Figure 4.5 shows the temperature control and AC power consumption for a day in summer. The

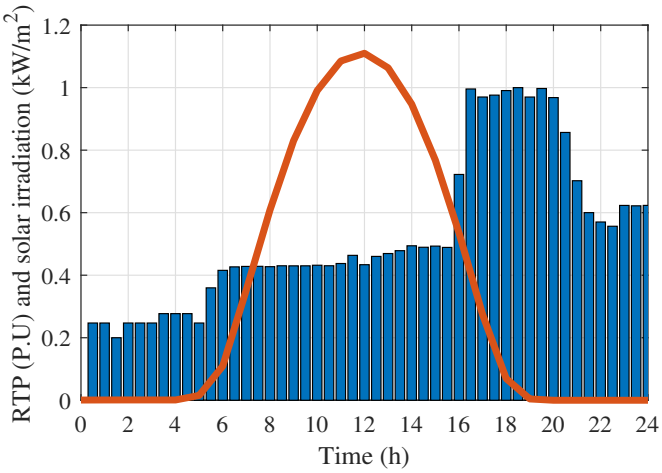

Figure 4.4: Normalised wholesale electricity market (blue bars) and solar irradiation (red line) for a day in summer.

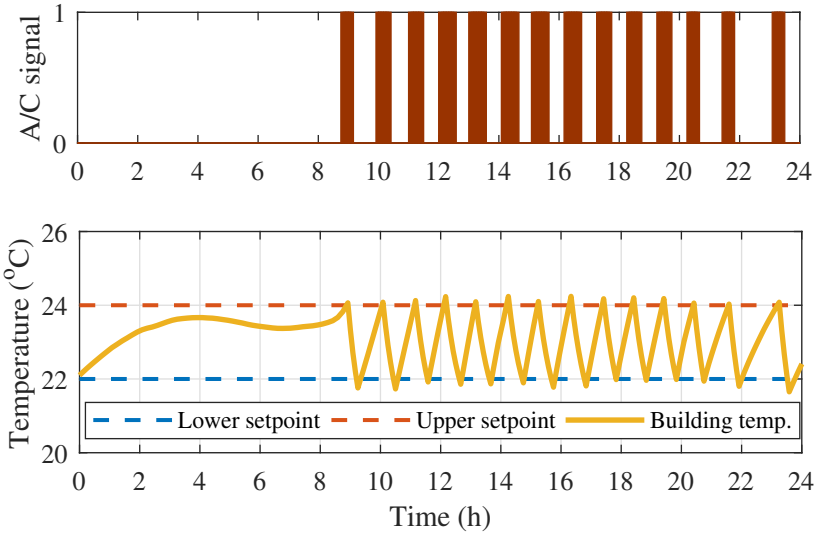

Figure 4.5: AC operation and indoor temperature for a day in summer.

temperature set-points are 22 ^oC-24 ^oC. The AC is run during peak-price to keep the indoor temperature within determined set-points.

4.6.2 Residential air-conditioning system with RTB

In this section, RTB is implemented in typical air-conditioning system to reduce AC power from peak-load hours and consequently it helps to reduce the electricity bill.

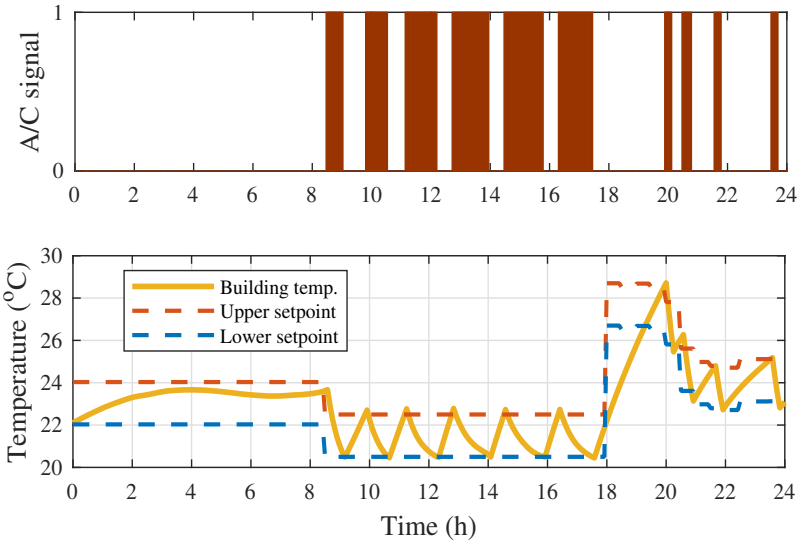

Figure 4.6: Proposed RTB: AC operation and indoor temperature for a day in summer.

Meanwhile, the indoor temperature is kept within thermal comfort zone. Figure 4.6 shows the temperature control and AC power consumption for a day in summer with the implementation of RTB. The maximum temperature offset ($\mathcal{U}_{max}$) is set to $4.5\,^{\circ}C$.

4.6.3 Residential air-conditioning system with storage tank and RTB

Houses with PV system require storage systems to reduce the electricity bill. The battery storage system is not cost-effective, whereas adding thermal energy storage to typical AC system can help to reduce a significant AC load from peak-load hours. However, adding TES to AC system requires an accurate controller to prevent wasting thermal energy. In this section, MPC controller is applied to store enough chilled water in TES. Thus, it can supply thermal load during peak-load period based on predicting weather condition. Figure 4.7 shows AC power consumption coupled with TES for the same day in Section 4.6.2 for the implementation of RTB. It can be seen that all AC load has shifted in PV power generation period. Figure 4.8 shows the percentage of stored chilled water in TES. To minimise the thermal losses, TES is charged in midday, when PV power is sufficient to run AC. TES is then discharged to supply thermal load during high electricity price period.

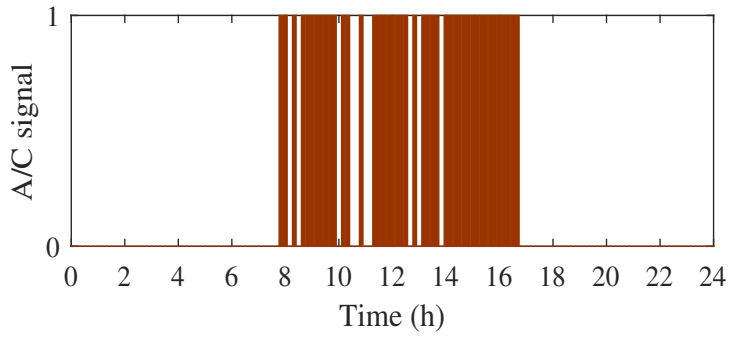

Figure 4.7: AC operation coupled with TES for a day in summer.

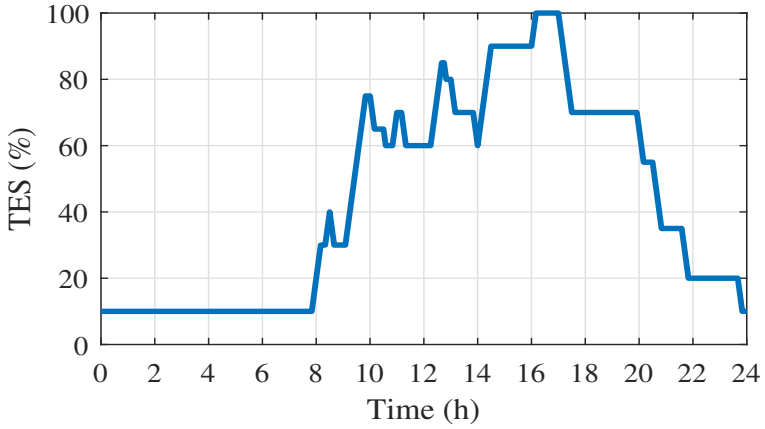

Figure 4.8: Percentage of thermal energy storage in TES.

4.7 Discussions

Simulation results representing by electrical energy cost, peak-load shifting, and average indoor temperature are summarised in Table 7.1. It is worth mentioning that by taking full advantage of TES, proposed controller has successfully reduced the overall energy cost and shifted the energy consumption from the peak-load hours. The proposed RTB with MPC controller based on RTP has enabled the end-users to efficiently increase the PV power self-consumption. According to the results shown in Table 4.1, the contributions of this work can be summarised as follows:

- The proposed RTB has reduced the total energy cost by 55%. The RTB reduced the HP load from peak-price period. This is achieved by taking advantage of

Table 4.1: Comparison of results (Figs. 4.5-4.8) with the percentage of improvement.

Cases	Electrical energy cost		Power consumption in peak hours		Increased PV self-consumption	Average temperature	Results
	$	%*	kWh	%*	kWh	°C	
AC without TES (Base case)	1.91	-	1.75	-	-	23.08	Fig. 4.5
AC with RTB and without TES	0.86	55	0.87	50	3.12	22.92	Fig. 4.6
AC with RTB and TES	0	100	0	100	4.4	22.92	Figs. 4.7,4.8

* Percentage of improvement with respect to base case.

building pre-cooling during PV power generation. However, only the proposed RTB has reduced the electricity cost by 55%.

- The MPC has effectively shifted 100% of HVAC load from the peak-load hours. In addition, TES has supplied the thermal load during peak-load period, and TES is totally discharged, as shown in Figure 4.8. The proposed method has successfully minimised thermal losses by charging and discharging TES in same day. The thermal energy may not be required for the next day.

4.8 Conclusion

In this chapter, the first part of RQ2 has been addressed. A thermal energy management strategy has been proposed to address the issue of the variations in rooftop PV power. This issue can cause a mismatch between generation and load demand in smart residential buildings. A real-time temperature boundary strategy based on real-time pricing tariff, is used to shift the heat pump load, thus minimises the operation cost of a smart building and reduces the export energy to the utility. Simulations are performed for residential air-conditioning systems without storage tank, with RTB, and with both storage tank and RTB. The proposed RTB with MPC controller based on RTP has increased the PV self-consumption by 4.4 kWh. It has also decreased the total energy cost by 55%. The RTB has effectively reduced the HP load from peak-price period.

Chapter 5

A Cost-effective Thermal and Electrical Energy Storage Management Strategy for Smart Buildings

This chapter presents an optimal energy management strategy for a model that encompasses heat pump coupled with thermal storage tank, rooftop PV modules, battery energy storage system, and electrical and thermal loads[1]. An integrated home energy management system with an optimal operation schedule is proposed to manage different resources based on time-of-use pricing tariff. This strategy is proposed to minimise the operation cost of a smart building, thus reduce the mismatch between generation and load. Extensive simulation results show the cost benefits and effectiveness of the proposed combined thermal and electrical energy management strategy.

[1]The presented chapter has been published as: **A. Baniasadi**, D. Habibi, W. Al-Saedi and M. A. S. Masoum, "A Cost-effective Thermal and Electrical Energy Storage Management Strategy for Smart Buildings," 2019 IEEE PES Innovative Smart Grid Technologies Europe (ISGT-Europe), Bucharest, Romania, 2019, pp. 1-5. doi: 10.1109/ISGTEurope.2019.8905537

5.1 Introduction

In recent years, the penetration of rooftop PV systems has been increasing in residential networks and commercial buildings. In 2017, small-scale PV systems participated in 20.3% of Australia's clean energy generation. These systems produced 3.4% of the country's total electricity [129]. However, the payback of renewable energy in some countries is insignificant. Load management is an important objective, which can help increase the penetration of renewable energy resources. This objective can be mainly achieved by considering the demand response on flexible loads such as heat pumps and electric vehicles [130], in particular when the customers are able to manage their usage manually or via an automatic system [39]. In fact, in most buildings, more than 40% of the power is consumed for space heating and cooling [118]. Therefore, an optimal energy management strategy is largely required for best utilisation of RESs. This strategy can be used for HPs as heating/cooling suppliers to meet the space heating/cooling, when it is possible. Thus, a significant cost-saving can be achieved while reducing stress on the grid during peak-load hours [79].

Many researchers have presented various strategies to minimise the energy cost of residential buildings with the integration of rooftop PVs and battery storage systems. The authors in [74] focused on HP water heaters to reduce energy cost based on TOU tariff, by utilising an optimal scheduling model. In [119], the authors presented an optimal model to minimise both energy and water consumption. The authors controlled an HP water heater and an instant heater which are integrated with a wind turbine, PV and diesel generator. However, space heating/cooling was not considered in both papers. In [88], end-users can earn additional cost-saving advantages from the thermal energy storage system. This cost-saving is achieved by implementing demand response programs (DRPs) and shift the heat pump load from peak-demand hours to off-peak periods. Ref [90] introduced an optimal demand response strategy to decrease the electricity cost of water heating based on TOU tariff. The authors considered the advantage of TES by assuming the consumption of hot water for a day. Ref [131] presented a a smart control strategy for an optimal integration of PV system, electrical HP and thermal energy storage to reduce electricity cost. However, considering an electrical storage is crucial to obtain maximum benefits from the rooftop PV system. A scheduling approach for an energy system with a battery was proposed in [120]. This approach is employed to

control HVAC systems regarding DRP. The authors in [121] introduced a cost-optimal schedule method. A mixed-integer linear programming optimisation technique is used for the better utilisation of solar energy in buildings. The demand caused by heating and partial thermal storage was investigated in [122]. An optimal thermal storage energy was determined by predicting the heat demand of the building.

This chapter presents a cost-effective approach to minimise the operation cost for smart homes. A model of an integrated home energy management system (IHEMS) is proposed in this work. This system encompasses rooftop PV system, battery and HP coupling with a thermal storage tank (TST) as a controllable load. Colonial competitive algorithm (CCA) is employed to minimise the operation cost. The efficiencies of battery charging and discharging are considered as well as battery charging method. HP coupled with the TST is considered to shift its load towards the low electricity price periods or whenever PV production is available. Furthermore, the occupants' thermal comfort is also taken into account while shifting HP electricity load. The IHEMS model is implemented in Smart Energy laboratory at Edith Cowan University to verify the simulation results.

5.2 Integrated Home Energy Management System Model

As shown in Figure 5.1, the proposed IHEMS model consists of a thermal energy system which includes an HP coupled with a TST, and an electrical energy system, including a battery, rooftop PV and electrical loads. The PV system is modelled in Section 4.2.3. Battery system and thermal energy system are modelled in Sections 5.2.1 and 5.2.2, respectively.

5.2.1 Battery model

The battery power in kW can be calculated as follows:

$$P_{batt,i} = P_{g,i} + P_{PV,i} - P_{HP,i} - P_{hl,i} \tag{5.1}$$

where P_g is the purchased power from grid, P_{PV} is the PV power output, P_{HP} is the HP load, and P_{hl} is the total households' load except HP load (P_{HP}). The efficiency

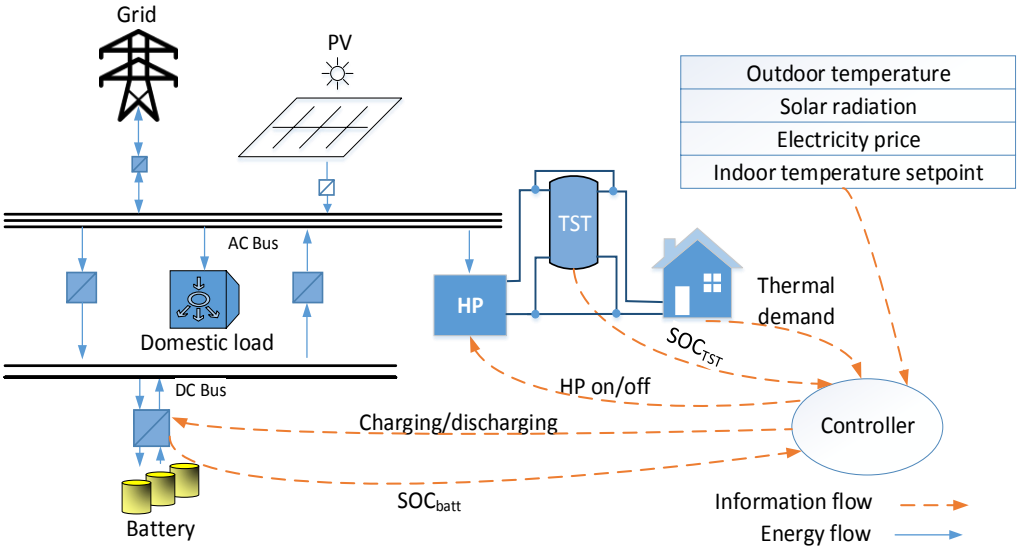

Figure 5.1: Schematic of the residential energy management system.

of the calculated charging (η_{ch}) and discharging (η_{dch}) battery can be considered in the battery energy storage (Ah) equations as follows:

$$E_{batt,i} = E_{batt,i-1} + P_{chbatt,i}\eta_{ch} - (\frac{P_{dchbatt,i}}{\eta_{dch}}) \tag{5.2}$$

$$P_{chbatt,i} = F(SOC_i^{batt}) \tag{5.3}$$

where Equation 5.3 represents the charging pattern which is a function of the battery state of charge (SOC), as a limitation for the charge power (P_{chbatt}). In this chapter, this function is determined by experimental data, and the battery SOC can be expressed as follows:

$$SOC_i^{batt} = \frac{E_{batt,i}}{E_{batt,max}} \times 100 \tag{5.4}$$

where $E_{batt,max}$ is the total stored energy in kWh. Taking into account the SOC limitation ($SOC_{min}^{batt} < SOC_i^{batt} < SOC_{max}^{batt}$).

5.2.2 Thermal energy system model

SELAB building is modelled by the heat dynamic state-space model in Section 3.2.2. The performance efficiency of the HP is represented by Equation 3.4.

The model of thermal-stratified two-layer tank is presented in [115]. Hot and cold water is separated by thermocline layer. In this chapter, TST is introduced in cooling mode to simplify the description of the model. In cooling mode, return water from heat distributor (HD) at temperature (T_w) is placed in the top of TST, while the chilled water produced by HP at temperature T_{HP} is stored in the bottom of TST. TST is connected to the closed-loop system. The total water (m) in TST is equal to the sum of the volume of return water (m_w) and chilled water (m_c), which is $m = m_w + m_c$. The SOC of TST model based on the heat and mass flow balance can be expressed as follows:

$$SOC_i^{TST} = SOC_{i-1}^{TST} + \sum_i \frac{\dot{m}_{HP} - \dot{m}_d}{m} \times 100 \tag{5.5}$$

where $\dot{m}_d$ is the mass water flow rate through the HD, and $\dot{m}_{HP}$ is the mass water flow rate of HP. In this work, constant rates of mass water flow are considered. The cooling energy stored in TST can be calculated as follows:

$$Q_{TST} = m_c c_p (T_w - T_{HP}) \tag{5.6}$$

Most of heat distributors are used to regulate the room temperature by using thermostats. The on-off state of the relay can be determined by the hysteresis control rule as follow:

$$\chi(t+1) = \begin{cases} 0 & \text{if } T_{in}(t) \leq \underline{T}_{in} \\ 1 & \text{if } T_{in}(t) \geq \overline{T}_{in} \\ \chi(t) & \text{otherwise,} \end{cases} \tag{5.7}$$

where the continuous state (T_{in}) is the building temperature, and the discrete state (χ) is the state of the relay, which switches the heat distributor on or off according to the hysteresis control rule.

5.3 IHEMS Formulation

The proposed CC algorithm is applied to manage the thermal and electrical energy systems. The aim is to minimise the operation cost while controlling the building temperature with an acceptable variation in thermal comfort. IHEMS is also employed to control the battery charging/discharging, in order to enhance the integration of the PV system with loads.

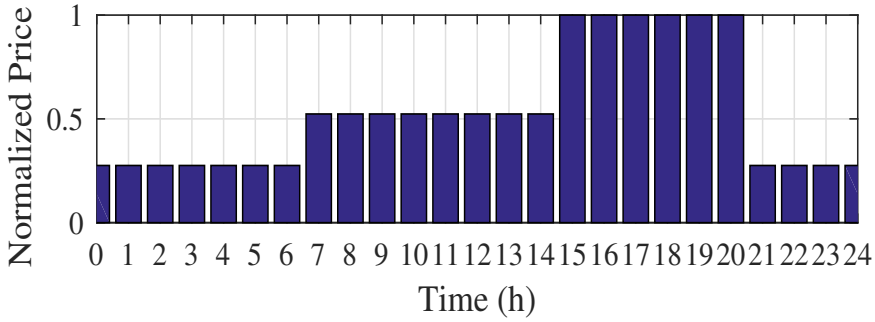

Figure 5.2: Normalised TOU electricity tariff.

5.3.1 Objective function

The objective function is a criterion which is used to evaluate the solution of CC algorithm. This evaluation is based on the minimum operation cost, which is calculated by the following expression:

$$\min \left(\sum_{i} C_{g,i} + \sum_{i} C_{batt,i} \right) \tag{5.8}$$

where

$$C_{g,i} = NP_i \cdot C \cdot P_{g,i} \cdot t \tag{5.9}$$

$$C_{batt,i} = \begin{cases} C_{batt_{om}} P_{batt,i} \cdot t & \text{if } P_{batt,i} \geq 0 \\ -C_{batt_{om}} P_{batt,i} \cdot t & \text{if } P_{batt,i} < 0 \end{cases} \tag{5.10}$$

where C_g is the total cost of grid power, C_{batt} is the total cost of battery, and $C_{batt_{om}}$ is the cost of battery operation and maintenance ($cent/kWh$). C is the peak TOU electricity price ($cent/kWh$), and NP is the normalised TOU tariff, as is shown in Figure 5.2 [132]. Prices are normalised based on the maximum electricity price in peak-hours.

5.3.2 Energy balance constraints

The model is proposed to supply the electrical and thermal demands without violating the thermal comfort. Therefore, the electrical energy balance can be written as:

$$P_{g,i} + P_{PV,i} - P_{batt,i} - P_{HP,i} - P_{hl,i} = 0 \tag{5.11}$$

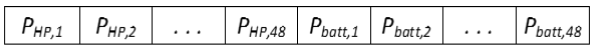

Figure 5.3: A Country (population) of variables for CCA.

where $P_{batt,i}$ is negative in discharging mode and positive in charging mode. The constraint of thermal energy balance can be expressed as follows:

$$Q_{HP,i} + Q_{TST,i} - Q_{hd,i} = 0 \tag{5.12}$$

where $Q_{TST,i}$ is positive in discharging mode and negative in charging mode.

5.3.3 Colonial Competitive Algorithm (CCA)

CCA is an evolutionary optimisation algorithm, which is inspired by imperialistic competition [133]. Similar to other evolutionary algorithms, CCA should be initialised to start the search process. Each individual in the first generation of CCA is called Country. According to the cost function, the algorithm countries can be classified into two groups: Imperialist for low cost or more power of countries, and Colonies for vice versa. Imperialist dominates Colonies based on their countries power, thus generates an empire. The Country dimensions are determined by the number of decision variables. In this chapter, P_{HP} and P_{batt} are two decision variables based on Equations 5.8-5.10, in each time step i. The time step is 0.5 hour, and IHEMS is implemented for 24 hours with two variables. Therefore, the dimension of the optimisation problem is 96 ($N = 24\times2\times2$). Figure 5.3 shows Country with the decision variables of the optimisation problem.Figure 5.4 shows the proposed IHEMS structure.

5.4 Simulation and Experimental Results

In this chapter, SELAB building is used as smart residential building. Figure 5.5 shows SELAB building, which is used to implement and test the proposed IHEMS. The thermal system consists of 1000 litre stainless steel TST with 100 mm insulation layer, and water source HP with 7.1 kW cooling capacity (1.92 kW power consumption) and 10.3 kW heating capacity. The electrical system consists of 12 series mono-crystalline PV

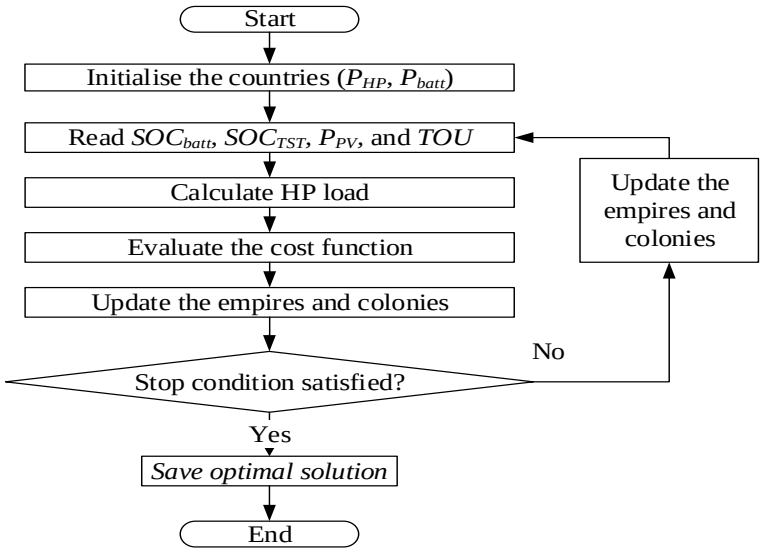

Figure 5.4: Flowchart of proposed IHEMS structure.

modules each with the rate of 285 W , which produce 3.4 kWp, 6 series poly-crystalline PV modules each with the rate of 250 W, which deliver 1.5 kWp, and $4 \times 12V$ series lead-acid battery modules MP12200 GEL CELL with nominal voltage $48V$ and total capacity of 4.8 kWh. All home appliances, except the HP, are modelled as uncontrollable loads.

The thermal demand of the SELAB building is calculated based on weather condition. Figures 5.6 and 5.7 show the building temperature control results including ambient temperature, solar irradiation, building temperature and heat distribution signal for a typical hot day in summer and a typical cold day in winter, respectively. Note that the building temperature are kept in thermal comfort zone (22 - 24 $^{\circ}C$). The simulation results have described the system performance for a typical day in summer and winter. The simulations are carried out for the following two scenarios.

- Scenario I: HP is considered as an uncontrollable load. Thus, the proposed IHEMS is used to minimise the utility bill by controlling the amount of buying/selling electricity from/to the grid.
- Scenario II: IHEMS is applied to the entire system which consists of HP coupling with TST as controllable load and battery storage. The building temperature is

Figure 5.5: SELAB at Edith Cowan University, Western Australia.

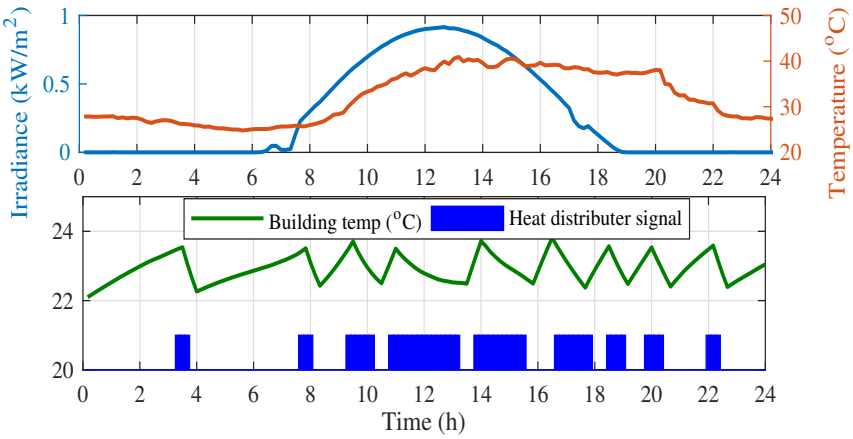

Figure 5.6: Building temperature control result of one day in summer.

maintained within a desirable temperature range. In this case, IHEMS is implemented to control the HP consumption to maximise the utilisation of PV production, and minimise the electricity bill by buying the grid power in off-peak periods.

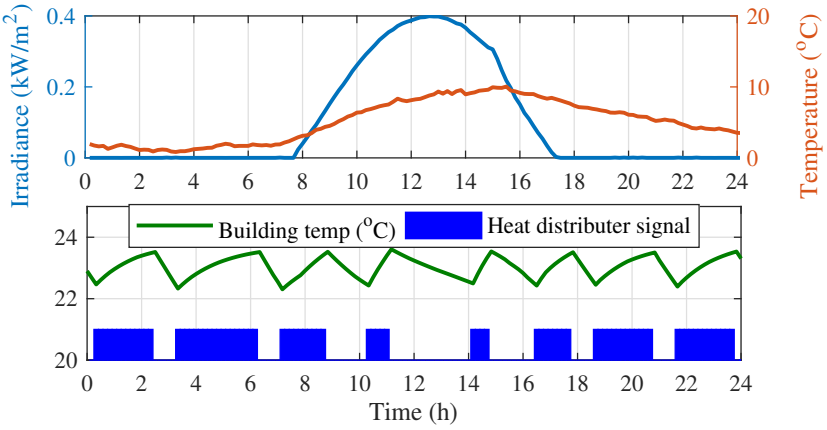

Figure 5.7: Building temperature control result of one day in winter.

Figures 5.8 and 5.9 show the results of scenario I for a typical day in summer and a typical day in winter, respectively. IHEMS has targeted the grid power and battery charging and discharging. In scenario I, the algorithm is used to import the grid power in low price tariff periods to charge the battery. However, the surplus PV output power is used to charge the battery by following charging pattern. The charging rate is decreased, while the SOC is increased. As shown in Figure 5.9, due to uncontrollable HP load and insufficient PV output power, the algorithm has responded to purchase power from the grid during peak-price tariff, thus avoid deep battery discharge.

In scenario II, the proposed algorithm has shifted the HVAC load based on TOU tariff, SOC of TST, and battery SOC. Figures 5.10 and 5.11 show the HP control results for a day in summer and winter, respectively. In summer, HP has produced chilled water to supply the thermal load and stored in TST. According to SOC of TST, HP is worked in midday, when PV power is available to increase the SOC of TST (see Figures 5.10-5.11). The thermal demand is then supplied by TST during peak-load hours. The majority of the thermal demand is in midday and evening, as shown in Figure 5.6. In winter, HP has delivered hot water to meet heat demand in midnight directly, and charged TST in early morning. Then TST supplies the thermal demand in high price period in evening. Figures 5.12 and 5.13 depict the IHEMS results of scenario II for a day in summer and winter, respectively.

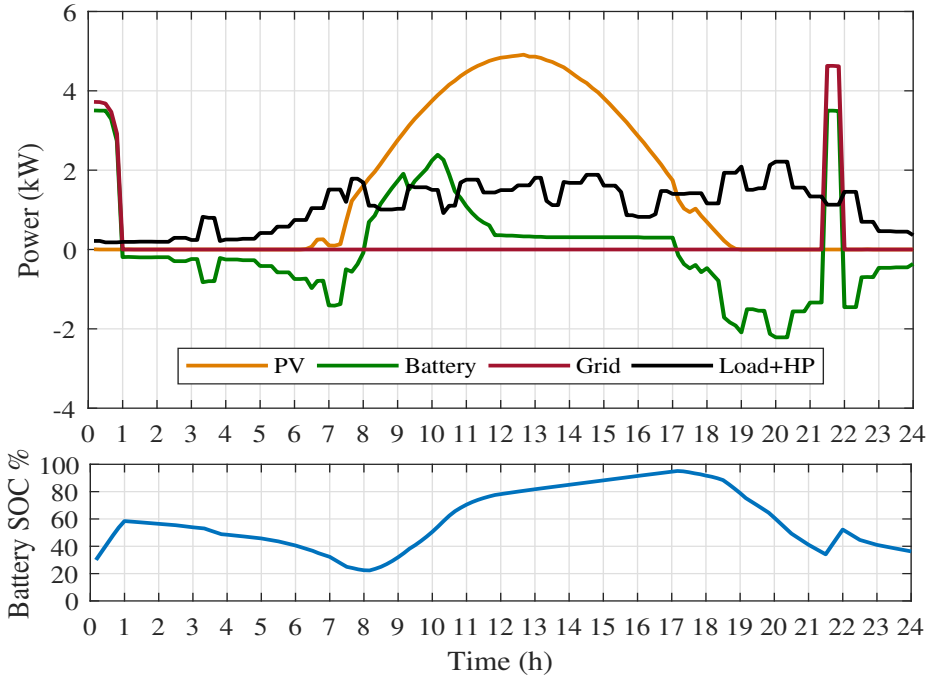

Figure 5.8: IHEMS results of day in summer without DR program on HP (scenario I).

5.5 Results Discussion

Figures 5.8-5.9 and 5.12-5.13 show the results of the system performance of a day in summer and winter for both scenarios (I and II). In scenario II, the proposed IHEMS has reduced the daily energy cost by 44.2% for the day in summer and 18.3% for the day in winter, in comparison to scenario I. Meanwhile, it has effectively reduced 2.3 kWh of the importing power from the grid in the summer day, and 0.3 kWh in the winter day. Table 5.1 summarises the annual results for both scenarios I and II, in case of importing power from the grid and exporting power to the grid as well as the electricity bill based on TOU tariff.

5.6 Conclusion

An IHEMS has been proposed and tested for economic operation of smart buildings and homes. This system consists an HP coupled with a TST, battery storage and a rooftop PV system. The aim of using HP is to minimise operation costs and maximise

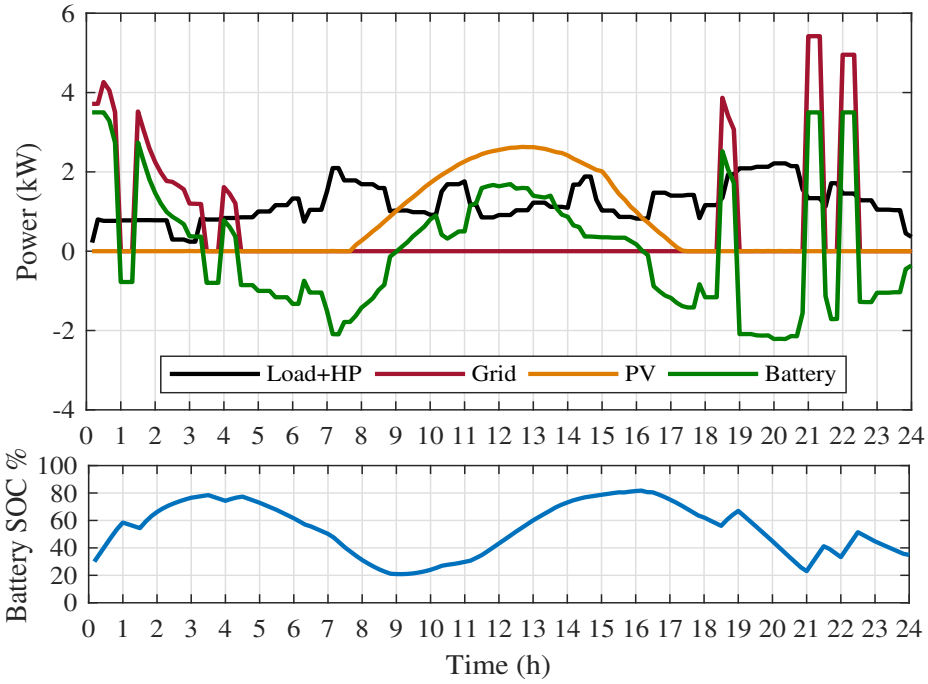

Figure 5.9: IHEMS results of day in winter without DR program on HP (scenario I).

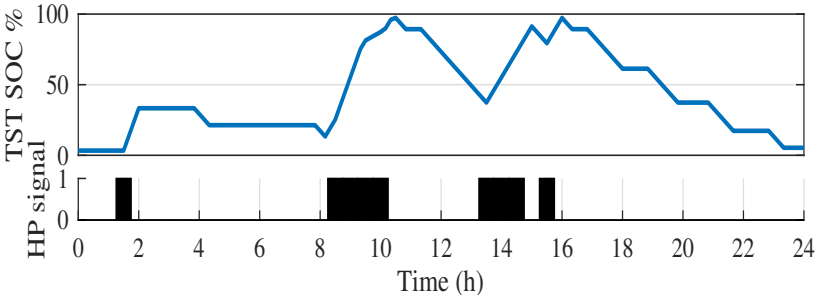

Figure 5.10: HP signal and TST SOC for day in summer.

Table 5.1: Annual results for scenarios I and II with the percentage of improvement (reduction) respect to scenario I.

	Scenario I	Scenario II	%
Electrical energy cost ($)	1159.5	718.2	38.05
Importing power from grid (kWh)	3865.2	3588.4	7.16
Exporting power to grid (kWh)	3960.7	3756.1	5.16

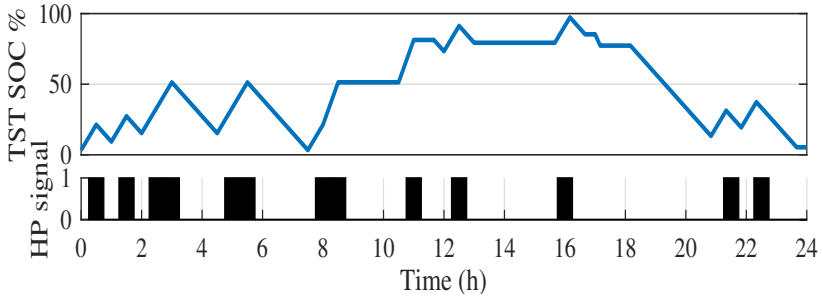

Figure 5.11: HP signal and TST SOC for day in winter.

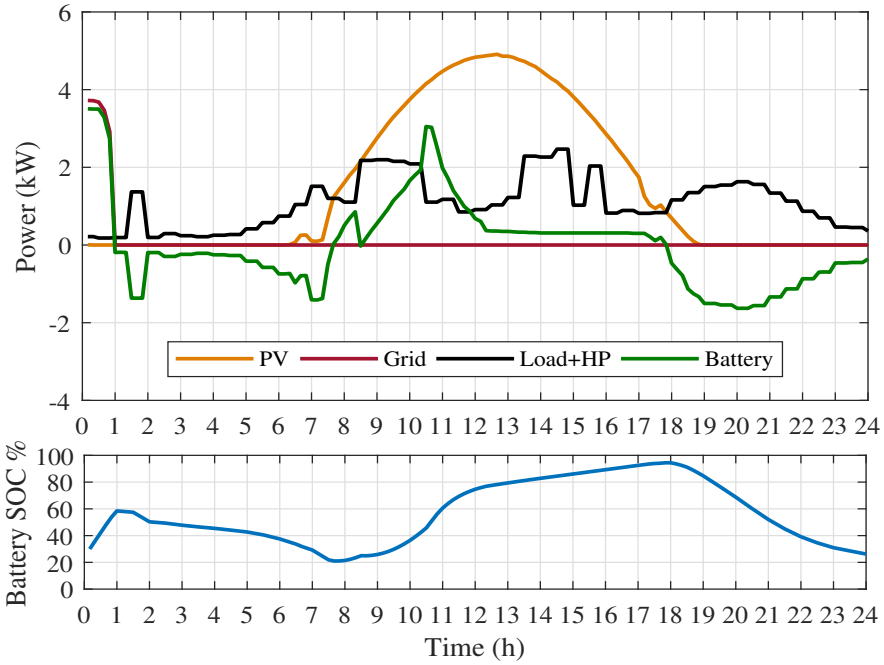

Figure 5.12: IHEMS results of day in summer with DR program on HP (scenario II).

the use of PV power. The battery charging strategy and battery efficiency are taken into account. The comparison of two scenarios indicates that an optimal schedule for the electrical and thermal storage systems has successfully achieved, thus reduced the operation costs of the system. The simulation results prove that the proposed IHEMS has effectively decreased the imported power from the grid by maximising the use of PV power.

Every part of RQ2 has been addressed in Chapters 4 and 5. In this chapter, the

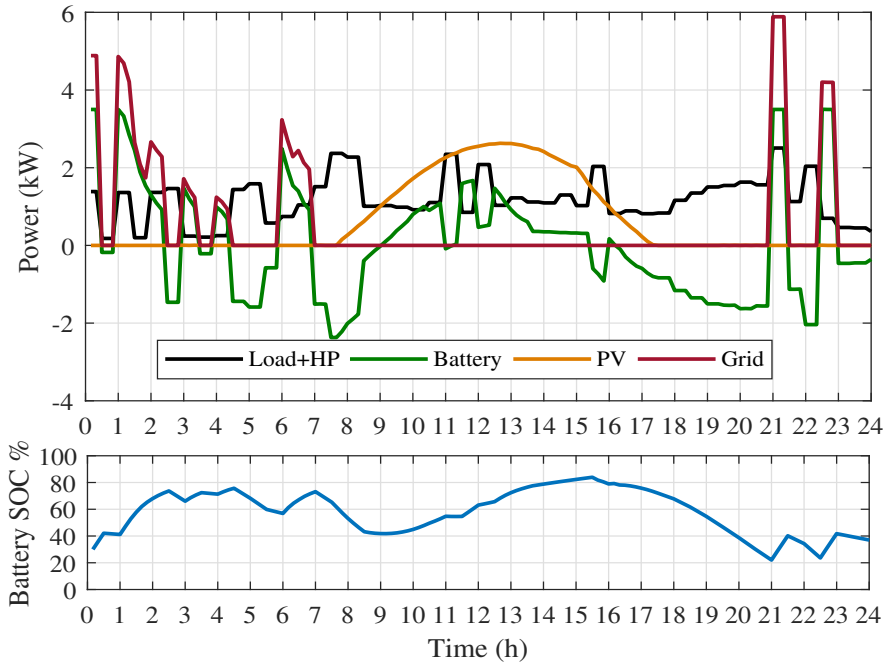

Figure 5.13: IHEMS results of day in winter with DR program on HP (scenario II).

second part of RQ2 has been addressed by applying a colonial competitive algorithm to manage the thermal and electrical energy systems in order to minimise the operation cost while controlling the building temperature with an acceptable variation in thermal comfort. IHEMS is also employed to control the battery charging/discharging, in order to enhance the integration of the PV system with loads.

Chapter 6

Optimal Sizing and Operation of Electrical and Thermal Energy Storage Systems in Smart Buildings

PV systems in residential buildings require energy storage to enhance their productivity. However, in present technology, battery storage systems are not the most cost-effective solutions. Comparatively, thermal storage systems can provide opportunities to enhance PV self-consumption while reducing life cycle costs. In this chapter, a new framework has been proposed for optimal sizing design and real-time operation of energy storage systems. The proposed framework is used for residential buildings that equipped with a PV system, heat pump, thermal and electrical energy storage systems[1]. For simultaneous optimal sizing of BSS and TSS, a particle swarm optimisation algorithm is implemented to minimise daily electricity and life cycle costs of the smart building. A model predictive controller is then developed to manage the energy flow of storage systems in order to minimise electricity costs for end-users. The main objective of the proposed controller is to optimally control HP operation and battery charge/discharge actions based on a

[1]The presented chapter has been published as: **A. Baniasadi**, D. Habibi, W. Al-Saedi, M. A. S. Masoum, C. K. Das, and N. Mousavi, "Optimal Sizing Design and Operation of Electrical and Thermal Energy Storage Systems in Smart Buildings" **Journal of Energy Storage**, 2020 Apr 1;28:101186.

demand response program. The controller can regulate the flow of water in the storage tank to meet the designated thermal energy requirements, by controlling HP operation. Furthermore, the power flow of battery is controlled to supply all loads during peak-load hours to minimise electricity costs. The results in this chapter demonstrate to rooftop PV system owners that investment in combined TSS and BSS can be more profitable as this system can minimise life cycle costs. The proposed methods for optimal sizing and operation of electrical and thermal storage system has reduced the annual electricity cost by more than 80% with over 42% reduction in the life cycle cost. Simulation and experimental results are presented in this chapter to validate the effectiveness of the proposed framework and controller.

6.1 Introduction

PV system is one of the top-ranked renewable resources in many countries such as USA, China, Japan, India, and Australia. In 2017, the global installed (on-grid and off-grid) PV capacity reached 98 GW, which is nearly one-third of the total 402 GW load [77]. However, the renewable energy buyback rate is expected to significantly drop in the near future. This buyback price reduction is due to power system challenges, such as frequency regulation, reverse power and voltage imbalance issues, which are caused by high PV penetration. A potential solution that may be beneficial for both end-users and utilities is to increase PV self-consumption. This can be efficiently achieved by using energy storage systems and residential flexible loads such as heat pumps and electric vehicles [39, 78]. Energy storage systems are frequently being applied to address various issues of RES-penetrated power networks. A comprehensive review of various energy storage systems is presented in [51].

Accordingly, residential customers can reduce their electricity costs by capitalizing their dispatched power. This can be done by: i) optimizing the capacities of renewable energy resources and energy storage systems, ii) utilizing HPs and HVAC systems coupled with thermal energy storage systems, and iii) implementing demand response programs to spread the HP load throughout the day based on electricity price tariffs and the availability of RESs [79, 80]. In Australia, residential end-users have moved to install rooftop PV systems to reduce electricity bills. However, they still have to pay for

electricity due to high electricity prices during peak-load hours when PV production is not sufficient. The practical solution is to implement demand response programs, flexible loads, and energy storage systems to take full advantage of PV power production.

Electrical storage systems (e.g., Lead-acid and Li-ion batteries) have limitations such as short lifespan, the limited number of cycles, and high initial cost. These limitations may make them unaffordable for most applications [81, 134]. Comparatively, thermal storage systems [51] and pumped-hydro storage systems [134, 135] are eco-friendly options that can provide more sustainable solutions. More importantly, TSSs can make HVAC systems flexible with suitable responses to time-varying electricity prices. Hence, a combination of TSSs and electrical storage systems would provide more economical and eco-friendly solution compared to utilisation of only electrical storage systems. Therefore, the motivation of this study is to provide a low-cost solution to end-users with low environmental impact, when using TSSs and battery storage systems for energy management applications.

Many researchers have focused on finding optimal component sizes of RES and storage systems for smart buildings. Some papers have applied flat electricity tariffs or average load as input data to find the optimal sizes of RESs and electrical energy storage [84, 85]. Most publications rely on simple charging algorithms [86, 87]. Recent research has considered optimal battery charging and discharging in their sizing strategies. However, the effect of flexible loads such as HPs and HVAC systems on RES and BSS sizes as well as PV self-consumption has not been investigated.

Accordingly, there is a research gap in developing effective sizing strategies for HPs coupled with TSS to respond to DRP while minimising life cycle cost. Therefore, the key goals of this chapter are first to find the optimal sizes of TSS and BSS based on TOU tariff to increase PV self-consumption. Second is to develop a management strategy to decrease the electricity cost of the residential buildings, after determining the optimal BSS and TSS sizes. The well-known heuristic PSO approach is applied to find optimal size for the thermal and electrical storage components. MCS is implemented to generate a set of random inputs using their probability density functions. After determining optimal BSS and TSS sizes, MPC is applied for real-time optimal operation of smart buildings.

The contributions of this research can be summarised as follows:

- A new optimal BSS and TSS sizing (OBTS) solution is proposed for thermal and electrical storage systems in order to minimise annual electricity costs of smart buildings with rooftop PVs while minimising the life cycle cost. Optimal BSS and TSS charging and discharging are key elements of the proposed OBTS that is considered in the optimal sizing. These elements have not been widely considered together by other researchers to determine the optimal TSS and BSS sizes. Furthermore, cost comparison for various case studies is presented.

- A control scheme is developed for a real-time smart building energy management system (SBEMS) to increase PV self-consumption and reduce electricity costs. The real-time charging and discharging of BSS and TSS are achieved by using the proposed SBEMS based on RTP.

- The proposed SBEMS is experimentally verified in a real-time environment using the available facilities in the Smart Energy Laboratory at Edith Cowan University, Australia. Furthermore, different sizes of BSS and TSS are applied to verify the results of proposed OBTS.

6.2 System Model

In this study, MCS is implemented in the proposed optimal BSS and TSS sizing (OBTS) strategy, to consider uncertainties associated with weather data such as solar radiation and ambient temperature. The uncertainties in weather prediction are described in MCS using the proper probability distribution functions (PDFs). The one-year weather data record is used as the input data for MCS. The daily inputs with 10-min discrete time steps for optimisation are then generated based on the daily recorded data. These data sets are sent to PV and building thermal models, to predict PV production and the thermal load profile of residential buildings. Then, the system model is described in two parts, the electrical system model and the thermal system model.

6.2.1 Electrical system model

Electrical loads can be incorporated with the base and HP loads as shiftable loads. In this work: i) the household appliances such as lighting, refrigerators, freezers, ovens, stoves and computers are considered as the base loads, ii) the input data for generating daily load profile by MCS is provided in [136] and, iii) the SELAB building at Edith Cowan University in Western Australia with an average daily power consumption of 18 kWh is selected as the residential building. PV system is modelled in Section 4.2.3.

Battery models are mainly determined by their charging and discharging limitations. The stored energy in battery for each time step can be calculated as:

$$E_{t+1}^{batt} = E_t^{batt} + P_{ch,t}\eta_{ch} - \frac{P_{dch,t}}{\eta_{dch}} \tag{6.1}$$

where η_{ch} and η_{dch} represent the efficiency during charging and discharging modes, respectively. Then, the battery state of charge can be expressed as:

$$SOC_{t+1} = \frac{E_{t+1}^{batt}}{E_{max}^{batt}} \times 100 \tag{6.2}$$

$$SOC_{min} < SOC_t < SOC_{max} \tag{6.3}$$

where E_{max}^{batt} is the maximum stored energy (kWh). An additional constraint is added to avoid the simultaneous charging and discharging:

$$P_{ch,t} \cdot P_{dch,t} = 0 \tag{6.4}$$

The depth of discharge (DOD) can be modelled by [137]:

$$E_t^{batt} \geq C_{batt}(1 - DOD) \tag{6.5}$$

where C_{batt} represents the size of BSS.

6.2.2 Thermal system model

In most buildings, air conditioners, radiators and fan coil units are employed to regulate room temperature by using thermostats. The state of the on/off relay can be

determined by the hysteresis control rule in cooling mode as follow [138]:

$$\mathbb{U}_{t+1} = \begin{cases} 0 & \text{if } T_{in,t} \leq \underline{T}_{in} \\ 1 & \text{if } T_{in,t} \geq \overline{T}_{in} \\ \mathbb{U}_t & \text{otherwise,} \end{cases} \tag{6.6}$$

where T_{in} is the indoor temperature which is function of outdoor temperature, solar radiation, internal heat gain, and building thermal mass. $\overline{T}_{in}$ and $\underline{T}_{in}$ are upper and lower boundaries of temperature set-point. $\mathbb{U}$ is the discrete state of the relay which switches the heat distributor on and off; according to the hysteresis control rule.

The Smart Energy laboratory building is modelled by the heat dynamic state-space model of [64] and [113] as follows:

$$\begin{bmatrix} \dot{T}_l \\ \dot{T}_{in} \end{bmatrix} = \begin{bmatrix} -\frac{1}{R_{in}C_l} & \frac{1}{R_{in}C_l} \\ \frac{1}{R_{in}C_{in}} & -(\frac{1}{R_{io}C_{in}} + \frac{1}{R_{in}C_{in}}) \end{bmatrix} \begin{bmatrix} T_l \\ T_{in} \end{bmatrix} + \begin{bmatrix} 0 \\ \frac{1}{C_{in}} \end{bmatrix} \mathbb{U}\dot{Q}_{td} + \begin{bmatrix} 0 & 0 & 0 \\ \frac{1}{R_{io}C_{in}} & \frac{\lambda}{C_{in}} & \frac{1}{C_{in}} \end{bmatrix} \begin{bmatrix} T_o \\ I_s \\ I_g \end{bmatrix} \tag{6.7}$$

where ideally $T_{TSS} = T_{HP}$, thus $\dot{Q}_{td} = \dot{m}_{td}c_p(T_{TSS} - T_{return})$. The model parameters are identified utilising a nonlinear regression algorithm by measuring T_{in}, T_o, I_s, I_g, and Q_{td} [79]. The building model is presented and validated in Chapter 3.

The daily thermal demand is calculated based on the building model of Equation (6.7). In each time step, the updated indoor temperature ($\dot{T}_{in}$) and building lumped thermal mass temperature ($\dot{T}_l$) are calculated based on the present temperatures, solar radiation, outdoor temperature, and heat gain. The calculated temperatures (Equation (6.6)) are used to determine the ON/OFF state of the heat distributor switch. When the heat distributor is ON, the required thermal energy is assumed to be $\dot{Q}_{td}$.

6.2.2.1 Heat pump model

The heating/cooling capacity of an HP ($\dot{Q}_{HP}$) can be calculated based on the flow rates and temperatures of water inlet and outlet of HP as well as the coefficient of

performance (COP) [53] as follows:

$$\dot{Q}_{HP} = \dot{m}_{HP} c_p (T_{HP} - T_{return}), \quad \text{COP} = \frac{\dot{Q}_{HP}}{P_{HP}} \tag{6.8}$$

In this study, a minimum runtime of 10 minutes is considered for HP, and the installed HP at the SELAB building is considered for the proposed model. HP is a ground source heat pump. Figure 6.1 shows the schematic of heat transfer of the HP. The heat transfer equations in heating and cooling are as follows:

$$\dot{Q}_{HP} = P_{HP} + \dot{Q}_e \tag{6.9}$$

$$\dot{Q}_{HP} + P_{HP} = \dot{Q}_e \tag{6.10}$$

where $\dot{Q}_{HP}$ is determined by consumed power by the compressor and the heat taken (given) from (to) the environment ($\dot{Q}_e$).

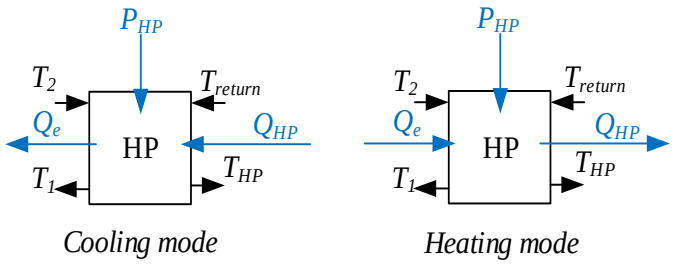

Figure 6.1: Heat transfer for HP system.

The COP depends on temperature difference between external source and internal source. The characteristics of COP can be explained by ideal Carnot heat pump cycle [139] as follows:

$$COP_h = \eta \cdot \frac{(T_e - \delta T)}{(T_{HP} + \delta T) - (T_e - \delta T)} + 1 \tag{6.11}$$

where $\eta = 0.55$ is the Carnot efficiency, δT is the temperature difference of the heat exchangers ($\delta T = 5^oC$), and T_e is the ground temperature which is 16^oC in WA.

The modelled HP is a single-phase ground source heat pump from Mammoth [140]. The HP model is MSR L024H. HP technical data are taken from the manufacturer datasheet ([140]) to evaluate the HP performance and power consumption.

6.2.2.2 Thermal storage system (TSS) model

TSS is modelled based on the stratified two-layer tank. Figure 6.2 shows the scheme of thermal system in cooling mode. As TSS is involved to the closed-loop system, the sum of the volume of return water (m_{return}) and chilled/hot water (m_{TSS}) is always constant and equal to the volume of TSS (m_{tot}):

$$m_{tot} = m_{TSS} + m_{return} \tag{6.12}$$

The dynamics of TSS system can be expressed by the change in volume (m_{TSS}) and temperature of the chilled/hot water layer of TSS (T_{TSS}). This model can be simplified by neglecting losses to the surrounding area. Therefore, based on the heat and mass flow balance concept, the TSS model can be described by the following first-order non-linear differential equation [79]:

$$\frac{\mathrm{d}m_{TSS}}{\mathrm{d}t} = \dot{m}_{HP} - \dot{m}_{td} \tag{6.13}$$

On the other hand, the product rule derivative of equation (3.8) is given by:

$$\frac{\mathrm{d}Q_{TSS}}{\mathrm{d}t}(m_{TSS},T_{TSS}) = c_p(\frac{\mathrm{d}m_{TSS}}{\mathrm{d}t} \cdot T_{TSS} + m_{TSS} \cdot \frac{\mathrm{d}T_{TSS}}{\mathrm{d}t}) \tag{6.14}$$

In charging mode ($\dot{m}_{HP} > \dot{m}_{td}$), a constant mass water flow rate is considered which is $\dot{m}_{HP} > \dot{m}_{td}$. Consequently, TSS is always charged and $T_{td} = T_{HP}$ since the HP is operating. Therefore, the following equation can be derived from Equations (3.8) and (6.14):

$$\frac{\mathrm{d}m_{TSS}}{\mathrm{d}t} \cdot T_{TSS} + m_{TSS} \cdot \frac{\mathrm{d}T_{TSS}}{\mathrm{d}t} = (\dot{m}_{HP} - \dot{m}_{td})T_{HP} \tag{6.15}$$

Subsequently, the temperature derivative of the bottom layer water at each time step can be expressed by substituting Eq. (6.13) into (6.15):

$$\frac{\mathrm{d}T_{TSS}}{\mathrm{d}t} = \frac{(\dot{m}_{HP} - \dot{m}_{td})(T_{HP} - T_{TSS})}{m_{TSS}} \tag{6.16}$$

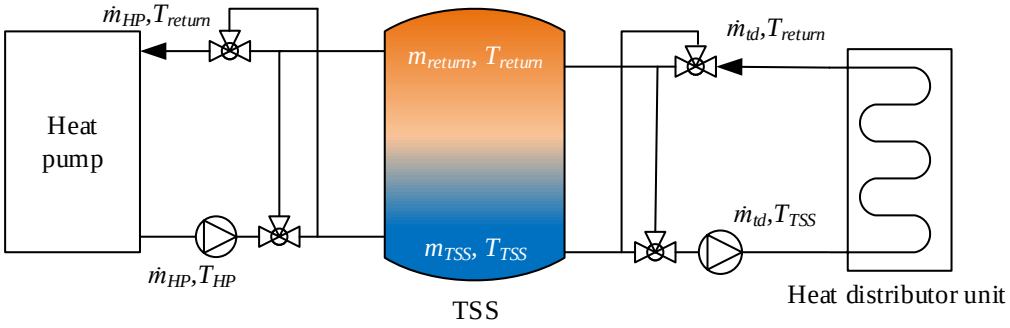

Figure 6.2: Scheme of thermal system (in cooling mode).

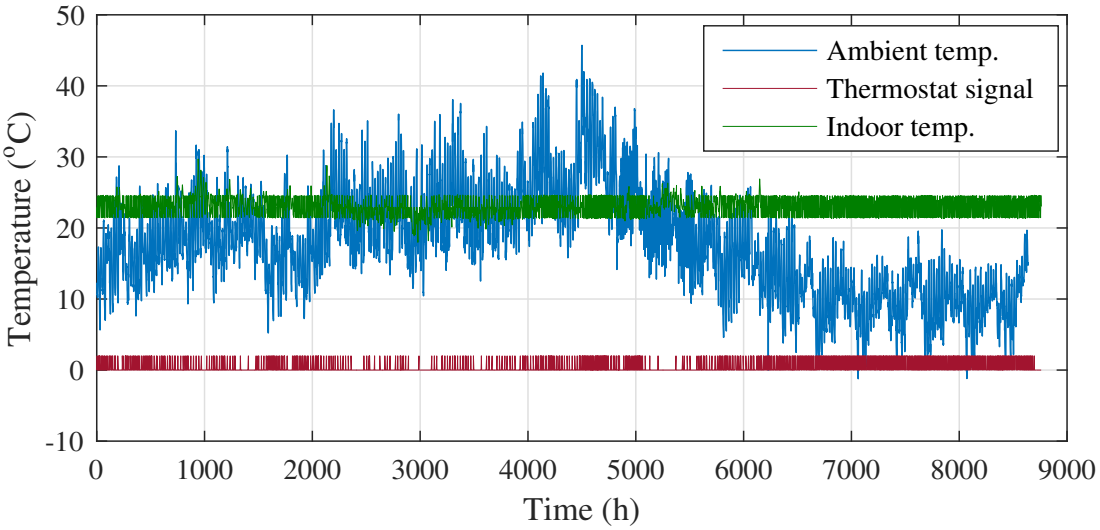

Figure 6.3: Thermostatic control simulation result.

Figure 6.3 shows the thermostatic control simulation result based on the annual ambient temperature data for Western Australia and SELAB building thermal model. The indoor temperature is kept within 22-24^oC. This simulation result verifies the model of thermal system.

6.3 Formulation of Optimum Design Problem

The system model presented in Section 6.2 is used to formulate and implement the proposed OBTS and SBEMS. The aim of this work is to design an optimal model for a smart home. This model encompasses rooftop PV, battery and HP system coupled with TSS. The sizes of battery and thermal storage tank are optimised considering the cost which is associated with the initial investment of each component, operation, maintenance, equipment replacement, and electricity purchase. Then, the proposed SBEMS is employed for the real-time management of the physical system which composed the smart building based on the optimal sizes of TSS and BSS.

6.3.1 Formulation of proposed OBTS

OBTS is presented with inner and main optimisation loops. These two loops are described in Sections 6.3.1.1 and 6.3.1.2.

6.3.1.1 Inner optimisation loop

Inner optimisation loop is proposed here to manage the thermal energy system. Thus, operation costs can be reduced, while the building temperature is within the thermal comfort zone. The inner loop is also used to control the battery charging/discharging to enhance the integration of the PV system with loads, based on TOU tariff.

During the peak and flat periods, the battery is charged by the surplus PV output power. Besides, the charging can also be performed over the night period to store enough energy. The load is supposed to cover first by the PV system, when it has a sufficient output power. While the redundant power is used to charge the battery, or it can be sent to the utility grid. Conversely, the battery is discharged, when the PV power is not enough to meet the load. The discharging continues until the minimum level of the SOC. Meanwhile, the power shortage is covered by purchasing power from the grid.

The objective function is used to minimise electricity costs with the aim of the most effective utilisation of PV generation. In this study, the objective function can be expressed as follows:

$$\min \quad \sum_{m} C_{g,m} \tag{6.17}$$

where

$$C_{g,m} = C_m \cdot P_{g,m} \tag{6.18}$$

Equation (6.17) is subject to:

$$m_{TSS}^{min} \leq m_{TSS} \leq m_{TSS}^{max} \tag{6.19}$$

$$P_{g,m} + P_{PV,m} + P_{dch,m} - P_{ch,m} - P_{HP,m} - P_{hl,m} = 0 \tag{6.20}$$

$$Q_{HP,m} - Q_{TSS,m} - Q_{td,m} = 0 \tag{6.21}$$

where C_m is the time-of-use electricity pricing tariff ($\$/kWh$), as described in Table 6.1 [132]. $Q_{TSS,m}$ represents the charging mode of TSS. The stored thermal energy is consumed on the same day and m_{TSS} reaches the initial stored thermal energy $m_{TSS,0}$ at the end of day. Note that the TSS model is simplified to reduce the complexity of solution. In proposed OBTS, it is assumed that HP can generate chilled/hot water at the required temperature. Therefore, TSS is modelled based on inlet and outlet water of TSS based on equation (6.13).

Table 6.1: Time-of-use electricity pricing tariff for Western Australia.

Time of day	Price ($)
7am-3pm	0.287
3pm-9pm	0.548
9pm-7am	0.151

6.3.1.2 Main optimisation loop

The main optimisation loop is incorporated to investigate the effect of the PV self-consumption system on BSS and TSS sizes for residential buildings. Accordingly, BSS and TSS sizes are determined by the end of this loop. The objective function of this loop is proposed to calculate the LCC of the system. Thus, optimal sizes are determined for minimum cost. The objective function of this loop is:

$$\min \quad \sum LCC \tag{6.22}$$

where

$$LCC = CC_{TSS} + CC_{BSS} + \sum_{y=1}^{Y} \frac{MC_{TSS} + MC_{BSS} + RC_{BSS} + (1+i)^y \sum_{d=1}^{365} C_{g,d}}{(1+l)^y} \tag{6.23}$$

In equation (6.23), y is the year of operation of the system, Y is the planned project lifetime, i is the expected annual energy price increase (inflation) during the project lifetime, and l is discount rate.

6.3.1.3 Constraints of main optimisation loop

Limitation of BSS and TSS: A fixed typical rooftop PV size of 5 kWp is used in this work. The limitations of BSS and TSS depend on the physical parameters of the residential building. Therefore, the battery and TSS are used as follows:

$$0 \leq m_{TSS} \leq 3000 \ L \tag{6.24}$$

$$0 \leq C_{batt} \leq 10 \ kWh \tag{6.25}$$

Life Cycle Cost of Thermal Storage System: The number of on/off HP cycles are reduced for higher TSS volumes. However, when the capacity of the tank is increased, the tank thermal losses and the initial capital cost will also increase. Therefore, the thermal losses of tank are compensated by energy-saving which is caused by the reduction of

Table 6.2: Number of full cycles based on depth of discharge [4].

DOD	10	20	30	40	50	60	70	80	90	100
N_{tot}	43000	35000	27500	20000	15000	10000	6250	3200	2700	2600

HP cycling losses. On the other hand, the stored chilled/hot water in TSS is produced and consumed on the same day. This constraint is to minimise thermal losses of TSS. Hence, the life cycle cost of TSS is determined by the initial capital cost (CC_{TSS}) and the maintenance cost (MC_{TSS}). The minimum lifetime of the water storage tank is 25 years. Therefore, the replacement cost of TSS is not considered in this work.

Life Cycle Cost of Battery Storage System: The charging and discharging cycles of the BSS is usually reduced due to battery degradation. The rate of this degradation largely depends on battery (calendar and cycle) aging, as well as the current state of life [141]. Therefore, the age of the battery is mainly determined by the number of cycles and time. The expected number of cycles (before the end of battery life) is often mentioned by manufacturers. The rain-flow-counting method is used to determine the number of cycles and subsequently the lifetime of BSS. The lifetime of the battery based on DOD is described [142] as follows:

$$L_{BSS} = \sum_{DOD=0.1}^{DOD=0.8} \frac{N_{cyc}(DOD)}{N_{tot}(DOD)} \tag{6.26}$$

where N_{cyc} is the number of full cycles in the specified DOD, and N_{tot} is the maximum number of full cycles based on DOD. The end of battery life with different DOD cycles is when $L_{BSS} = 1$. Table 6.2 shows the number of full cycles N_{tot} versus DOD [4].

This work considers battery degradation costs within the operational and maintenance costs (MC_{BSS}). The replacement cost of battery (RC_{BSS}) should be considered in addition to battery operation and maintenance costs. Table 6.3 shows the costs which associated with initial capital costs of BSS (CC_{BSS}) and TSS, as well as replacement and maintenance costs. CC_{BSS} represents the capital cost which associated with the battery and its inverter.

Table 6.3: Costs associated with BSS and TSS.

CC_{TSS}	MC_{TSS}	CC_{BSS}[143]	RC_{BSS}	MC_{BSS}
100 \$/100L	1 \$/100L	850 \$/kWh	850 \$/kWh	2% of CC_{BSS}

6.3.1.4 Proposed optimisation approach

Figure 6.4 shows the proposed OBTS structure. The PSO algorithm is used as the main optimisation tool to minimise the LCC of the system. PSO is a heuristic algorithm for solving complex optimisation problems by a population (swarm) of named particles [144]. Each particle is a vector which consists of N decision variables and defines a position of the search space. During the iterations, each particle moves randomly based on the swarm's experience and its own best knowledge. Note that each particle moves toward the location of the current global best position (*pbest*) and the group's best experience (*gbest*). This process is repeated until the termination criterion is reached. In each iteration (t), the updating pattern of particles is given by:

$$v_j(t+1) = w(t) \times v_j(t) + c_1 \times r_1(pbest_j(t) - x_j(t)) + c_2 \times r_2(gbest_j(t) - x_j(t)) \quad (6.27)$$

$$x_j(t+1) = v_j(t+1) + x_j(t) \qquad (t = 1, 2, ..., t_{max}) \quad (6.28)$$

where x_j and v_j are the position and the velocity of jth particle, respectively. j is the index of particle ($j = 1, 2, ..., N_p$), N_p is the size of particle, r_1 and r_2 represent uniform random numbers between 0 and 1 which are independently generated for each particle in each update, c_1 and c_2 represent learning factors which are usually between 0 and 2, t_{max} is the maximum iteration times, and w is the inertia constant.

PSO is applied to simultaneously determine the BSS and TSS sizes, while optimising the operations of battery and HP. Integer variables such as HP on-off cannot be included in the convex optimisation problem. PSO is a well developed technique to deal with non-linear and nonconvex constrained problems to find global optima [145]. PSO is a promising tool that does not require the computation of derivatives. Therefore, PSO is applied in the inner loop to optimise HP on-off and battery charging and discharging. In main optimisation loop, PSO creates a random population of possible solutions named

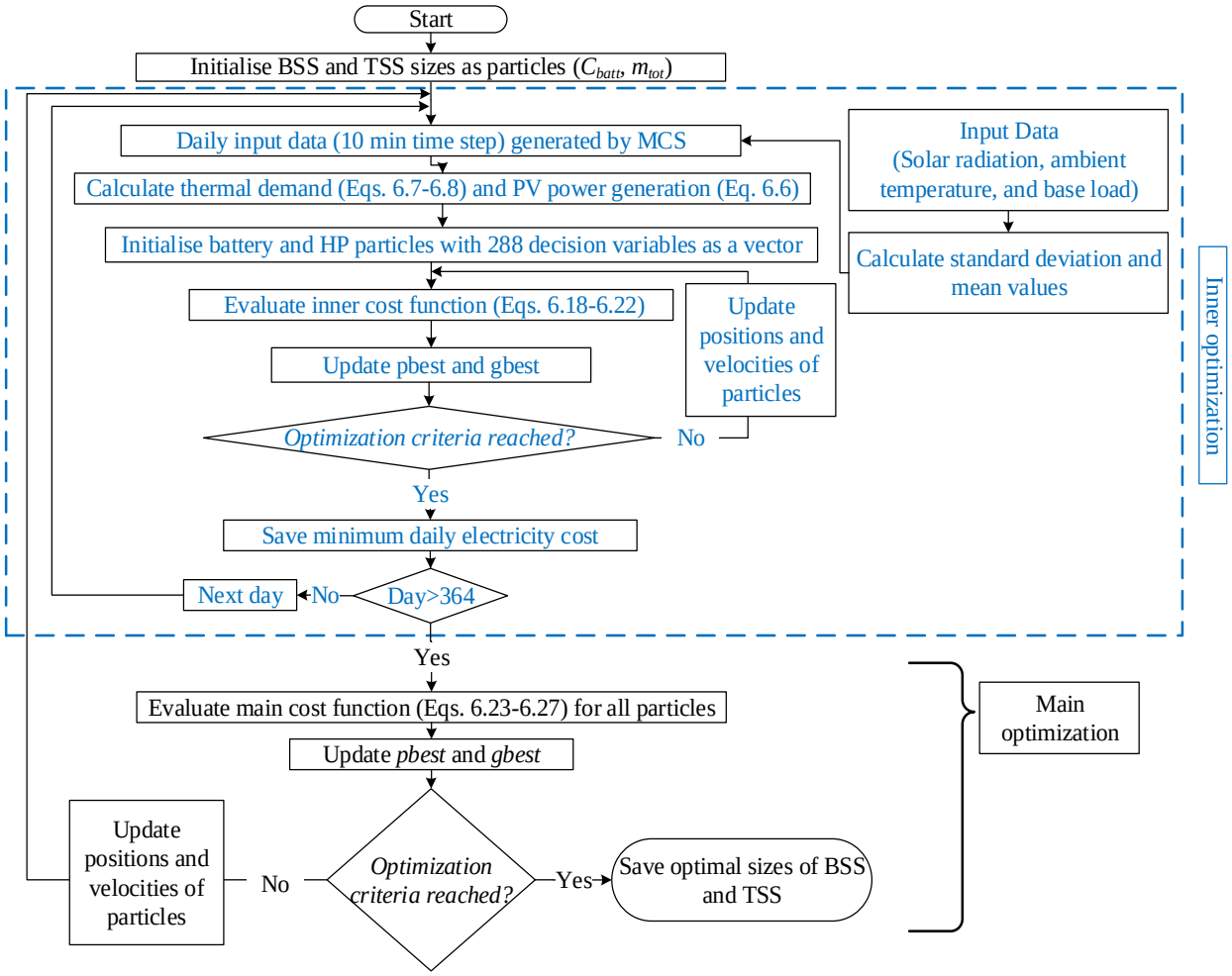

Figure 6.4: Flowchart of proposed OBTS.

particles. Each particle consists of the random sizes of BSS and TSS. In each iteration, particles are sent to the inner optimisation loop. The objective of inner loop is to minimise the daily electricity cost, and maximise the PV self-consumption. The annual electricity cost is then evaluated for each particle. Particles then move toward local and global solutions by evaluating LCC. Consequently, the optimal sizes of TSS and BSS are determined by minimising LCC.

6.3.2 Formulation of real-time optimal operation

The proposed SBEMS is employed to manage the physical system that composed the smart building based on the optimal sizes of TSS and BSS. The building is equipped

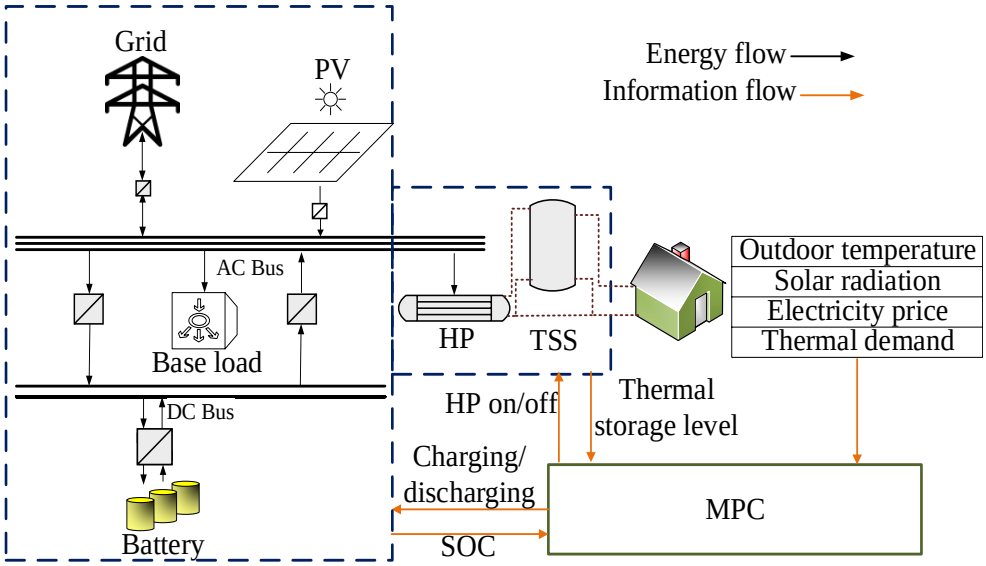

Figure 6.5: Schematic of energy management system.

with PV panels and BSS and connected to the grid. Total electrical base load is supplied by PV, BSS, and the grid. While the thermal load is supposed to be supplied by the HP coupled with TSS. In general, the daily HP input and electrical load can be met by the grid, PV panels, and batteries. The objective is to propose an SBEMS that can achieve minimum electricity cost and maximum PV self-consumption. The main advantage of the proposed SBEMS is the possibility to simultaneously control the BSS and HP coupled with TSS. After determining the optimal BSS and TSS sizes, MPC is used for the real-time optimal operation of the smart building. The schematic diagram of the proposed SBEMS is shown in Figure 6.5. MPC uses the system model to predict the future evolution of the smart building and perform real-time control actions [146]. The main objective of using MPC is to control the HP (on/off), in order to shift HP load based on the DRP, by producing sufficient chilled/hot water. Moreover, this controller is responsible to manage the charging and discharging of BSS. The cost function of the MPC based on RTP tariffs is the trade-off between the minimum cost of the total daily electricity and PV power exportation to the grid. At the same time, producing enough chilled/hot water, which is subject to the dynamic constraints as follows:

$$\min_{u_k} \quad \sum_{j=k}^{k+N-1} C_g(j|k) \tag{6.29}$$

subject to

$$x(j+1|k) = f(x(j|k), u(j|k), d(j|k)), \quad \forall j = k, k+1, \ldots, k+N-1 \tag{6.30}$$

$$y(j|k) = g(x(j|k), u(j|k), d(j|k)), \quad \forall j = k, k+1, \ldots, k+N \tag{6.31}$$

where N is the prediction horizon, u is the binary decision variable, x is the state variable which represents T_{in}, m_{TSS} and SOC, y is the output which represents P_g, and d is the disturbance. The model-based optimisation problem is solved over the finite horizon. The horizon prediction is N which is equal to 24 hours. The control sampling time is 5 minutes. The prediction horizon is considered equal to the control horizon. In this study, the MPC optimisation problem is defined as the problem of finding an optimal reference power for the heat pump and the discharge/charge reference power for BSS to supply the load. This can be described as follows: The electrical system dynamic Equations (6.1)-(6.2.1) and the thermal system dynamic Equations (6.6)-(6.16) are the main dynamics of the MPC, while Equations (6.20)-(6.21) and Table 6.4 correspond to the constraints of the system. Figure 6.6 shows the overview of the MPC which is implemented in the proposed SBEMS. The problem of control is formulated and solved in each time step to obtain the control signal. The control signal can be calculated based on the current system conditions, the prediction of external influences, and the future system state. The model of the system is used to evaluate the impacts of controls on the state of the system and to compute the optimal control solution. The first part of the computed solution is applied to the system. The procedure continues to find the control trajectory of u that minimises the cost function (Equation (6.29)).

6.4 Simulation Study of Proposed OBTS

In this study, SELAB building is considered as a residential building with an average of 18 kWh daily power consumption in Western Australia. This building is equipped with 5-kWp rooftop PV system and 10-kW water source HP system for space heating and cooling. The project lifetime is assumed to be 25 years based on average of PV panel lifetime. The simulations are performed with operating constraints as presented in

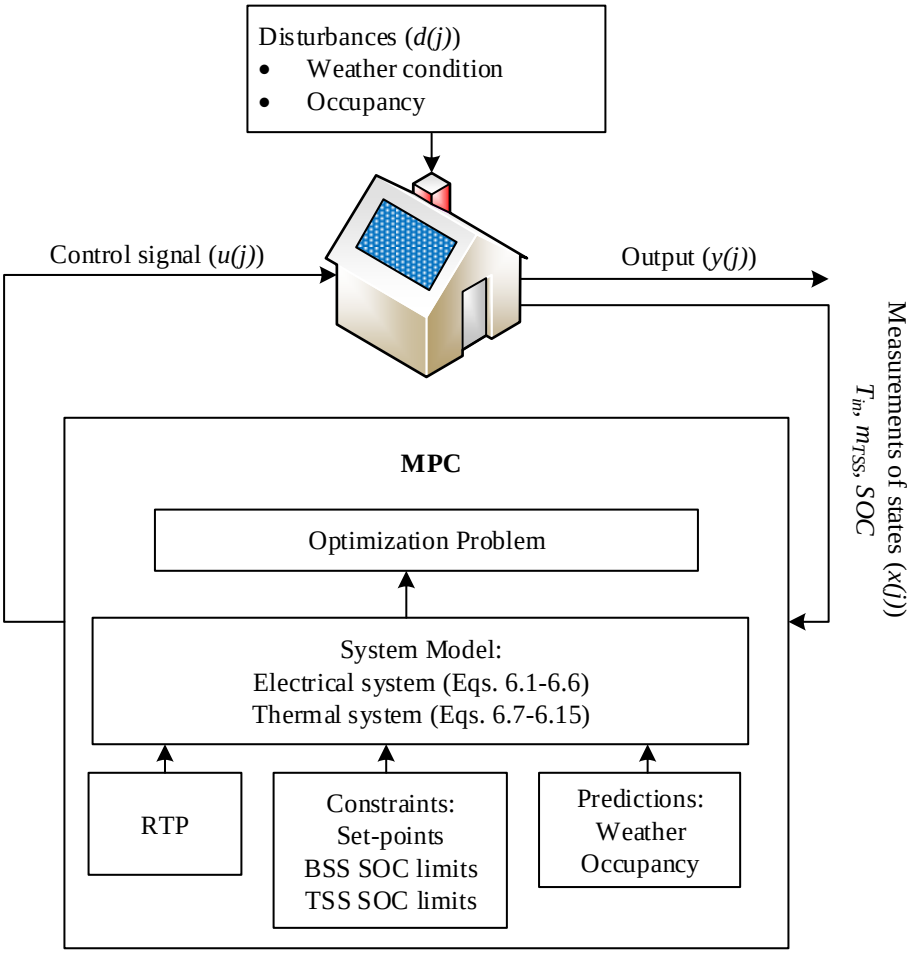

Figure 6.6: Flowchart of the MPC procedure.

Table 6.4. The percentages of m_{TSS} are associated with the volume of TSS (m_{tot}). In the grid-side, it is preferred for the renewable output power to be consumed locally, to avoid the risk of causing rapid ramp generation on the conventional generators. Furthermore, selling power price rates are appealing. Therefore, the revenue of selling PV power to the grid is not considered in this study. The main objective of OBTS is to find optimal sizes of thermal and electrical systems, with the aim of decreasing LCC and increasing PV self-consumption. Detailed simulations are performed for four cases.

Table 6.4: Operating constraints used in simulations.

SOC_0	SOC_{min}	SOC_{max}	m_{TSS}^{min}	m_{TSS}^{max}	$m_{TSS,0}$
50%	10%	90%	5%	100%	5%

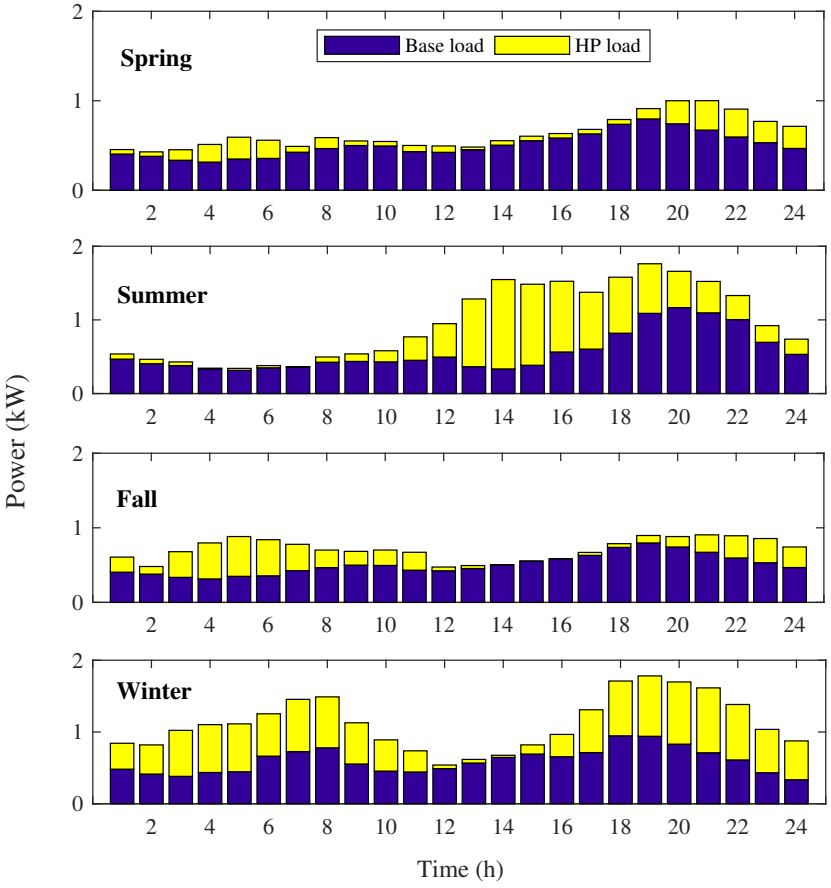

Figure 6.7: Case I: Average hourly power consumption for four seasons.

6.4.1 Case I: Base case

In this case, SELAB building is simulated without BSS and TSS. The reason for this is to use this base case results to evaluate and analyse other scenarios. Figure 6.7 shows the average hourly power consumption for four seasons. The base load and HP load are without any storage systems. The thermostatic control is utilised to determine the HP on-off signal, thus supplied the thermal load. The demand is increased in the peak-load period due to HP operation, in particular in summer and winter seasons.

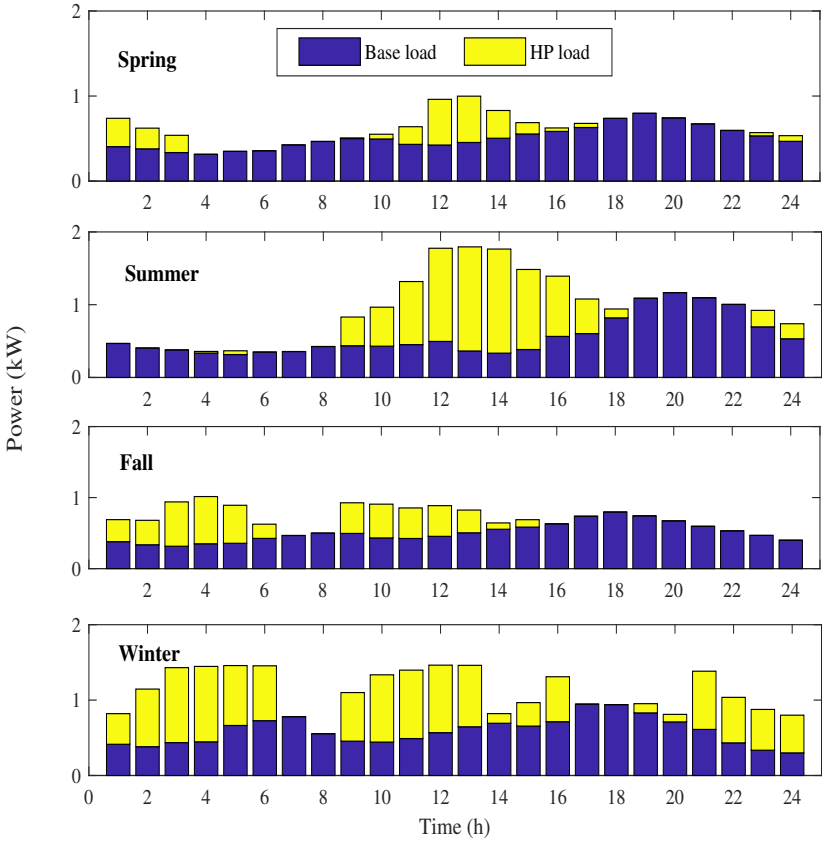

Figure 6.8: Case II: Average hourly power consumption for four seasons (TSS = 2000 $liters$).

6.4.2 Case II: TSS only

The HP system is employed with a TSS. The optimal size/volume of TSS (determined by the proposed OBTS) is 2000 liters. The life cycle cost of TSS is considered in this scenario. The HP system can be operated without an initial stored thermal energy in TSS, at first time step in each day. In order to avoid TSS thermal losses, it is assumed that: i) the TSS is covered with 100 mm insulation layer, and ii) the OBTS algorithm keeps the TSS without stored chilled/hot water at the end of the day. Figure 6.8 shows the base load and shifted HP load by the OBTS algorithm for four seasons. The results show that most of the HP load is shifted from peak-load hours (6pm-9pm) to periods with PV generation or the periods with lower electricity prices.

6.4.3 Case III: BSS only

The building is simulated with BSS and HP systems without any TSS. The optimal size of BSS, considering the operating and economic constraints indicated in Table 7.1, is 6.5 kWh. It is assumed that the initial SOC is 50%. The SOC of the battery is also considered to be equal to the initial SOC at the end of each day. The HP system is considered as nonshiftable load due to the lack of TSS. A possible economic solution for cases without significant load flexibility is to store PV generation in the BSS. However, this requires larger battery size which can subsequently raise capital cost and consequently the total life cycle cost. Figure 6.9 shows the simulation results of the average hourly power dispatch for four seasons. Note that the grid power is purchased in low electricity tariff rates. However, in summer and winter, BSS is unable to fully supply the total load during the peak-load period; consequently, some power is imported from the grid.

6.4.4 Case IV: BSS and TSS

In this case, BSS and TSS are considered to find their optimal sizes in a residential building with a 5-kWp PV system. Figure 6.10 shows the average power dispatch for four seasons with optimal sizes of BSS (4.7 kWh) and TSS (1800 liters). The simulation results prove that adding TSS to the HVAC system acquires more flexibility to the system. The introduction of TSS (with optimal size of 1800 liters) positively affects the BSS by reducing the size from 6.5 kWh to 4.7 kWh. This is achieved by shifting the HP load from the peak-load hours to either lower electricity tariff or mid-day hours, when PV generation is available.

6.4.5 Comparison of simulation results of optimal sizing

Simulation results and cost analysis of Cases I to IV are summarised and compared in Table 7.1. This Table shows the optimal BSS and TSS sizes, annual PV self-consumption, annual electricity cost, life cycle cost, payback period, and the percentage of return on investment (ROI). The payback period is the time that it takes an option to have the same LCC as the base case. The payback periods of Cases II, III and IV are calculated

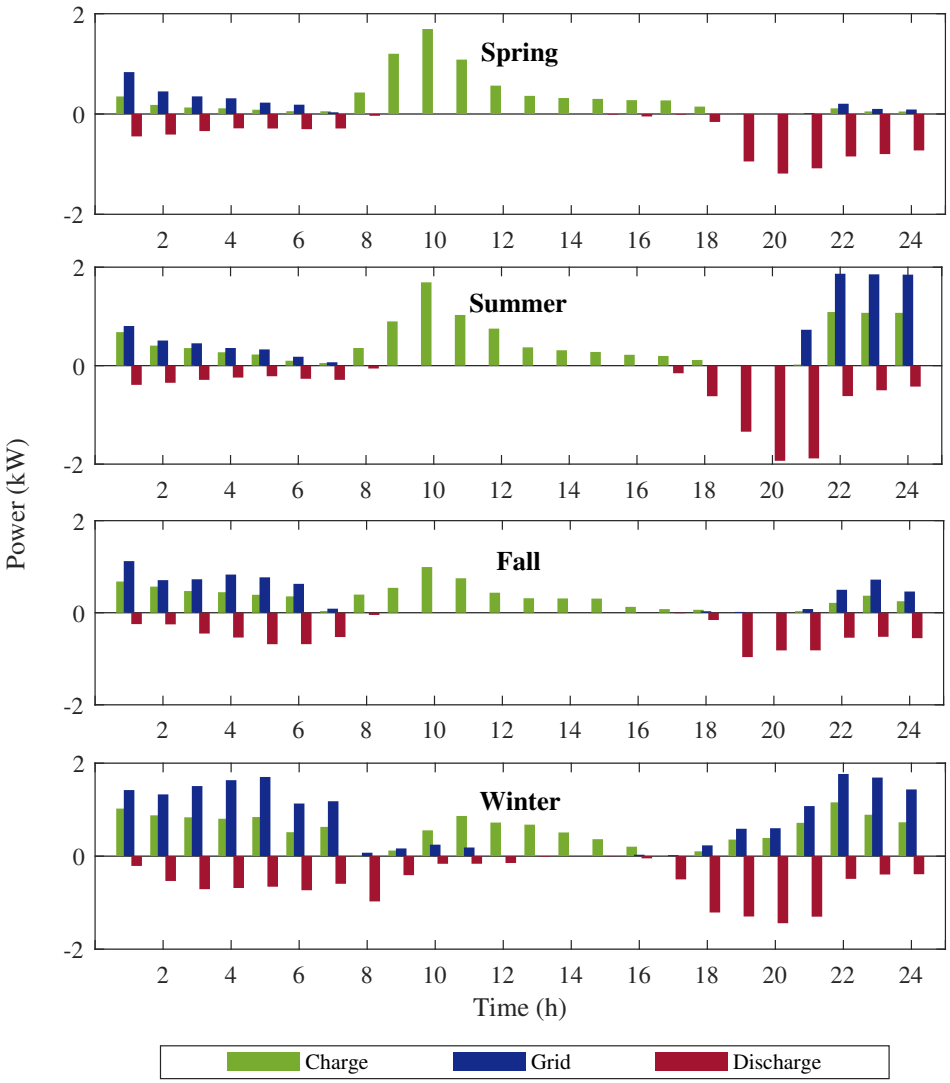

Figure 6.9: Case III: Average hourly power dispatch for four seasons ($BSS = 6.5\ kWh$).

based on the initial investment divided by the annual net cash flow. ROI is the ratio of gain to the investment. ROI is defined over a life cycle of the system as follows [147]:

$$ROI = \frac{Return - Investment}{Investment} = \frac{Avoided\ Cost}{Investment} - 1 \tag{6.32}$$

However, ROI does not include the project lifetime. Thus, annualised return on investment (AROI) is necessary to amortise the full investment cost over the lifetime of the

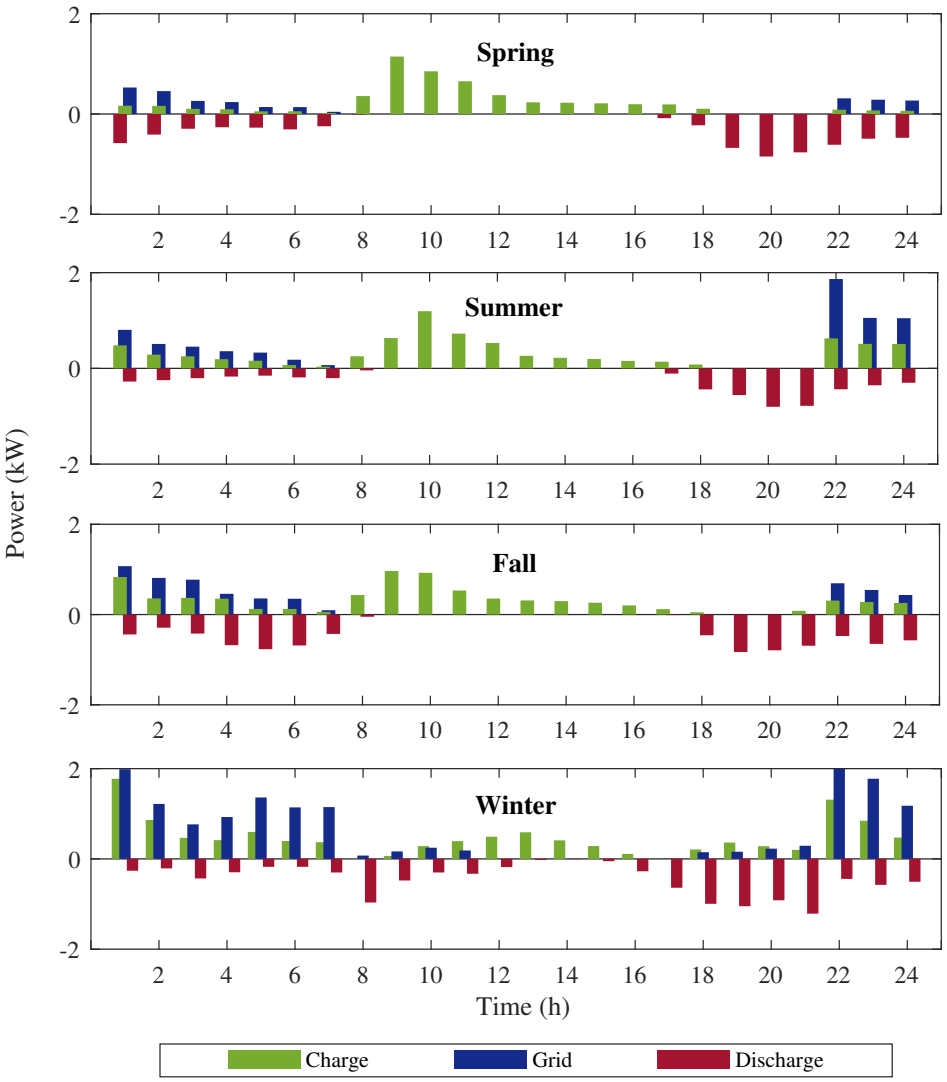

Figure 6.10: Case IV: Average hourly power dispatch for four seasons ($TSS = 1800$ *liters* and $BSS = 4.7$ kWh).

system. AROI can be described as follows:

$$AROI = [(1 + ROI)^{1/Y} - 1] \times 100\% \tag{6.33}$$

AROI is useful to compare the returns on Cases as investment opportunities. The total average annual PV generation is 8150 kWh. In Case I, the results show that the annual PV self-consumption is only 37.1% due to the lack of any storage systems. In this case, 62.9% of the total PV power is exported to the grid. In Case II, the introduction of TSS

with the optimal volume of 2000 liters has decreased the annual electricity cost by 26.2%, while PV self-consumption increased to 43.5%. As expected, this case is associated with a relatively short payback time of 5.1 years and a relatively high AROI of 6.5% over 25 years of project lifetime. In Case III, the annual electricity cost is reduced by 69.8% when adding a battery with an optimal size of 6.5 kWh to Case I; while the PV self-consumption increased to 53.3%. Moreover, LCC is improved by only 4.7% from Case II. However, the payback period and AROI are 10 years and 3.7%, respectively. In Case IV (proposed cost-effective framework of this chapter), the introduction of TSS (with the new optimal volume of 1800 liters) to Case III reduces the size of BSS to 4.7 kWh. In this case, the annual electricity cost is decreased by 80.4%. Moreover, PV self-consumption is increased to 57.3%. Interestingly, the payback period is dropped to 6.8 years, while the AROI is increased to 5.3%. As a result, this case has the lowest LCC in compared with other cases. Accordingly, the main advantages of using the proposed OBTS model are as follows:

- Adding the TSS in Case II with the optimal volume of 2000 liters to the residential HP system effectively increases the PV self-consumption by 17.1%, in compared with Case I. Consequently, the flexible HP system reduces annual electricity cost to $1066 (73.7% of Case I). The main advantage of this option is the short payback period of 5.1 years along with the higher AROI of 6.5%.

- The results of Case III show that the option of adding BSS significantly reduces the electricity bill to $436.2 (30% of Case I). However, this solution may not be very attractive for some consumers due to the low return on investment (3.7%) and the long payback period (10 years).

- The proposed OBTS of Case IV reveals the significant economic impacts of introducing HP coupled with TSS to Case III. This is the most attractive solution for the consumers since the battery size is reduced by 28% (from 6.5 kWh to 4.7 kWh) and the annual electricity cost is reduced by 81% (from $1445.4 to only $282.7) with the acceptable LCC.

Table 6.5: Comparison of results for Cases I-IV.

Cases	TSS size	BSS size	Annual PV self-consumption		Annual electricity cost		LCC	Payback period*	AROI**
	Liter	kWh	kWh	%	$	%	$/year	Year	%
Case I (No BSS/TSS)	-	-	3028	37.1	1445.4	-	1445.4	-	-
Case II (TSS only)	2000	-	3548	43.5	1066.4	26.2	1140.3	5.1	6.5
Case III (BSS only)	-	6.5	4351	53.3	436.2	69.8	1086	10	3.7
Case IV (BSS and TSS)	1800	4.7	4678	57.3	282.7	80.4	832.6	6.8	5.3

* Payback period is calculated based on project lifetime (25 years) and without buyback.
** Annualised return on investment.

6.5 Verification of Proposed OBTS and SBEMS

6.5.1 Verification of proposed OBTS

In order to verify the optimal sizing solutions of Case IV, different sizes of BSS and TSS are chosen and the corresponding costs are calculated. Sensitivity analysis results are presented and compared in Figures 6.11 - 6.14. Figure 6.11 describes simulation results for the annual electricity cost. As expected, the annual electricity cost decreases when BSS and TSS sizes are increased. However, increasing storage sizes results in higher payback period (Figure 6.12) and lower AROI (Figure 6.13) due to the increasing trend of capital cost. Figures 6.12 and 6.13 show that increasing the size of BSS without adding TSS to HVAC system remarkably increases the payback period and subsequently decreases AROI. Therefore, the results of Figures 6.11 - 6.14 verify that the captured optimal solution (marked in Figure 6.14) corresponds to the lowest life cycle cost. In order to the analysis of optimal TSS and BSS design for different sizes of PV system, it is necessary to consider the whole costs of PV system within LCC. The average cost of a PV system in Australia is about $1.09/W [148]. Two per cent of the initial cost of PV system is considered as the annual operational and maintenance costs. Four PV sizes are chosen and results are presented in Table 6.6. The optimal BSS and TSS sizes for different PV sizes show that increasing the size of PV increases the size of storage systems, while the trend is not linear. The optimal sizes of TSS and BSS are required for taking advantage of PV generation in the higher size of PV. It is not economical to increase the storage sizes due to i) rising initial costs of PV, TSS and BSS which leads

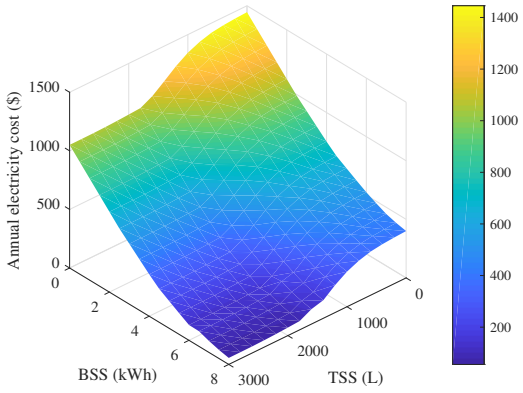

Figure 6.11: Sensitivity analysis of annual electricity cost.

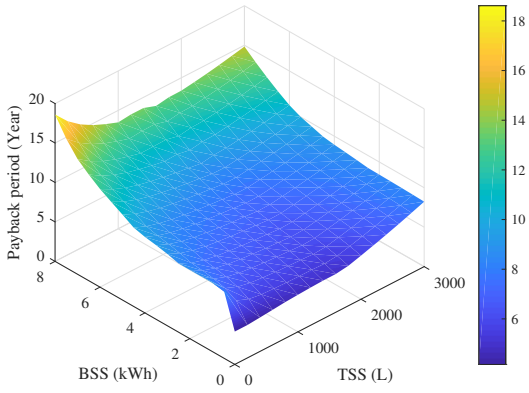

Figure 6.12: Sensitivity analysis of payback period.

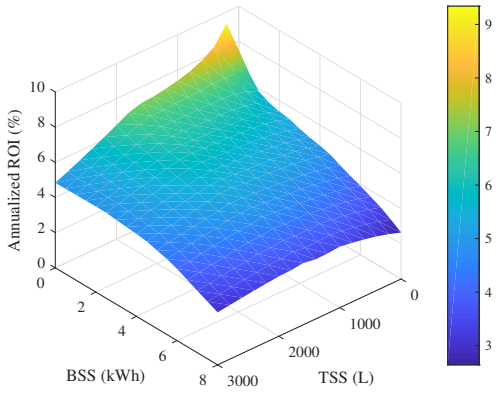

Figure 6.13: Sensitivity analysis of return on investment.

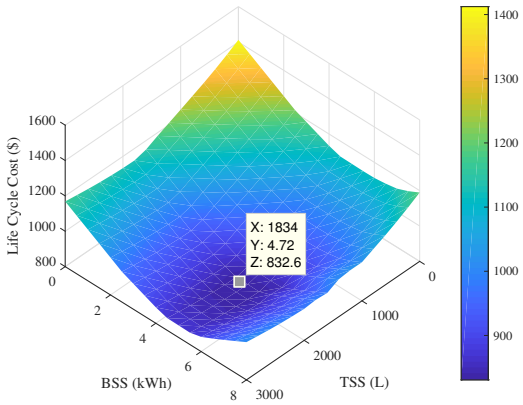

Figure 6.14: Sensitivity analysis of life cycle costs.

Table 6.6: OBTS results for different PV sizes.

PV size	kWp	2	4	6	8
TSS size	Liter	1200	1700	2200	2200
BSS size	kWh	3.4	4.2	5.0	5.2
Annual PV power	kWh	3380	6760	10140	13520
PV self-consumption	kWh	2984	4042	4708	4830
Annual electricity cost	$	958	396	233	195
LCC*	$	1464	1139	1206	1311
Payback period*	year	6.6	6.9	8.6	10.2
AROI*	%	5.4	5.2	4.2	3.4

* The life cycle cost of PV system is considered in LCC, payback period, and AROI.

to increase the LCC, and ii) the sizes of TSS and BSS are mostly limited by households load.

The seasonal performance factor (SPF) on the ground source heat pump is 4.4 in heating mode and 4.8 in cooling mode for the optimal TSS size. In this work, increasing the temperature of the TSS has not been considered to increase PV self-consumption. Additionally, TSS is considered to be correctly insulated. OBTS optimises the stored thermal energy in TSS to supply daily thermal demand and avoid tank heat loss. Therefore, different sizes of TSS do not significantly impact the SPF of HP. However, the higher sizes of TSS decreases the SPF slightly due to the increase in tank heat loss.

6.5.2 Experimental validation of SBEMS

Figure 6.15 shows the SELAB at Edith Cowan University, Western Australia. Experimental validations have been performed for the thermal and electrical energy systems installed at the SELAB. The thermal system consists of 3×1000 liters stainless steel tank (100 mm insulation layer), and ground source HP with 10.3 kW heating capacity and 7.1 kW cooling capacity (the power consumption of the HP is between 1.5-2 kW). The electrical system encompasses 12×285 W series mono-crystalline PV modules (3.5 kWp), 6×250 W series poly-crystalline PV modules (1.5 kWp), and $4 \times 4 \times 12$ V series lead-acid

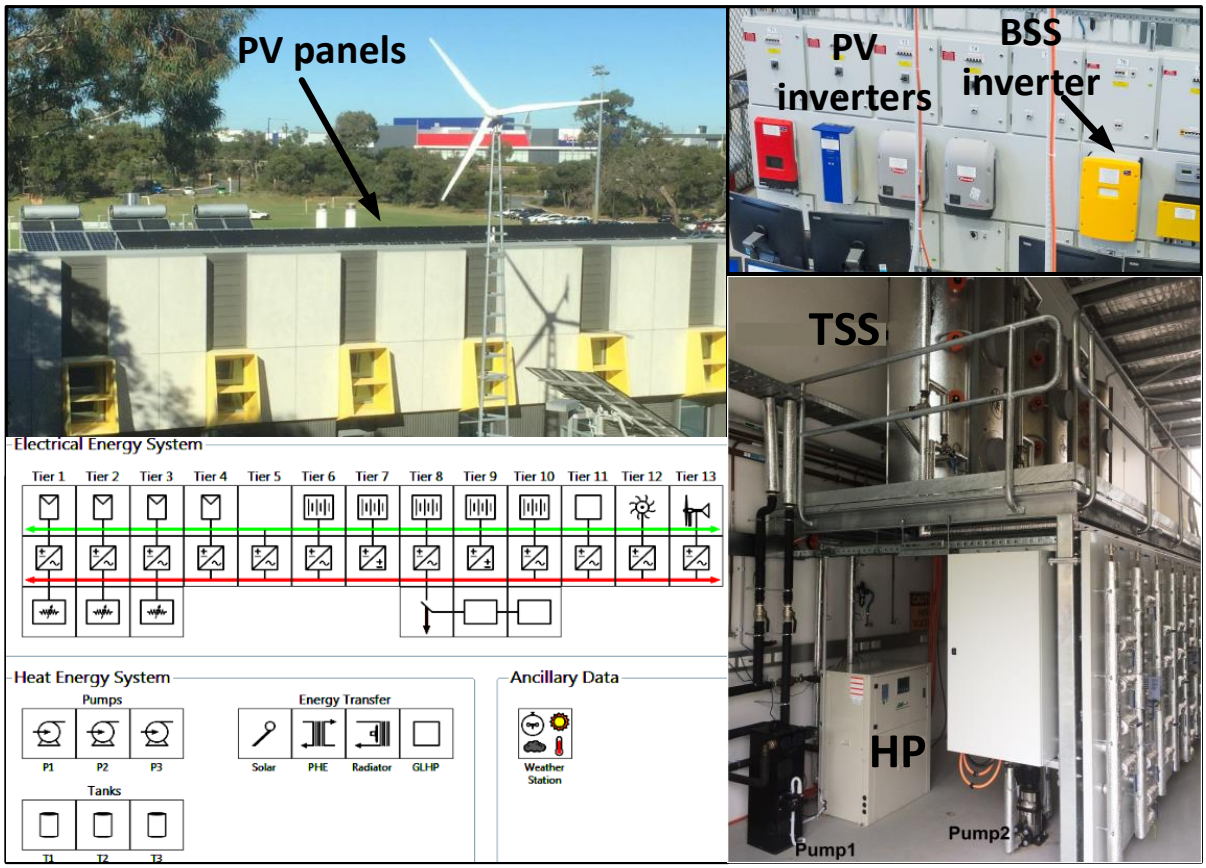

Figure 6.15: Smart Energy Laboratory (SELAB) at Edith Cowan University (ECU), Western Australia.

batteries modules MP12200 GEL CELL with nominal voltage of 48 V and total capacity of 4×4.8 kWh. All home appliances, except the HP, are modelled as uncontrollable loads. The base load is the data of a smart meter for a house in Perth, Australia, as shown in Figure 6.17b. The experiments are performed at SELAB with the operating constraints shown in Table 6.4. TSS is set to $m_{TSS} = 0.1$ m^3 in the first time step. The stored chilled/hot water volume in TSS is calculated by measuring the difference between the inlet and outlet water flow rates of the TSS. The indoor temperature set-point is considered between 22 °C and 24 °C. Figure 6.16 shows the real-time pricing profile used in this study. This profile is based on wholesale electricity market from the Australian energy market operator (AEMO) website [1]. The RTP is for two typical days in January 2019. A horizon prediction of $N = 24$ h and a control sampling time of

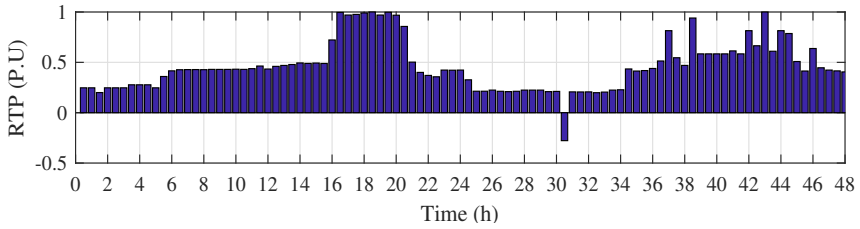

Figure 6.16: Wholesale electricity market price for two days in Jan-2019 [1].

5 min are chosen in this test. The proposed algorithm shifts the HP load based on RTP tariff and availability of PV generation, taking into account the stored thermal energy in the TSS (m_{TSS}) and the battery SOC. To verify the SBEMS results by experimental tests, TSS with the volume of 2000 liters and BSS with the capacity of 4.8 kWh are used as installed in SELAB.

Figure 6.17 shows SBEMS results of two days in summer. These results are obtained based on the actual system. Based on weather prediction, SBEMS calculates PV production and thermal demand over the prediction horizon. In each time step, the indoor temperature is predicted and thermostat signal ($\mathbb{U}$) determines the total required thermal demand of the building for the next time step (Figure 6.17f). The SBEMS optimises to run HP at midnight to directly supply thermal demand (Figure 6.17c). Figure 6.17d shows that SBEMS is applied to import power from the grid during midnight to avoid deep BSS discharging in the early morning. In second day, SBEMS runs the HP when the real-time price is negative. The power is also imported from the grid when the price is negative. It is assumed that the SOC of battery is 50% in the first time step. Figure 6.17e shows that the battery is charged by the grid power during low electricity price-period, based on RTP, which has shown in Figure 6.16, to supply base load and HP load during midnight and early morning. Then, BSS is fully charged by PV power to supply the load during peak-load hours (Figure 6.17a). Figure 6.17e also demonstrates that HP is operated to charge TSS in midnight and when PV generation is sufficient to charge battery as well as supply the total load. The results show that according to m_{TSS}, the HP is run in mid-day when the PV power is available, to increase stored chilled water m_{TSS}. The thermal demand is then supplied by TSS during peak-load hours.

To show the effectiveness of SBEMS, test is done for the PV system without BSS and TSS. Figures 6.18 and 6.19 show the experimental results of power dispatch for the

system without the storage and with TSS and BSS, respectively. The HP load causes an increase in the total load during peak-load hours when the electricity price is high. This is due to the lack of storage systems. Thus, the total purchased grid power is 10.81 kWh in base case, while it is decreased to 3.16 kWh in the presence of TSS and BSS. In addition, the electricity cost is decreased by 84% from \$8.4 to \$1.3. The PV self-consumption is increased from 14.38 kWh (35.6 %) to 19.81 kWh (49.1 %).

Figure 6.20 and Table 6.7 show the comparison between the model results and the experimental measurements. Figure 6.20 demonstrates that the experimental measurements of BSS power and the grid power verify the simulation results with minor differences. Table 6.7 shows the PV power, PV self-consumption, HP electrical load, and the grid power for the first day for both simulations and measurements. The difference between the experimental results and the simulation results is mainly due to the 5-min time step. It can be seen that the results have verified the effectiveness of the proposed model. However, Table 6.7 shows 0.5 kWh difference in HP power consumption. This difference is due to the ground circulation pump of the ground source heat pump. The ground circulation pump operates about 2 min earlier than the HP and turns off 2 min after turning off the HP.

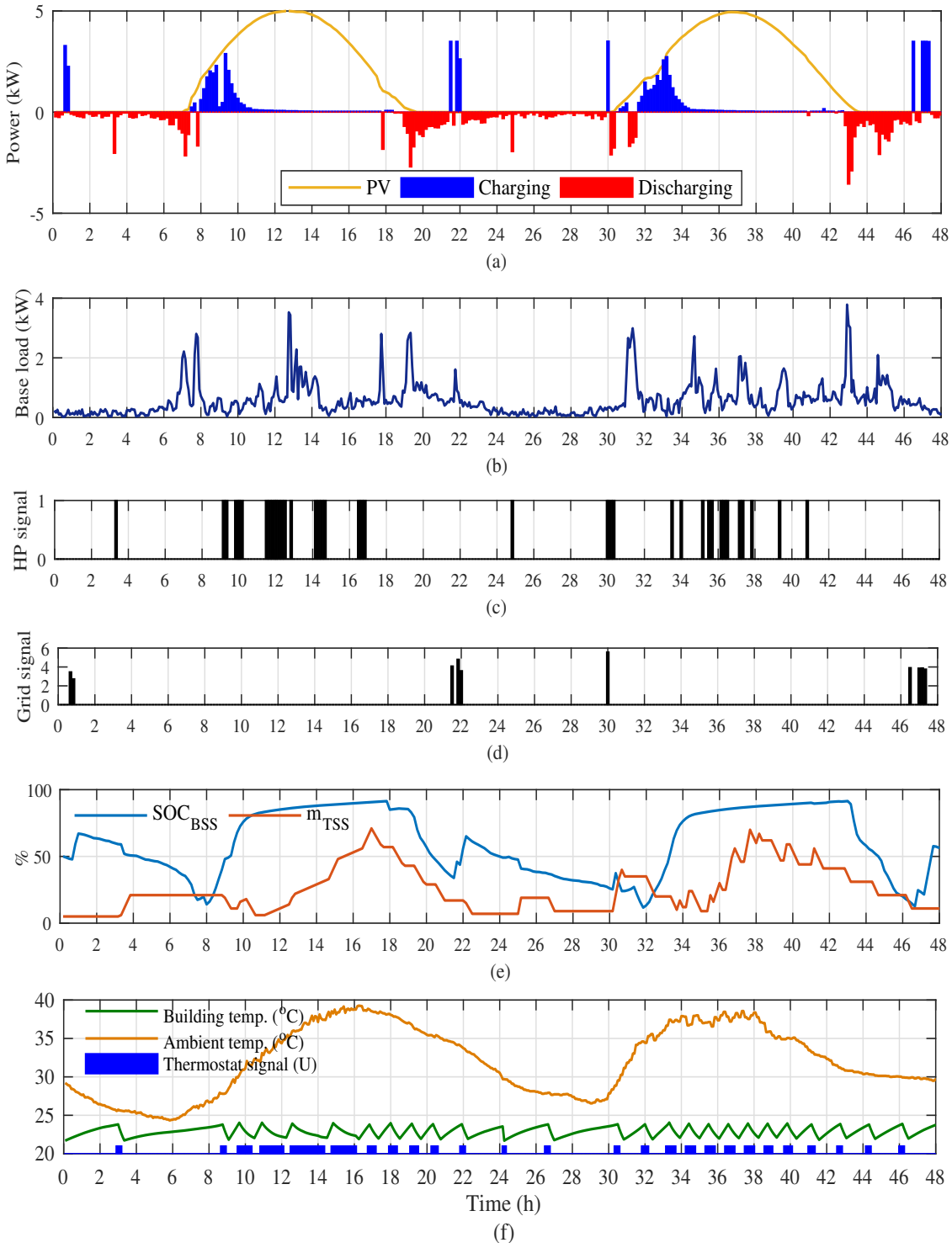

Figure 6.17: Power dispatch for a day in summer with the 4.8 kWh BSS and 2000 liters TSS. (a) PV production and battery power flow. (b) Base load. (c) HP operation signal. (d) Signal of imported power from the grid. (e) Percentages of the stored electrical and thermal energy in BSS and TSS. (f) Building temperature control result based on weather condition.

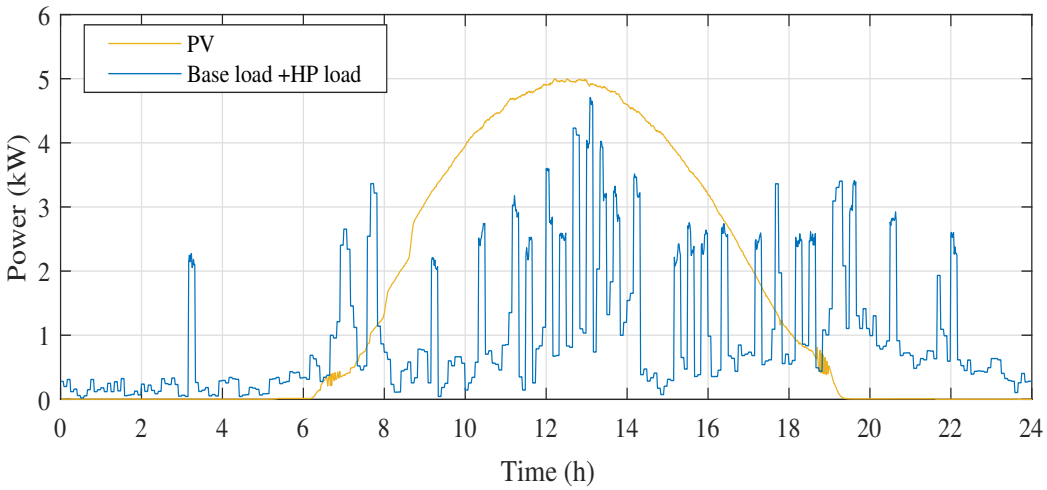

Figure 6.18: Experimental results of power dispatch for PV system without BSS and TSS.

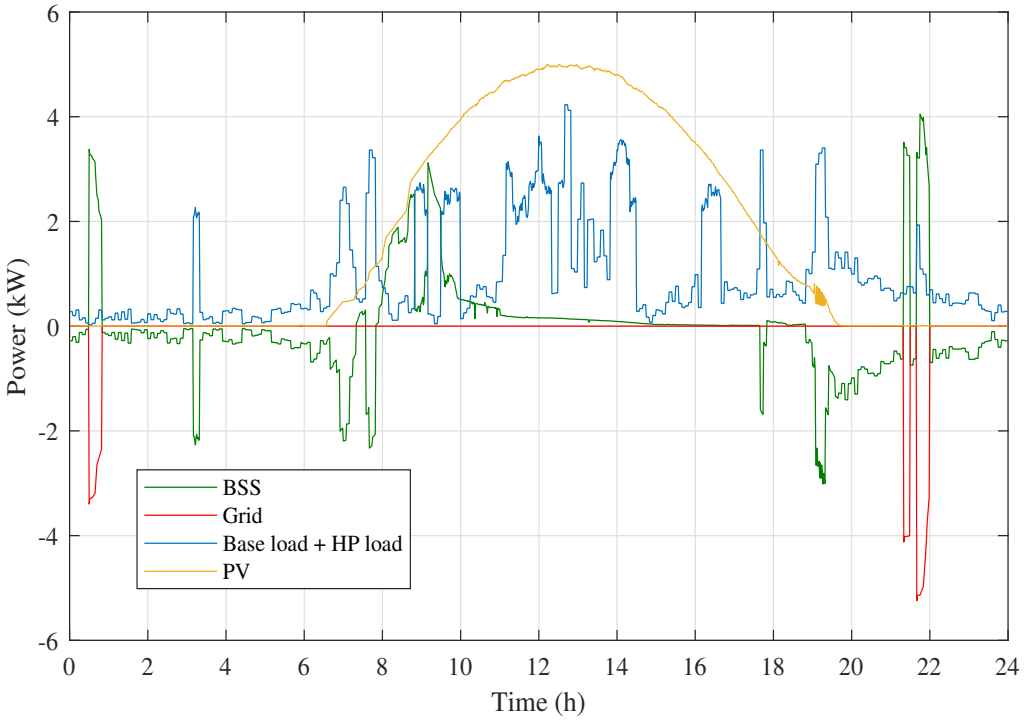

Figure 6.19: Experimental results of power dispatch for the PV system with 4.8 kWh BSS and 2000 liters TSS.

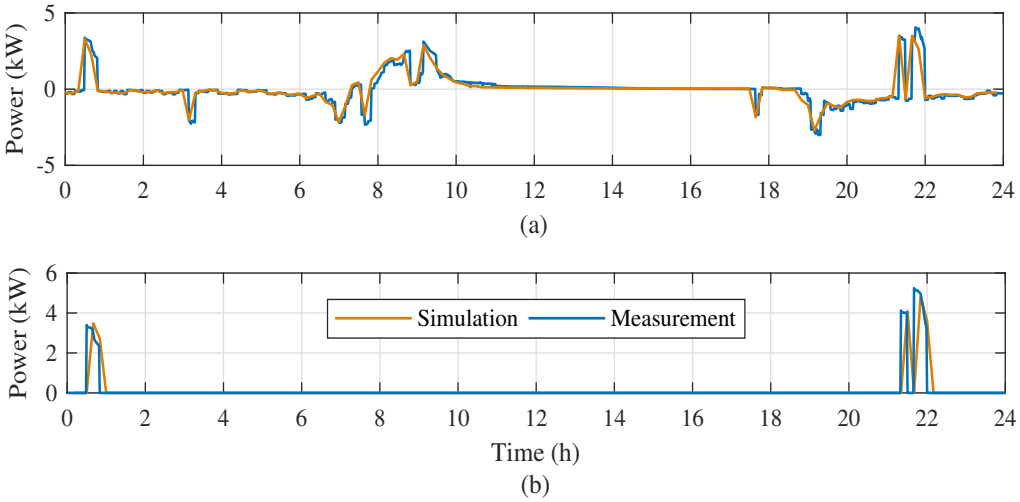

Figure 6.20: Comparison of experimental measurements and simulation results. (a) BSS power. (b) grid power.

Table 6.7: Comparison of experimental measurements and simulation results.

		Simulation	Experiment
PV power	kWh	38.4	39.3
PV self-consumption	kWh	19.6	20.1
HP load	kWh	12.1	12.6
Grid power	kWh	3.16	3.19

6.6 Conclusion

This chapter presents a cost-effective framework for energy management of residential buildings with rooftop PVs, heat pumps, and thermal storage system and battery storage system. Two methods are proposed and tested: 1) optimal BSS and TSS sizing (OBTS) to determine the optimal sizes of BSS and TSS, and 2) a smart building energy management system (SBEMS) to manage real-time operation of storage systems based on the OBTS results. The performance of OBTS and SBEMS are verified using detailed simulations and experimental tests. In addition, the cost benefits of the proposed OBTS are demonstrated for different scenarios by oversizing and undersizing both TSS and BSS components. The key outcomes of this study can be described as follows:

- The proposed OBTS reveals significant economic benefits in smart buildings with

rooftop PVs by introducing BSS and TSS systems coupled with HP. The results demonstrate that buildings with TSS only are a low investment solution in terms of short payback period and reasonable AROI. However, buildings with either thermal or battery storage (Table 7.1, Cases II and III) are not as cost-effective as the proposed TSS+BSS systems of Case IV, in terms of low annual electricity and life cycle costs. In particular, the control of residential HP coupled with TSS reduces building demand from peak-load hours. Consequently, the BSS size is decreased. Accordingly, thermal and battery storage systems significantly increase PV self-consumption.

- With optimal sizing of BSS and TSS, the proposed SBEMS significantly reduces the total electricity cost of the smart building by shifting the HP loads based on DRP. This is achieved by charging the battery either during low-price electricity hours or when PV power is available.

In this chapter, the issues related to research question RQ3 have been addressed. The results of this study demonstrate that residential rooftop PV systems can rely on HPs coupled with TSS systems as shifting technologies. This can help avoid power system challenges which caused by exporting excess PV power to the grid. The enhanced system can significantly reduce the burden of residential loads at peak hours by increasing rooftop PV self-consumption. Due to the high initial investment and operating costs of BSS, adding TSS to air-conditioning systems is more economical since end-users can take full advantage of rooftop PV systems with a reasonable investment cost. Accordingly, distribution network operators can support customers by introducing an incentive framework to foster HP systems. The proposed framework can be modified to consider the power sharing within buildings. It can also be applied in peer-to-peer trading with other types of HVAC systems and renewable energy resources.

Simulation results and cost analysis of Cases I to IV show that adding the TSS in Case II with the optimal volume of 2000 liters to the residential HP system effectively increases the PV self-consumption by 17%. The results of Case III show the option of adding BSS significantly reduces the electricity bill and Case IV reveals the significant economic impacts of introducing HP coupled with TSS to Case III. The proposed OBTS

reveals significant economic benefits in smart buildings with rooftop PVs by simultaneously introducing BSS and TSS systems coupled with the HP. The results demonstrate that buildings with TSS only are a low investment solution in terms of short payback period and reasonable AROI. However, buildings with either thermal or battery storage are not as cost-effective as the proposed TSS+BSS systems of Case IV, in terms of low annual electricity and life cycle costs. In particular, the control of residential HP coupled with TSS reduces building demand from peak-load hours. Consequently, the BSS size is decreased. Accordingly, thermal and battery storage systems significantly increase PV self-consumption. With optimal sizing of BSS and TSS, the proposed SBEMS significantly reduces the total electricity cost of the smart building by shifting the HP loads based on DRP. This is done by charging the battery either during low-price electricity hours or when PV power is available. The performance of OBTS and SBEMS are verified using detailed simulations and experimental tests. In addition, the cost benefits of the proposed OBTS are demonstrated for different scenarios by oversizing and undersizing both TSS and BSS components.

Chapter 7 is not included in this version of the thesis

Potential Integration of Residential Heat Pump Systems into Reserve Capacity Market

Chapter 8

Conclusions and Recommendations for Future Research

8.1 Conclusions

This PhD research focuses on grid-side and demand-side issues related to the high penetration of PV generation in residential areas. The power system challenges, such as frequency regulation, reverse power and voltage imbalance issues are caused by high PV penetration. A potential solution that may be beneficial for both end-users and utilities is to increase PV self-consumption. This can be efficiently achieved using energy storage systems and residential flexible loads such as heat pumps. The research objectives and significances are presented in Section 1.1. The integration of HPs into microgrids as load responsive and ancillary service providers have been addressed in the earlier literature in Chapter 2. Based on the literature survey of Chapter 2, four research questions (RQ1 to RQ4) are identified and addressed in Chapters 3-7. Controlling residential thermal loads and thermal energy storage is a viable strategy to engage end-users in demand response programs. This thesis has focused on the development of an optimal real-time thermal energy management system for residential buildings to resolve various issues in microgrids. This research has mainly targeted residential HPs with the aim of (i) minimising

HPs power consumption during peak-load hours while improving the energy efficiency of HP and maintaining the indoor temperature within a desirable thermal comfort range, (ii) enhancing the PV self-consumption in residential buildings, (iii) minimising the electricity costs for end-users, (iv) minimising the operation cost of battery in residential buildings with PV and HP, (v) sizing thermal and electrical energy storage systems to minimise annual electricity costs of building with rooftop PVs while minimising life cycle costs of the system, and (vi) aggregating and controlling residential HPs load to participate in reserve capacity market. Overall, the investigations carried out within this thesis will benefit both distribution network operators and end-users by providing solutions to recent power network issues. These issues have been investigated, and different solution approaches have been proposed. This concluding chapter summarises the main findings and the contributions of this thesis. In addition, several research directions for future works are suggested.

8.2 Key findings

Based on the work described in the preceding chapters, the key findings of this thesis are summarised as follows:

- This research has performed studies on the implementation of optimal real-time thermal energy management strategies for smart buildings with GSHP, WST and FCUs. The total power consumption of the GSHP and FCUs is decreased from peak-load hours by shifting HP loads based on DRP while providing adequate thermal comfort levels. Two online closed-loop MPCs are applied to manage two thermal energy storage systems, a water storage tank and the building thermal mass. The main advantages and contributions of the proposed MPC with DTS based on RTP tariffs compared to the existing technologies based on thermostatic control are (i) the proposed MPC with DTS can significantly reduce the total energy cost and overall cost by shifting up to 100% of HVAC (GSHP and FCUs) loads based on DRP depending on weather conditions while maintaining the indoor temperature within a desirable comfort range, and (ii) the proposed MPC with DTS allows the end-user to take more advantage of RTP by increasing the DTS intensity coefficient. Large values of β will significantly shift HVAC loads from

high price periods and consequently reduce the cost while the indoor temperature is maintained within the thermal comfort zone.

- This research has demonstrated a practical approach to resolve the issues associated with variations in rooftop PV power causing a mismatch between generation and load demand in smart residential buildings. A real-time temperature boundary strategy based on real-time pricing tariff is used to shift heat pump load to minimise the operation cost of a smart building and reduce the export energy to the utility. Simulations are performed for residential air-conditioning systems without storage tank, with RTB, and with both storage tank and RTB. The proposed RTB with MPC controller based on RTP increases the PV self-consumption. The proposed RTB reduces the total energy cost by shifting the HP load from the peak-price period.

- An IHEMS has been proposed and tested for economic operation of smart buildings and homes that include HPs coupled with thermal energy storage, battery storage, and rooftop PV system. The potential of HPs to minimise operation costs and maximise the use of PV power has been investigated. The battery charging strategy and battery efficiency are taken into account. The comparison of two different cases has indicated that the optimal scheduling of the electrical and thermal storage systems simultaneously can significantly reduce the operation costs of the system. The results demonstrate that the proposed IHEMS effectively decreases power consumption from the grid by maximising the use of PV power.

- This research has performed a cost-effective framework for energy management of residential buildings with rooftop PVs, heat pumps, thermal storage system and battery storage system. Two methods were proposed and tested: 1) optimal BSS and TSS sizing (OBTS) to determine the optimal sizes of BSS and TSS, and 2) a smart building energy management system (SBEMS) to manage the real-time operation of storage systems based on the OBTS results. The performance of OBTS and SBEMS are verified using detailed simulations and experimental tests. The cost benefits of the proposed OBTS are demonstrated for different scenarios by oversizing and undersizing both TSS and BSS components. The key findings of this study are: (i) the proposed OBTS achieves significant economic benefits in smart buildings with rooftop PVs by introducing BSS and TSS systems coupled with the

HP. The results demonstrate that buildings with only TSS are a low investment solution in terms of a short payback period and reasonable AROI. However, buildings with either thermal or battery storage are not as cost-effective as the proposed TSS and BSS systems, in terms of low annual electricity and life cycle costs. In particular, the control of a residential HP coupled with TSS reduces building demand from peak-load hours. Consequently, the BSS size is decreased. Accordingly, thermal and battery storage systems significantly increase PV self-consumption; (ii) with optimal sizing of BSS and TSS, the proposed SBEMS significantly reduces the total electricity cost of smart buildings by shifting the HP loads based on DRP. This is done by charging the battery either during low-price electricity hours or when PV power is available.

- The results of this research have demonstrated that residential rooftop PV systems can rely on HPs coupled with TSS systems as shifting technologies to avoid power system challenges caused by exporting excess PV power to the grid. The enhanced system can significantly reduce the burden of residential loads during peak hours by increasing rooftop PV self-consumption. Due to the high initial investment and operating costs of BSS, adding TSS to air-conditioning systems is more economical since end-users can take full advantage of rooftop PV systems with a reasonable investment cost. Accordingly, distribution network operators can support customers by introducing an incentive framework to foster the deployment of HP systems.

- In this research, a business energy aggregate model for residential heat pumps has been proposed to allow energy aggregators to participate in individual reserve capacity requirement. The model determines trading intervals capacity requirements through forecasting peak demand and renewable energy generation. A dynamic model of RHPs coupled with thermal energy storage was presented to implement the control strategy to provide demand side management capacity reserve. A rebound effect reduction strategy was introduced. The results of this study have demonstrated that the aggregate RHPs model is accurate to capture all power fluctuations. This model helps energy aggregators to implement a control strategy for different purposes, like mitigating the fluctuations of renewable energy resources, frequency regulation, and peak-load shaving. The control strategy is

used to minimise the RHPs load during reserve capacity trading intervals in trading days. The results show that energy aggregators can take advantage of TESs to earn capacity credits. The aggregate RHPs coupled with TES model provides reliable and long period load reduction to receive capacity credits. The control of the aggregate RHPs is suitable for IRCR reduction which results in decreasing the cost for energy aggregators. However, the rebound effect is crucial to mitigate. Therefore, the proposed RER reduces the peak rebound.

8.3 Future recommendations

This PhD project has considered and addressed several issues in power networks with renewable energy sources, including modelling, analysing, and establishing HPs application benefits. However, there are still several scopes for further studies with the focus on the following research factors:

- In this thesis, a GSHP as an energy-efficient heating/cooling device has been used to satisfy DRPs. However, the effect of borehole thermal energy storage (BTES) as seasonal thermal energy storage on cost savings as well as PV self-consumption has not been evaluated for buildings with RESs. Therefore, the potential impacts of using BTES for a PV and wind hybrid system integrated with a GSHP at building level can be investigated. The feasibility of the BTES for injection/extraction of heat from the ground on the long-term operation and storage of surplus renewable energy can also be evaluated. Furthermore, control techniques can be applied to manage thermal energy in BTES to minimise energy costs.

- Developing an optimal bidding strategy for the residential HPs to participate in the distribution day-ahead and real-time markets. Appropriate building energy management systems, coupled with an optimised bidding strategy, can provide significant cost savings for consumers with RESs and/or storage systems when they participate in bi-directional trading. An energy management system can be applied for HP systems with an optimisation-based scheduling and bidding strategy for residential customers to determine optimal day-ahead energy-quantity bids.

- A framework can be applied to consider the power-sharing within buildings with HP systems and RESs. It can also be applied in peer-to-peer trading with the implementation of residential demand response through heat pumps and thermal energy storage systems. In a case that prosumers are equipped with heat pumps and renewable generation with energy storage units, a novel strategy can be applied that encourages sharing surplus electricity between different prosumers, in order to maximise the overall cost savings and the utilisation of renewable energy in the district.

- Cloud coverage transients cause rapid fluctuations in the output of PV power generation, which can considerably impact the voltage levels in a low-voltage (LV) distribution network with high penetration of PV systems. These voltage fluctuations may lead to violation of the existing power quality standards. A control system can be applied in the HP unit coupled with thermal energy storage for the mitigation of PV output fluctuations.

Appendix

Appendix A: Model Predictive Control

Model predictive control was proposed in the late 1970s and has developed noticeably ever since [3]. MPC is a control methodology that utilises a process model to predict and optimise the future evolution of a plant. The main ideas of predictive control methods are as follows:

- Explicit use of a model to predict the process result up to a future time instant (horizon),
- Achieving control signal by minimising an objective function,
- Using receding strategy, at each instant, the horizon extends for the same period into the future.

Furthermore, MPC for buildings is an active research area [73]. The use of weather prediction to control building climate has recently gained attention. In this research MPC is applied to multi input and multi output systems and also considering multiple control objectives at the same time.

MPC structure

The control objective and the mathematical model is formulated as a real-time optimisation problem that repeatedly computes the control inputs. The basic structure of the MPC is indicated in Figure 1. The model uses past inputs and outputs data and combines this data with potential future inputs to estimate how the system will respond. Then the predicted output is delivered to the future time step and is compared with a reference trajectory to determine the deviation of the systems. These future errors are then fed into an optimiser, which operates to maximise profit, minimise operational costs, or keeping the system around set point trajectory. In order to satisfy constraints on outputs, inputs and states of the system, the optimiser tries different sequences of future inputs, which are fed back into the main model for evaluation. Once the optimisation has converged, and the best sequence of control inputs has been found, the first step of these is applied to the real system. At the next time step, the process is repeated using the new measurement. This leads to what is known as "receding horizon optimisation".

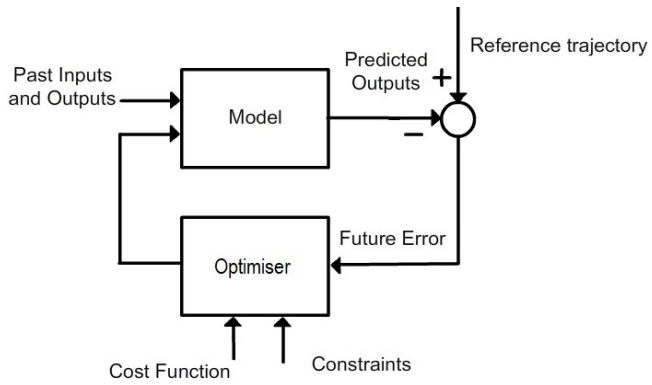

Figure 1: The basic structure of the MPC [3].

MPC Strategy

Predictive control is a receding horizon method. This means the horizon will be shifted after computing the optimal sequence and the optimisation is restarted with new data of the measurements. There are four steps to describe the methodology of the MPC, represented in Figure 2.

Step 1 At time k the future control signals $\{u(k \mid k), ..., u(k + N_c - 1 \mid k)\}$ are optimised to minimise an objective function. The objective function induces the outputs to follow the reference trajectory as close as possible. This optimisation is performed using backwards simulation.

Step 2 The model predicts the future outputs for a known prediction horizon N at each time step k using forward simulation. These predicted outputs depend on past inputs, system state, and (initial) future control signals and disturbances.

Step 3 The constraints of the system are checked, and if they are violated, changes are applied to make sure that they are satisfied. Several different optimisation strategies exist for this step, but they all require some amount of iteration between the continuous optimisation of the control inputs and the discrete optimisation of the limits at each time step. This step is the main reason that a long time horizon (and especially a long

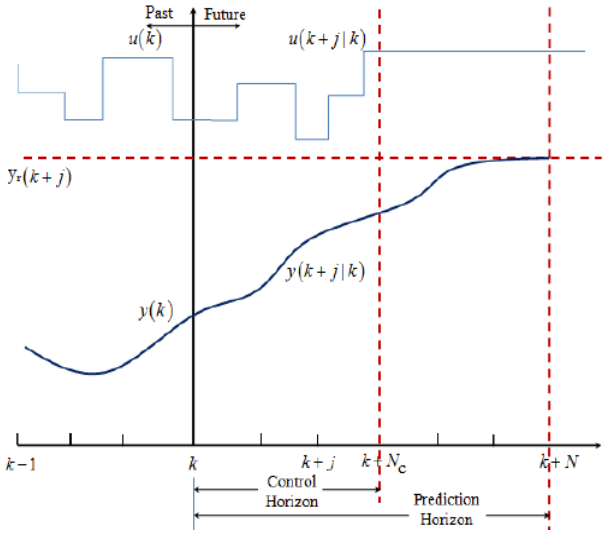

Figure 2: MPC strategy [3].

control horizon) can make the MPC problem very difficult to solve, because the limits have to be considered at each time step and therefore the total number of limits is much higher than first it seems.

Step 4 Once the solution is found, the first step of the control input is sent to the process. All further steps are discarded, because at the next sampling instant $y(k+1)$ is already known, the prediction horizon can be increased, and a more accurate control input can be calculated by repeating from step 1.

Process model and disturbance model The MPC makes use of a process model of the plant to predict the control signal during a specified horizon. A linear model is commonly used to make an estimation of the future response of the system. Therefore, the state space model is well-suited for the most general system description. The following state space form will be adopted:

$$\begin{aligned} x_{k+1} &= Ax_k + Bu_k \\ y_k &= Cx_k \end{aligned} \tag{1}$$

where A is the state matrix, B is the input matrix and C is the output matrix of dimensions $A \in \mathbb{R}^{nx \times nx}$, $B \in \mathbb{R}^{ny \times nx}$ and $C \in \mathbb{R}^{ny \times nx}$. Also x_k is the state of the system, u_k is all predicted disturbance, and y_k is the output of the system.

Cost function The ability of the MPC control approach to define a detailed objective function makes this control strategy one of the most flexible advanced control strategies. The MPC makes use of a model of the plant to obtain the control signal by minimising this objective function. The predictive controller iterates the model plant n steps forward in time (prediction horizon) to see how the system will behave in the future for a given set of predicted disturbances based on the current states, and adjusts the inputs, u_k, which include both the measured disturbances and controlled inputs. At each discrete sampling time k, the vector of system states x_k is measured or estimated.

The cost function of a MPC generally has the following structure:

$$J(u,k) = \sum_{j=N_m}^{N} Q(j)(y(k+j|k) - y_r(k+j)^2 + \sum_{j=1}^{N_c} \omega(\Delta u(k+j-1|k))^2 \qquad (2)$$

where Q is the weighted process output signal, $y_r(k)$ is the reference trajectory, $y(k)$ is the process output signal, $\Delta u(k)$ is the process control increment signal, N_m is the minimum cost-horizon, N is the prediction horizon, N_c is the control horizon, ω is the weighting on the control signal.

where $y(k+j|k)$ is the prediction of $y(k+j)$, based on knowledge up to time k, the increment input signal is $\Delta u(k) = u(k) - u(k-1)$ and $\Delta u(k+j) = 0$ for $j \geq N_c$. The coefficient ω determines the trade-off between tracking accuracy (first part) and control effort (second part).

Constraint Model predictive control has the ability to include constraints in the MPC formulation. The capability of MPC to cope with these constraints directly is one of the key strengths of MPC. Specific signals must not violate specified bounds due to safety limitations, environmental regulations, consumer specifications and physical restrictions such as minimum and/or maximum temperature. Accurate tuning of the controller parameters may keep these values away from the bounds. The constraints can be on the inputs, the control, the outputs or states. The constraints used in this work are linear constraints and can be given by the following kind of equation;

$$u_{min,k} \leq u_k \leq u_{max,k} \qquad (3)$$

Linear constraints are the most commonly used constraints, because they are comparatively easy to resolve.

References

[1] "Australian energy market operator." `https://www.aemo.com.au/Electricity/Wholesale-Electricity-Market-WEM/Data-dashboard`. Accessed: 2018-12-20.

[2] J. H. Yoon, R. Baldick, and A. Novoselac, "Dynamic demand response controller based on real-time retail price for residential buildings," *IEEE Transactions on Smart Grid*, vol. 5, no. 1, pp. 121–129, 2014.

[3] E. F. Camacho and C. B. Alba, *Model predictive control*. Springer Science & Business Media, 2013.

[4] N. Omar, M. A. Monem, Y. Firouz, J. Salminen, J. Smekens, O. Hegazy, H. Gaulous, G. Mulder, P. Van den Bossche, T. Coosemans, *et al.*, "Lithium iron phosphate based battery–assessment of the aging parameters and development of cycle life model," *Applied Energy*, vol. 113, pp. 1575–1585, 2014.

[5] D. Fischer and H. Madani, "On heat pumps in smart grids: A review," *Renewable and Sustainable Energy Reviews*, vol. 70, pp. 342–357, 2017.

[6] M. Behrangrad, "A review of demand side management business models in the electricity market," *Renewable and Sustainable Energy Reviews*, vol. 47, pp. 270–283, 2015.

[7] Q. QDR, "Benefits of demand response in electricity markets and recommendations for achieving them," *US Dept. Energy, Washington, DC, USA, Tech. Rep*, 2006.

[8] H. T. Haider, O. H. See, and W. Elmenreich, "A review of residential demand response of smart grid," *Renewable and Sustainable Energy Reviews*, vol. 59, pp. 166–178, 2016.

[9] M. H. Albadi and E. El-Saadany, "A summary of demand response in electricity markets," *Electric power systems research*, vol. 78, no. 11, pp. 1989–1996, 2008.

[10] P. Cappers, "Mass market demand response and variable generation integration issues: A scoping study," tech. rep., Lawrence Berkeley National Laboratory, 2012.

[11] G. Strbac, "Demand side management: Benefits and challenges," *Energy policy*, vol. 36, no. 12, pp. 4419–4426, 2008.

[12] P. D. Lund, J. Lindgren, J. Mikkola, and J. Salpakari, "Review of energy system flexibility measures to enable high levels of variable renewable electricity," *Renewable and Sustainable Energy Reviews*, vol. 45, pp. 785–807, 2015.

[13] K. Chua, S. Chou, and W. Yang, "Advances in heat pump systems: A review," *Applied energy*, vol. 87, no. 12, pp. 3611–3624, 2010.

[14] F. Staff, "Assessment of demand response and advanced metering," *Federal Energy Regulatory Commission, Docket AD-06-2-000*, 2006.

[15] A. Chiasson and C. Yavuzturk, "A design tool for hybrid geothermal heat pump systems in cooling-dominated buildings.," *ASHRAE Transactions*, vol. 115, no. 2, 2009.

[16] P. Zhao, S. Suryanarayanan, and M. G. Simoes, "An energy management system for building structures using a multi-agent decision-making control methodology," *IEEE Transactions on Industry Applications*, vol. 49, no. 1, pp. 322–330, 2013.

[17] A. Ghalebani and T. K. Das, "Design of financial incentive programs to promote net zero energy buildings," *IEEE Transactions on Power Systems*, vol. 32, no. 1, pp. 75–84, 2017.

[18] Australian-Government, "http://www.cleanenergyregulator.gov.au/ret," 2019.

[19] A. G. Tsikalakis and N. D. Hatziargyriou, "Centralized control for optimizing microgrids operation," in *Power and Energy Society General Meeting, 2011 IEEE*, pp. 1–8, IEEE, 2011.

[20] B. Zhang and J. Baillieul, "Control and communication protocols based on packetized direct load control in smart building microgrids," *Proceedings of the IEEE*, vol. 104, no. 4, pp. 837–857, 2016.

[21] J. Hua, Q. Ai, and Y. Yao, "Dynamic equivalent of microgrid considering flexible components," *IET Generation, Transmission & Distribution*, vol. 9, no. 13, pp. 1688–1696, 2015.

[22] B. Nordman, "Nanogrids: evolving our electrical systems from the bottom up," *Environmental Energy Technologies Division*, 2010.

[23] D. Burmester, R. Rayudu, W. Seah, and D. Akinyele, "A review of nanogrid topologies and technologies," *Renewable and Sustainable Energy Reviews*, vol. 67, pp. 760–775, 2017.

[24] I. Patrao, E. Figueres, G. Garcerá, and R. González-Medina, "Microgrid architectures for low voltage distributed generation," *Renewable and Sustainable Energy Reviews*, vol. 43, pp. 415–424, 2015.

[25] A. Werth, N. Kitamura, and K. Tanaka, "Conceptual study for open energy systems: distributed energy network using interconnected dc nanogrids," *IEEE Transactions on Smart Grid*, vol. 6, no. 4, pp. 1621–1630, 2015.

[26] R. Asad and A. Kazemi, "A novel distributed optimal power sharing method for radial dc microgrids with different distributed energy sources," *Energy*, vol. 72, pp. 291–299, 2014.

[27] L. Ma, N. Liu, J. Zhang, W. Tushar, and C. Yuen, "Energy management for joint operation of chp and pv prosumers inside a grid-connected microgrid: A game theoretic approach," *IEEE Transactions on Industrial Informatics*, vol. 12, no. 5, pp. 1930–1942, 2016.

[28] G. Mantovani, G. T. Costanzo, M. Marinelli, and L. Ferrarini, "Experimental validation of energy resources integration in microgrids via distributed predictive control," *IEEE Transactions on Energy Conversion*, vol. 29, no. 4, pp. 1018–1025, 2014.

[29] M. Marinelli, F. Sossan, G. T. Costanzo, and H. W. Bindner, "Testing of a predictive control strategy for balancing renewable sources in a microgrid," *IEEE Transactions on Sustainable Energy*, vol. 5, no. 4, pp. 1426–1433, 2014.

[30] M. Marzband, F. Azarinejadian, M. Savaghebi, and J. M. Guerrero, "An optimal energy management system for islanded microgrids based on multiperiod artificial bee colony combined with markov chain," *IEEE Systems Journal*, 2015.

[31] J. Tian, Z. Liu, J. Shu, J. Liu, and J. Tang, "Base on the ultra-short term power prediction and feed-forward control of energy management for microgrid system applied in industrial park," *IET Generation, Transmission & Distribution*, vol. 10, no. 9, pp. 2259–2266, 2016.

[32] A. Chaouachi, R. M. Kamel, R. Andoulsi, and K. Nagasaka, "Multiobjective intelligent energy management for a microgrid," *IEEE Transactions on Industrial Electronics*, vol. 60, no. 4, pp. 1688–1699, 2013.

[33] Z. Ding and W.-J. Lee, "A stochastic microgrid operation scheme to balance between system reliability and greenhouse gas emission," in *Industrial & Commercial Power Systems Technical Conference (I&CPS), 2015 IEEE/IAS 51st*, pp. 1–9, IEEE, 2015.

[34] K. Yeager, "Striving for power perfection," *IEEE Power and Energy Magazine*, vol. 6, no. 6, pp. 28–35, 2008.

[35] G. G. Dranka and P. Ferreira, "Review and assessment of the different categories of demand response potentials," *Energy*, vol. 179, pp. 280–294, 2019.

[36] W. W. Hogan, "Time-of-use rates and real-time prices," *John F. Kennedy School of Government, Harvard University*, 2014.

[37] G. Barbose, C. Goldman, and B. Neenan, "A survey of utility experience with real time pricing," *Lawrence Berkeley National Laboratory*, 2004.

[38] B. Biegel, P. Andersen, J. Stoustrup, L. H. Hansen, and A. Birke, "Sustainable reserve power from demand response and fluctuating production-two danish demonstrations," *Proceedings of the IEEE*, vol. 104, no. 4, pp. 780–788, 2016.

[39] K. M. Tsui and S.-C. Chan, "Demand response optimization for smart home scheduling under real-time pricing," *IEEE Transactions on Smart Grid*, vol. 3, no. 4, pp. 1812–1821, 2012.

[40] A. D. Carvalho, P. Moura, G. C. Vaz, and A. T. de Almeida, "Ground source heat pumps as high efficient solutions for building space conditioning and for integration in smart grids," *Energy Conversion and Management*, vol. 103, pp. 991–1007, 2015.

[41] E. Kjellsson, G. Hellström, and B. Perers, "Optimization of systems with the combination of ground-source heat pump and solar collectors in dwellings," *Energy*, vol. 35, no. 6, pp. 2667–2673, 2010.

[42] C. Underwood, M. Royapoor, and B. Sturm, "Parametric modelling of domestic air-source heat pumps," *Energy and Buildings*, 2017.

[43] R. Halvgaard, N. K. Poulsen, H. Madsen, and J. B. Jørgensen, "Economic model predictive control for building climate control in a smart grid," in *Innovative Smart Grid Technologies (ISGT), 2012 IEEE PES*, pp. 1–6, IEEE, 2012.

[44] G. Papaefthymiou, B. Hasche, and C. Nabe, "Potential of heat pumps for demand side management and wind power integration in the german electricity market," *IEEE Transactions on Sustainable Energy*, vol. 3, no. 4, pp. 636–642, 2012.

[45] N. Good, E. Karangelos, A. Navarro-Espinosa, and P. Mancarella, "Optimization under uncertainty of thermal storage-based flexible demand response with quantification of residential users discomfort," *IEEE Transactions on Smart Grid*, vol. 6, no. 5, pp. 2333–2342, 2015.

[46] A. Hesaraki, S. Holmberg, and F. Haghighat, "Seasonal thermal energy storage with heat pumps and low temperatures in building projects-a comparative review," *Renewable and Sustainable Energy Reviews*, vol. 43, pp. 1199–1213, 2015.

[47] J. Salpakari and P. Lund, "Optimal and rule-based control strategies for energy flexibility in buildings with pv," *Applied Energy*, vol. 161, pp. 425–436, 2016.

[48] H. Kobayashi, M. Asari, and H. Hatta, "Integrated control techniques of supply and demand for japanese style smart grid," in *Power and Energy Society General Meeting, 2010 IEEE*, pp. 1–7, IEEE, 2010.

[49] S. Deilami, A. S. Masoum, P. S. Moses, and M. A. Masoum, "Real-time coordination of plug-in electric vehicle charging in smart grids to minimize power losses and improve voltage profile," *IEEE Transactions on Smart Grid*, vol. 2, no. 3, pp. 456–467, 2011.

[50] Z. Moghaddam, I. Ahmad, D. Habibi, and Q. V. Phung, "Smart charging strategy for electric vehicle charging stations," *IEEE Transactions on Transportation Electrification*, vol. 4, no. 1, pp. 76–88, 2018.

[51] C. K. Das, O. Bass, G. Kothapalli, T. S. Mahmoud, and D. Habibi, "Overview of energy storage systems in distribution networks: Placement, sizing, operation, and power quality," *Renewable and Sustainable Energy Reviews*, vol. 91, pp. 1205–1230, 2018.

[52] F. Ruelens, B. Claessens, S. Quaiyum, B. D. Schutter, R. Babuska, and R. Belmans, "Reinforcement learning applied to an electric water heater: From theory to practice," *IEEE Transactions on Smart Grid*, pp. 1–1, 2016.

[53] I. Staffell, D. Brett, N. Brandon, and A. Hawkes, "A review of domestic heat pumps," *Energy & Environmental Science*, vol. 5, no. 11, pp. 9291–9306, 2012.

[54] C. Shao, Y. Ding, P. Siano, and Z. Lin, "A framework for incorporating demand response of smart buildings into the integrated heat and electricity energy system," *IEEE Transactions on Industrial Electronics*, pp. 1–1, 2017.

[55] M. Avci, M. Erkoc, A. Rahmani, and S. Asfour, "Model predictive hvac load control in buildings using real-time electricity pricing," *Energy and Buildings*, vol. 60, pp. 199–209, 2013.

[56] J. E. Braun, "Load control using building thermal mass," *Journal of solar energy engineering*, vol. 125, no. 3, pp. 292–301, 2003.

[57] G. P. Henze, C. Felsmann, and G. Knabe, "Evaluation of optimal control for active and passive building thermal storage," *International Journal of Thermal Sciences*, vol. 43, no. 2, pp. 173–183, 2004.

[58] Y. Kim, "Optimal price-based demand response of hvac systems in multi-zone office buildings considering thermal preferences of individual occupants," *IEEE Transactions on Industrial Informatics*, pp. 1–1, 2018.

[59] E. Atam, D. Patteeuw, S. P. Antonov, and L. Helsen, "Optimal control approaches for analysis of energy use minimization of hybrid ground-coupled heat pump systems," *IEEE Transactions on Control Systems Technology*, vol. 24, no. 2, pp. 525–540, 2016.

[60] V. Rostampour and T. Keviczky, "Probabilistic energy management for building climate comfort in smart thermal grids with seasonal storage systems," *IEEE Transactions on Smart Grid*, pp. 1–1, 2018.

[61] G. Mantovani and L. Ferrarini, "Temperature control of a commercial building with model predictive control techniques," *IEEE Transactions on Industrial Electronics*, vol. 62, no. 4, pp. 2651–2660, 2015.

[62] M. Liu, Y. Shi, and X. Liu, "Distributed mpc of aggregated heterogeneous thermostatically controlled loads in smart grid," *IEEE Transactions on Industrial Electronics*, vol. 63, no. 2, pp. 1120–1129, 2016.

[63] J. Yao, G. T. Costanzo, G. Zhu, and B. Wen, "Power admission control with predictive thermal management in smart buildings," *IEEE Transactions on Industrial Electronics*, vol. 62, no. 4, pp. 2642–2650, 2015.

[64] D. Molina, C. Lu, V. Sherman, and R. G. Harley, "Model predictive and genetic algorithm-based optimization of residential temperature control in the presence of time-varying electricity prices," *IEEE Transactions on Industry Applications*, vol. 49, no. 3, pp. 1137–1145, 2013.

[65] Y. Ma, F. Borrelli, B. Hencey, B. Coffey, S. Bengea, and P. Haves, "Model predictive control for the operation of building cooling systems," *IEEE Transactions on control systems technology*, vol. 20, no. 3, pp. 796–803, 2012.

[66] J. Vasilj, S. Gros, D. Jakus, and M. Zanon, "Day-ahead scheduling and real-time economic mpc of chp unit in microgrid with smart buildings," *IEEE Transactions on Smart Grid*, pp. 1–1, 2017.

[67] M. Razmara, G. R. Bharati, M. Shahbakhti, S. Paudyal, and R. D. Robinett, "Bilevel optimization framework for smart building-to-grid systems," *IEEE Transactions on Smart Grid*, vol. 9, pp. 582–593, March 2018.

[68] I. D. de Cerio Mendaza, I. G. Szczesny, J. R. Pillai, and B. Bak-Jensen, "Flexible demand control to enhance the dynamic operation of low voltage networks," *IEEE Transactions on Smart Grid*, vol. 6, no. 2, pp. 705–715, 2015.

[69] I. D. de Cerio Mendaza, I. G. Szczesny, J. R. Pillai, and B. Bak-Jensen, "Demand response control in low voltage grids for technical and commercial aggregation services," *IEEE Transactions on Smart Grid*, vol. 7, no. 6, pp. 2771–2780, 2016.

[70] S. Huang and Q. Wu, "Dynamic subsidy method for congestion management in distribution networks," *IEEE Transactions on Smart Grid*, 2016.

[71] S. Huang and Q. Wu, "Real-time congestion management in distribution networks by flexible demand swap," *IEEE Transactions on Smart Grid*, 2017.

[72] Y.-J. Kim, E. Fuentes, and L. K. Norford, "Experimental study of grid frequency regulation ancillary service of a variable speed heat pump," *IEEE Transactions on Power Systems*, vol. 31, no. 4, pp. 3090–3099, 2016.

[73] M. Killian and M. Kozek, "Ten questions concerning model predictive control for energy efficient buildings," *Building and Environment*, vol. 105, pp. 403–412, 2016.

[74] S. M. Sichilalu and X. Xia, "Optimal power dispatch of a grid tied-battery-photovoltaic system supplying heat pump water heaters," *Energy Conversion and Management*, vol. 102, pp. 81–91, 2015.

[75] S. M. Sichilalu and X. Xia, "Optimal energy control of grid tied pv-diesel-battery hybrid system powering heat pump water heater," *Solar Energy*, vol. 115, pp. 243–254, 2015.

[76] S. Sichilalu, H. Tazvinga, and X. Xia, "Optimal control of a fuel cell/wind/pv/grid hybrid system with thermal heat pump load," *Solar Energy*, vol. 135, pp. 59–69, 2016.

[77] REN21-Secretariat, "Renewables 2018 global status report," 2018.

[78] Z. Moghaddam, I. Ahmad, D. Habibi, and M. A. Masoum, "A coordinated dynamic pricing model for electric vehicle charging stations," *IEEE Transactions on Transportation Electrification*, vol. 5, no. 1, pp. 226–238, 2019.

[79] A. Baniasadi, D. Habibi, O. Bass, and M. A. S. Masoum, "Optimal real-time residential thermal energy management for peak-load shifting with experimental verification," *IEEE Transactions on Smart Grid*, pp. 1–1, 2018.

[80] Y. Kim, "Optimal price-based demand response of hvac systems in multi-zone office buildings considering thermal preferences of individual occupants," *IEEE Transactions on Industrial Informatics*, 2018.

[81] M. Shabani and J. Mahmoudimehr, "Techno-economic role of pv tracking technology in a hybrid pv-hydroelectric standalone power system," *Applied energy*, vol. 212, pp. 84–108, 2018.

[82] N. Mousavi, G. Kothapalli, D. Habibi, C. K. Das, and A. Baniasadi, "A novel photovoltaic-pumped hydro storage microgrid applicable to rural areas," *Applied Energy*, vol. 262, p. 114284, 2020.

[83] N. Mousavi, G. Kothapalli, D. Habibi, C. K. Das, and A. Baniasadi, "Modelling, design, and experimental validation of a grid-connected farmhouse comprising a photovoltaic and a pumped hydro storage system," *Energy Conversion and Management*, vol. 210, p. 112675, 2020.

[84] G. Yang and M. Chen, "The methodology for size optimization of the photovoltaic/wind hybrid system," *Energy Sources, Part A: Recovery, Utilization, and Environmental Effects*, vol. 32, no. 17, pp. 1644–1650, 2010.

[85] G. Mokhtari, G. Nourbakhsh, and A. Gosh, "Optimal sizing of combined pv-energy storage for a grid-connected residential building," *Advances in Energy Engineering*, vol. 1, no. 3, pp. 53–65, 2013.

[86] T. K. Brekken, A. Yokochi, A. Von Jouanne, Z. Z. Yen, H. M. Hapke, and D. A. Halamay, "Optimal energy storage sizing and control for wind power applications," *IEEE Transactions on Sustainable Energy*, vol. 2, no. 1, pp. 69–77, 2010.

[87] D. Parra, M. Gillott, S. A. Norman, and G. S. Walker, "Optimum community energy storage system for pv energy time-shift," *Applied Energy*, vol. 137, pp. 576–587, 2015.

[88] A. Arteconi, N. J. Hewitt, and F. Polonara, "Domestic demand-side management (dsm): Role of heat pumps and thermal energy storage (tes) systems," *Applied thermal engineering*, vol. 51, no. 1-2, pp. 155–165, 2013.

[89] T. Scholten, C. D. Persis, and P. Tesi, "Modeling and control of heat networks with storage: The single-producer multiple-consumer case," *IEEE Transactions on Control Systems Technology*, vol. 25, pp. 414–428, March 2017.

[90] J. J. Shah, M. C. Nielsen, T. S. Shaffer, and R. L. Fittro, "Cost-optimal consumption-aware electric water heating via thermal storage under time-of-use pricing," *IEEE Transactions on Smart Grid*, vol. 7, no. 2, pp. 592–599, 2016.

[91] X. Jin, J. Wu, Y. Mu, M. Wang, X. Xu, and H. Jia, "Hierarchical microgrid energy management in an office building," *Applied Energy*, vol. 208, pp. 480–494, 2017.

[92] T. Jiang, Z. Li, X. Jin, H. Chen, X. Li, and Y. Mu, "Flexible operation of active distribution network using integrated smart buildings with heating, ventilation and air-conditioning systems," *Applied Energy*, vol. 226, pp. 181–196, 2018.

[93] F. Benavente, A. Lundblad, P. E. Campana, Y. Zhang, S. Cabrera, and G. Lindbergh, "Photovoltaic/battery system sizing for rural electrification in bolivia: Considering the suppressed demand effect," *Applied energy*, vol. 235, pp. 519–528, 2019.

[94] X. Wu, X. Hu, X. Yin, C. Zhang, and S. Qian, "Optimal battery sizing of smart home via convex programming," *Energy*, vol. 140, pp. 444–453, 2017.

[95] R. Hemmati and H. Saboori, "Stochastic optimal battery storage sizing and scheduling in home energy management systems equipped with solar photovoltaic panels," *Energy and Buildings*, vol. 152, pp. 290–300, 2017.

[96] O. Talent and H. Du, "Optimal sizing and energy scheduling of photovoltaic-battery systems under different tariff structures," *Renewable energy*, vol. 129, pp. 513–526, 2018.

[97] O. Erdinc, N. G. Paterakis, I. N. Pappi, A. G. Bakirtzis, and J. P. Catalão, "A new perspective for sizing of distributed generation and energy storage for smart households under demand response," *Applied Energy*, vol. 143, pp. 26–37, 2015.

[98] R. Atia and N. Yamada, "Sizing and analysis of renewable energy and battery systems in residential microgrids," *IEEE Transactions on Smart Grid*, vol. 7, pp. 1204–1213, May 2016.

[99] J. Koskela, A. Rautiainen, and P. Järventausta, "Using electrical energy storage in residential buildings–sizing of battery and photovoltaic panels based on electricity cost optimization," *Applied Energy*, vol. 239, pp. 1175–1189, 2019.

[100] T. Beck, H. Kondziella, G. Huard, and T. Bruckner, "Optimal operation, configuration and sizing of generation and storage technologies for residential heat pump systems in the spotlight of self-consumption of photovoltaic electricity," *Applied energy*, vol. 188, pp. 604–619, 2017.

[101] D. Fischer, K. B. Lindberg, H. Madani, and C. Wittwer, "Impact of pv and variable prices on optimal system sizing for heat pumps and thermal storage," *Energy and Buildings*, vol. 128, pp. 723–733, 2016.

[102] M. Kharseh and H. Wallbaum, "The effect of different working parameters on the optimal size of a battery for grid-connected pv systems," *Energy Procedia*, vol. 122, pp. 595–600, 2017.

[103] L. Zhou, Y. Zhang, X. Lin, C. Li, Z. Cai, and P. Yang, "Optimal sizing of pv and bess for a smart household considering different price mechanisms," *IEEE access*, vol. 6, pp. 41050–41059, 2018.

[104] B. Boeckl and T. Kienberger, "Sizing of pv storage systems for different household types," *Journal of Energy Storage*, vol. 24, p. 100763, 2019.

[105] D. Wu, M. Kintner-Meyer, T. Yang, and P. Balducci, "Analytical sizing methods for behind-the-meter battery storage," *Journal of Energy Storage*, vol. 12, pp. 297–304, 2017.

[106] J. von Appen, "Incentive design, sizing and grid integration of residential pv systems with heat pumps and battery storage systems," in *2018 15th International Conference on the European Energy Market (EEM)*, pp. 1–5, IEEE, 2018.

[107] J. von Appen and M. Braun, "Sizing and improved grid integration of residential pv systems with heat pumps and battery storage systems," *IEEE Transactions on Energy Conversion*, vol. 34, no. 1, pp. 562–571, 2019.

[108] G. Angenendt, S. Zurmühlen, F. Rücker, H. Axelsen, and D. U. Sauer, "Optimization and operation of integrated homes with photovoltaic battery energy storage systems and power-to-heat coupling," *Energy Conversion and Management: X*, vol. 1, p. 100005, 2019.

[109] P. Huang, M. Lovati, X. Zhang, C. Bales, S. Hallbeck, A. Becker, H. Bergqvist, J. Hedberg, and L. Maturi, "Transforming a residential building cluster into electricity prosumers in sweden: Optimal design of a coupled pv-heat pump-thermal storage-electric vehicle system," *Applied Energy*, vol. 255, p. 113864, 2019.

[110] M. Lovati, G. Salvalai, G. Fratus, L. Maturi, R. Albatici, and D. Moser, "New method for the early design of bipv with electric storage: A case study in northern italy," *Sustainable Cities and Society*, vol. 48, p. 101400, 2019.

[111] S. Bahrami, M. H. Amini, M. Shafie-khah, and J. P. Catalao, "A decentralized electricity market scheme enabling demand response deployment," *IEEE Transactions on Power Systems*, vol. 33, no. 4, pp. 4218–4227, 2018.

[112] J. A. Pinzon, P. P. Vergara, L. C. P. da Silva, and M. J. Rider, "Optimal management of energy consumption and comfort for smart buildings operating in a microgrid," *IEEE Transactions on Smart Grid*, pp. 1–1, 2018.

[113] E. Vrettos, E. C. Kara, J. MacDonald, G. Andersson, and D. S. Callaway, "Experimental demonstration of frequency regulation by commercial buildings- part i: Modeling and hierarchical control design," *IEEE Transactions on Smart Grid*, pp. 1–1, 2017.

[114] *ASHRAE Guideline 14-2002: "Measurement of Energy and Demand Savings," ASHRAE, Atlanta, Georgia (2002).*

[115] B. Mayer, M. Killian, and M. Kozek, "Management of hybrid energy supply systems in buildings using mixed-integer model predictive control," *Energy conversion and management*, vol. 98, pp. 470–483, 2015.

[116] R. K. Shah and D. P. Sekulic, *Fundamentals of heat exchanger design.* John Wiley & Sons, 2003.

[117] L. Pérez-Lombard, J. Ortiz, and C. Pout, "A review on buildings energy consumption information," *Energy and buildings*, vol. 40, no. 3, pp. 394–398, 2008.

[118] R. Tang, S. Wang, K. Shan, and H. Cheung, "Optimal control strategy of central air-conditioning systems of buildings at morning start period for enhanced energy efficiency and peak demand limiting," *Energy*, vol. 151, pp. 771–781, 2018.

[119] E. M. Wanjiru, S. M. Sichilalu, and X. Xia, "Model predictive control of heat pump water heater-instantaneous shower powered with integrated renewable-grid energy systems," *Applied Energy*, vol. 204, pp. 1333–1346, 2017.

[120] F. Jabari, S. Nojavan, B. M. Ivatloo, and M. B. Sharifian, "Optimal short-term scheduling of a novel tri-generation system in the presence of demand response programs and battery storage system," *Energy conversion and management*, vol. 122, pp. 95–108, 2016.

[121] S. Baldi, A. Karagevrekis, I. T. Michailidis, and E. B. Kosmatopoulos, "Joint energy demand and thermal comfort optimization in photovoltaic-equipped interconnected microgrids," *Energy Conversion and Management*, vol. 101, pp. 352–363, 2015.

[122] M. Ali, J. Jokisalo, K. Siren, and M. Lehtonen, "Combining the demand response of direct electric space heating and partial thermal storage using lp optimization," *Electric Power Systems Research*, vol. 106, pp. 160–167, 2014.

[123] D. Keiner, M. Ram, L. D. S. N. S. Barbosa, D. Bogdanov, and C. Breyer, "Cost optimal self-consumption of pv prosumers with stationary batteries, heat pumps, thermal energy storage and electric vehicles across the world up to 2050," *Solar Energy*, vol. 185, pp. 406–423, 2019.

[124] E. Bee, A. Prada, and P. Baggio, "Demand-side management of air-source heat pump and photovoltaic systems for heating applications in the italian context," *Environments*, vol. 5, no. 12, p. 132, 2018.

[125] R. Gelleschus, M. Böttiger, and T. Bocklisch, "Optimization-based control concept with feed-in and demand peak shaving for a pv battery heat pump heat storage system," *Energies*, vol. 12, no. 11, p. 2098, 2019.

[126] S. Chen, H. B. Gooi, and M. Wang, "Sizing of energy storage for microgrids," *IEEE Transactions on Smart Grid*, vol. 3, no. 1, pp. 142–151, 2012.

[127] K. Khadka, H. Pourgharibshahi, and H. Zargarzadeh, "Comparative analysis of mppt methods for pv system with dc-dc three-level converter," in *2018 Clemson University Power Systems Conference (PSC)*, pp. 1–6, IEEE, 2018.

[128] C. Perfumo, E. Kofman, J. H. Braslavsky, and J. K. Ward, "Load management: Model-based control of aggregate power for populations of thermostatically controlled loads," *Energy Conversion and Management*, vol. 55, pp. 36–48, 2012.

[129] C. E. Council, "Clean energy australia report 2018," *Clean Energy Council, Melbourne, VIC, Australia*, 2018.

[130] Z. Moghaddam, I. Ahmad, D. Habibi, and M. A. S. Masoum, "A coordinated dynamic pricing model for electric vehicle charging stations," *IEEE Transactions on Transportation Electrification*, pp. 1–1, 2019.

[131] A. L. Facci, V. K. Krastev, G. Falcucci, and S. Ubertini, "Smart integration of photovoltaic production, heat pump and thermal energy storage in residential applications," *Solar Energy*, 2018.

[132] "Western australian electricity generator and retailer corporation.." `https://www.synergy.net.au/Your-home/Energy-plans/Smart-Home-Plan`. Accessed: 2018-11-10.

[133] E. Atashpaz Gargari, F. Hashemzadeh, R. Rajabioun, and C. Lucas, "Colonial competitive algorithm: a novel approach for pid controller design in mimo distillation column process," *International Journal of Intelligent Computing and Cybernetics*, vol. 1, no. 3, pp. 337–355, 2008.

[134] N. Mousavi, G. Kothapalli, D. Habibi, M. Khiadani, and C. K. Das, "An improved mathematical model for a pumped hydro storage system considering electrical, mechanical, and hydraulic losses," *Applied Energy*, vol. 247, pp. 228–236, 2019.

[135] N. Mousavi, G. Kothapalli, D. Habibi, and C. K. Das, "Operational cost reduction of pv-phs systems in farmhouses: Modelling, design, and experimental validation," in *IOP Conference Series: Earth and Environmental Science*, vol. 322, p. 012011, IOP Publishing, 2019.

[136] A. Marszal-Pomianowska, P. Heiselberg, and O. K. Larsen, "Household electricity demand profiles–a high-resolution load model to facilitate modelling of energy flexible buildings," *Energy*, vol. 103, pp. 487–501, 2016.

[137] M. I. Hlal, V. K. Ramachandaramurthy, A. Sarhan, A. Pouryekta, and U. Subramaniam, "Optimum battery depth of discharge for off-grid solar pv/battery system," *Journal of Energy Storage*, vol. 26, p. 100999, 2019.

[138] A. Baniasadi, D. Habibi, W. Al-Saedi, and M. A. Masoum, "A cost-effective thermal and electrical energy storage management strategy for smart buildings," in *2019 IEEE PES Innovative Smart Grid Technologies Europe (ISGT-Europe)*, pp. 1–5, IEEE.

[139] J. Salpakari, T. Rasku, J. Lindgren, and P. D. Lund, "Flexibility of electric vehicles and space heating in net zero energy houses: an optimal control model with thermal dynamics and battery degradation," *Applied energy*, vol. 190, pp. 800–812, 2017.

[140] "Water source heat pump (package type e series) 3.0kw-20.1kw (50hz).." `https://www.academia.edu/16499984/Mammoth_WSHP_Package_E_series_50HZ_R410A_catalogue_1_`. Accessed: 2019-10-19.

[141] B. Xu, A. Oudalov, A. Ulbig, G. Andersson, and D. S. Kirschen, "Modeling of lithium-ion battery degradation for cell life assessment," *IEEE Transactions on Smart Grid*, vol. 9, pp. 1131–1140, March 2018.

[142] D. U. Sauer and H. Wenzl, "Comparison of different approaches for lifetime prediction of electrochemical systems using lead-acid batteries as example," *Journal of Power sources*, vol. 176, no. 2, pp. 534–546, 2008.

[143] `https://www.solarquotes.com.au/battery-storage/comparison-table/`. Accessed: 2019.

[144] W. Al-Saedi, S. W. Lachowicz, D. Habibi, and O. Bass, "Power flow control in grid-connected microgrid operation using particle swarm optimization under variable load conditions," *International Journal of Electrical Power & Energy Systems*, vol. 49, pp. 76–85, 2013.

[145] N. Ming, W. Can, and X. Zhao, "A review on applications of heuristic optimization algorithms for optimal power flow in modern power systems," *Journal of Modern Power Systems and Clean Energy*, vol. 2, no. 4, pp. 289–297, 2014.

[146] M. Killian and M. Kozek, "Ten questions concerning model predictive control for energy efficient buildings," *Building and Environment*, vol. 105, pp. 403–412, 2016.

[147] K. Feldman, T. Jazouli, and P. A. Sandborn, "A methodology for determining the return on investment associated with prognostics and health management," *IEEE Transactions on Reliability*, vol. 58, no. 2, pp. 305–316, 2009.

[148] `https://www.solarchoice.net.au/blog/solar-power-system-prices`. Accessed: 2019.

[149] I. A. Sajjad, G. Chicco, and R. Napoli, "Definitions of demand flexibility for aggregate residential loads," *IEEE Transactions on Smart Grid*, vol. 7, no. 6, pp. 2633–2643, 2016.

[150] f. zhang, Z. Hu, K. Meng, L. Ding, and Z. Y. Dong, "Hess sizing methodology for an existing thermal generator for the promotion of agc response ability," *IEEE Transactions on Sustainable Energy*, pp. 1–1, 2019.

[151] A. Baniasadi, D. Habibi, O. Bass, and M. A. Masoum, "Optimal real-time residential thermal energy management for peak-load shifting with experimental verification," *IEEE Transactions on Smart Grid*, 2018.

[152] Y. Cao, W. Wei, L. Wu, S. Mei, M. Shahidehpour, and Z. Li, "Decentralized operation of interdependent power distribution network and district heating network: A market-driven approach," *IEEE Transactions on Smart Grid*, vol. 10, pp. 5374–5385, Sep. 2019.

[153] M. S. H. Nizami, J. Hossain, and E. Fernandez, "Multi-agent based transactive energy management systems for residential buildings with distributed energy resources," *IEEE Transactions on Industrial Informatics*, pp. 1–1, 2019.

[154] A. E. M. Operator, "Electricity statement of opportunities," 2019.

[155] N. Lu and Y. Zhang, "Design considerations of a centralized load controller using thermostatically controlled appliances for continuous regulation reserves," *IEEE Transactions on Smart Grid*, vol. 4, no. 2, pp. 914–921, 2012.

[156] H. Hui, Y. Ding, W. Liu, Y. Lin, and Y. Song, "Operating reserve evaluation of aggregated air conditioners," *Applied energy*, vol. 196, pp. 218–228, 2017.

[157] J. Hu, J. Cao, M. Z. Chen, J. Yu, J. Yao, S. Yang, and T. Yong, "Load following of multiple heterogeneous tcl aggregators by centralized control," *IEEE Transactions on Power Systems*, vol. 32, no. 4, pp. 3157–3167, 2016.

[158] D. Xie, H. Hui, Y. Ding, and Z. Lin, "Operating reserve capacity evaluation of aggregated heterogeneous tcls with price signals," *Applied energy*, vol. 216, pp. 338–347, 2018.

[159] M. Song, C. Gao, M. Shahidehpour, Z. Li, J. Yang, and H. Yan, "State space modeling and control of aggregated tcls for regulation services in power grids," *IEEE Transactions on Smart Grid*, 2018.

[160] H. Khalkhali and S. H. Hosseinian, "Novel residential energy demand management framework based on clustering approach in energy and performance-based regulation service markets," *Sustainable cities and society*, vol. 45, pp. 628–639, 2019.

[161] L. Zhang, N. Good, and P. Mancarella, "Building-to-grid flexibility: Modelling and assessment metrics for residential demand response from heat pump aggregations," *Applied energy*, vol. 233, pp. 709–723, 2019.

[162] S. Wang and R. Tang, "Supply-based feedback control strategy of air-conditioning systems for direct load control of buildings responding to urgent requests of smart grids," *Applied Energy*, vol. 201, pp. 419–432, 2017.

[163] L. R. Rodríguez, M. Brennenstuhl, M. Yadack, P. Boch, and U. Eicker, "Heuristic optimization of clusters of heat pumps: A simulation and case study of residential frequency reserve," *Applied energy*, vol. 233, pp. 943–958, 2019.

[164] F. Müller and B. Jansen, "Large-scale demonstration of precise demand response provided by residential heat pumps," *Applied energy*, vol. 239, pp. 836–845, 2019.

[165] C. Batlle and P. Rodilla, "A critical assessment of the different approaches aimed to secure electricity generation supply," *Energy Policy*, vol. 38, no. 11, pp. 7169–7179, 2010.

[166] B. Lu, A. Blakers, and M. Stocks, "90–100% renewable electricity for the south west interconnected system of western australia," *Energy*, vol. 122, pp. 663–674, 2017.

[167] H. Bazine and M. Mabrouki, "Chaotic dynamics applied in time prediction of photovoltaic production," *Renewable energy*, vol. 136, pp. 1255–1265, 2019.

[168] K. B. Debnath and M. Mourshed, "Forecasting methods in energy planning models," *Renewable and Sustainable Energy Reviews*, vol. 88, pp. 297–325, 2018.

[169] L. Ruiz, M. Cuéllar, M. Calvo-Flores, and M. Jiménez, "An application of non-linear autoregressive neural networks to predict energy consumption in public buildings," *Energies*, vol. 9, no. 9, p. 684, 2016.